

**“Reversible DNMT/G9a blockade activates viral mimicry,
myelomonocytic differentiation and TSG expression in
MDS/AML *in vitro* models”**

Dissertation

Zur Erlangung des Grades
Doktor der Naturwissenschaften

Am Fachbereich Biologie
Der Johannes Gutenberg-Universität Mainz

Angelique Schönefeld (geborene Ziegfeld)
geboren am 11.07.1991 in Sömmerda

Mainz, 2022

Dekan: Prof. Dr. Eckhard Thines

Betreuer: Dr. rer. nat. Borhane Guezguez

Erster Berichterstatter: Univ.-Prof. Dr. med. Matthias Theobald

Zweiter Berichterstatter: Univ.-Prof. Dr. rer. nat. Thomas Hankeln

Tag der mündlichen Prüfung: 24.07.2023

1 Summary

Acute myeloid leukemia (AML) is one of the most aggressive cancers of the hematopoietic system. It is characterized by malignant hematopoiesis leading to the generation of fast-growing myeloblasts found in the bone marrow and blood. The development of AML can be favored by myelodysplastic syndromes (MDS), which are a heterogeneous group of clonal hematopoietic stem cell disorders. MDS/AML initiation and maintenance are based on genomic and epigenomic alterations including dysregulated activity of the histone methyltransferase G9a and DNA methyltransferases (DNMTs). This is associated with transcriptionally silencing of tumor suppressor genes (TSGs) as well as tumor metastasis, increased proliferation and cancer progression.

The DNMT inhibitors (DNMTi), azacytidine (AZA) and decitabine (DAC) have been successfully used to treat MDS and AML patients with poor-prognosis by reversing critical epigenetic events driving the cancer phenotype. However, only half of the patients respond to the treatment and all responder develop drug resistance. Moreover, DNMTi have a short half-life and induce high cytotoxicity due to irreversible DNA incorporation and DNA double strand breaks that eventually trigger pro-oncogenic chromosomal translocation and leukemic evolution. Therefore, it is important to find stable, highly potent but less toxic epigenetic inhibitors for MDS and AML patients.

Recently, a new generation of hypomethylating agents (HMAs) were discovered including CM-272 being a small molecule dually inhibiting G9a and DNMTs by reversible binding. Based on these findings, the dual blockage of the enzymes in different MDS/AML *in vitro* models was investigated. CM-272 induced cytotoxicity in nanomolar (nM) range in various MDS/AML cell lines and primary AML cells with a heterogeneous mutational background. Anti-tumor effects such as reduced proliferation and colony forming potential, cell-cycle arrest, and increased apoptosis without DNA damage were detected particularly in OCI-AML3 upon DNMT/G9a protein inactivation and degradation.

OCI-AML3 is a *de novo* AML cell line harboring AML-driver mutations DNMT3A^{R882C} and nucleophosmin 1 (NPM1c). CM-272 induced myelomonocytic differentiation of OCI-AML3 cells, which was linked to a suppressed expression of the nuclear export protein exportin 1 (XPO1). Consequently, NPM1c was seen to translocate to the nucleus, causing a reduced HOX9A/MEIS1 signaling pathway and enhanced differentiation of OCI-AML3 cells.

Summary

In MDS-L, F-36P, and OCI-AML3, dual inhibition of DNMT/G9a resulted in a transcriptomic reprogramming seen by chromatin remodeling and activated transcription factors (TFs). Furthermore, double stranded (ds)RNA of LTR-elements of endogenous retroviruses (ERVs) and the type I interferon (IFN) signaling pathway were upregulated, which could be linked to the anti-tumor response in MDS/AML cell lines treated with CM-272.

In addition, an AML fluorescence reporter gene cell line with THP-1 cells was generated as a screening tool for epigenetic inhibitors. Controlled by the epigenetically suppressed promoter of the TSG secreted frizzled-related protein 1 (SFRP1), fluorescent expression (mCherry) expression was investigated in response to DAC and CM-272 versus vehicle control. Signal intensity and number of mCherry positive cells increased upon drug treatment seen by high-throughput FACS analysis. These initial experiments verified the functionality of the recombinant THP-1 cell line and showed that DAC and CM-272 similarly activate the SFRP1 promoter.

In summary, the dual inhibitor of DNMT/G9a, CM-272 showed highly potent effects on MDS/AML cells that are comparable with the DNMTi DAC. These *in vitro* data indicated that CM-272 could be a promising alternative to the conventional epigenetic therapy in MDS and AML. However, further investigations by *in vivo* experiments and sequencing analysis has to be performed to understand the therapeutic effects and the mode of action of CM-272.

2 Zusammenfassung

Die akute myeloische Leukämie (AML) ist eine der aggressivsten Krebserkrankungen des blutbildenden Systems. Sie ist durch eine maligne Hämatopoese gekennzeichnet, die zur Entwicklung schnell wachsender Myeloblasten im Knochenmark und Blut führt. Die Entwicklung der AML kann durch myelodysplastische Syndrome (MDS) begünstigt werden, welche eine heterogene Gruppe klonaler hämatopoetischer Stammzellerkrankungen darstellen. Die Entstehung und Aufrechterhaltung von MDS/AML beruht auf genomischen und epigenomischen Veränderungen, einschließlich einer dysregulierten Aktivität der Histon-Methyltransferase G9a und der DNA-Methyltransferasen (DNMTs). Dies wird mit der transkriptionellen Stilllegung von Tumorsuppressorgen (TSG) sowie mit der Metastasierung von Tumoren, der verstärkten Proliferation und dem Fortschreiten von Krebs in Verbindung gebracht.

Die DNMT-Inhibitoren (DNMTi), Azacytidin (AZA) und Decitabin (DAC) wurden erfolgreich zur Behandlung von MDS- und AML-Patienten mit schlechter Prognose eingesetzt, indem sie kritische epigenetische Ereignisse, die den Krebsphänotyp bestimmen, rückgängig machen. Allerdings spricht nur etwa die Hälfte der Patienten auf die Behandlung an und alle Patienten, welche auf die Behandlung ansprechen, entwickeln eine Arzneimittelresistenz. Außerdem weisen DNMTi eine kurze Halbwertszeit auf und wirken hoch zytotoxisch. Ihre Toxizität wird durch eine irreversible DNA-Inkorporation verursacht, was zu DNA-Doppelstrangbrüchen führen kann und pro-onkogene chromosomale Translokationen und die Entstehung von Leukämie begünstigt. Daher ist es wichtig stabile, hochwirksame, aber weniger toxische epigenetische Inhibitoren für MDS- und AML-Patienten zu finden.

Kürzlich wurde eine neue Generation von hypomethylierenden Agenzien (HMA) entdeckt, darunter CM-272, ein kleines Molekül, das die Enzyme G9a und DNMT durch reversible Bindung gleichzeitig hemmt. Darauf aufbauend wurde in dieser Arbeit die duale Blockade der Enzyme in verschiedenen MDS/AML-*in-vitro*-Modellen untersucht. Medikamentenbehandlung von CM-272 im nanomolaren (nM) Bereich wirkten sich zytotoxisch auf verschiedene MDS/AML-Zelllinien und primären AML-Zellen mit heterogenem Mutationshintergrund aus. Antitumoreffekte, wie verringerte Proliferation und Koloniebildung, Zellzyklus-Arrest und erhöhte Apoptose ohne DNA-Schäden wurden insbesondere bei OCI-AML3 nach DNMT/G9a-Protein-Inaktivierung und -Degradation festgestellt.

Zusammenfassung

OCI-AML3 ist eine *de novo* AML-Zelllinie, welche die AML-treibenden Mutationen DNMT3A^{R882C} und Nukleophosmin 1 (NPM1c) aufweist. In diesen Zellen führte CM-272 zu einer myeloisch-monozytären Differenzierung. Unsere Daten zeigten eine verringerte Expression des nuklearen Exportproteins Exportin 1 (XPO1) durch CM-272 Behandlung, welches mit einer Translokation von NPM1c im Nukleus verbunden war. Weiterhin deuten die Ergebnisse darauf hin, dass die Akkumulation von NPM1c im Nukleus zu einem unterdrückten HOX9A/ MEIS1-Signalweg führte und sich die Zellen verstärkt differenzierten.

Bei MDS-L, F-36P und OCI-AML3 führte die duale Hemmung von DNMT/G9a zu einer transkriptomischen Umprogrammierung, was eine Umstrukturierung von Chromatin und eine Aktivierung von Transkriptionsfaktoren auslöste. Darüber hinaus wurden dsRNAs von LTR-Elementen endogener Retroviren (ERV) mit einer Hochregulierung des Interferon (IFN)-Signalwegs vom Typ I in Zusammenhang gebracht. Wir vermuten, dass dieser Signalweg für die Anti-Tumorantwort der CM-272-behandelten MDS/AML-Zelllinien mitverantwortlich ist.

Basierend auf dem epigenetisch unterdrückten TSG SFRP1 wurde eine AML-Zelllinie mit dem Reporter gen mCherry generiert, um epigenetische Inhibitoren zu testen. Dafür verwendete man THP-1-Zellen und untersuchte die mCherry-Expression nach Behandlung mit DAC und CM-272 im Vergleich zur Vehikelkontrolle. Die Signalintensität und die Anzahl der mCherry-positiven Zellen nahm nach der Behandlung mit den Medikamenten zu, wie die FACS-Analyse im Hochdurchsatz zeigte. Diese ersten Experimente bestätigten die Funktionalität der rekombinanten THP-1-Zelllinie und zeigten, dass DAC und CM-272 den SFRP1-Promotor ähnlich potent aktivieren.

Zusammenfassend lässt sich sagen, dass CM-272 aufgrund der dualen Inhibierung von DNMT/G9a spezifisch auf MDS/AML-Zellen wirkt und eine Anti-Tumorreaktion auslöst. Dieser Effekt ist mit dem DNMTi DAC vergleichbar. Deshalb deuten diese *in-vitro*-Daten darauf hin, dass CM-272 eine vielversprechende Alternative zur herkömmlichen epigenetischen Therapie bei MDS und AML sein könnte. Es müssen jedoch noch weitere Untersuchungen durch *in-vivo*-Experimente und Sequenzierungsanalysen durchgeführt werden, um die therapeutischen Effekte und die Wirkungsweise von CM-272 aufzudecken.

3 List of Abbreviations

μ micro (10^6)

% percentage

°C degree Celsius

3'UTR 3' untranslated region

5hmC 5-hydroxymethylcytosine

5mC 5-methylcytosines

ac acetylation

ADME absorption, distribution, metabolism and excretion properties

AdoMet or SAM S-Adenosyl-L-methionine

ALL acute lymphocytic leukemia

Allo SCT allogenic hematopoietic stem cell transplantation

AML acute myeloid leukemia

AML-MRC AML with myelodysplasia-related changes

APC adenomatous polyposis coli

APL acute promyelocytic leukemia

APS ammonium persulfate

ATP adenosine triphosphate

AXIN axis inhibitor

AZN azanucleosides

b2M β2 microglobulin

BCL-2 B-Cell Leukemia/Lymphoma 2

BET bromodomain and extraterminal

BrdU bromodeoxyuridine

BSA bovine serum albumine

c centi (10^2)

C cytosines

ca. circa

CBF-AML core-binding factor AML

cdNA complementary DNA

CEPBA CCAAT enhancer binding protein alpha

CFU colony forming unit

CHIP Clonal Hematopoiesis of Indeterminate Potential

CK1α casein kinase 1α

c-Kit receptor tyrosine kinase

CLL chronic lymphocytic leukemia

CML chronic myeloid leukemia

CpG 5'-desoxycytidine-phosphate-desoxyguanosine-3'

CRC colorectal cancer

CRISPR Clustered Regularly Interspaced Short Palindromic Repeats

Ct threshold cycle

DAPI 4',6-diamidino-2-phenylindole

DGE differential gene expression

DKK1 dickkopf WNT signaling pathway inhibitor 1

DMSO dimethyl sulfoxide

DNA deoxyribonucleic acid

DNMT1, 3A, 3B DNA methyltransferases 1, 3A, 3B

DNMTi DNMT inhibitors

DSC3 desmocollin 3

DTT dithiothreitol

dUTPs deoxyuridine 5-triphosphate

e.g. exempli gratia - for example

EGR2 early growth response 2

EHMT2 euchromatic histone-lysine N-methyltransferase 2

EMA European Medicine Agency

EPO erythropoietin

et al. et alii - and others

FACS fluorescence-activated single cell sorting

FBP1 fructose-1,6-bisphosphatase

FBS fetal bovine serum

FCS forward scatter

FDA Food and drug Administration

FL full-length

FLT3 FMS-like tyrosine kinase 3

FOSB FosB Proto-Oncogene

fw forward

g gram

G-CSF granulocyte colony stimulating factor

gDNA genomic DNA

GLP glucagon-like peptide-1

GM-CSF granulocyte-macrophage colony-stimulating factor

gRNA guide RNA

GSEA gene set enrichment analysis

GSK3β glycogen synthase kinase-3 beta

List of Abbreviations

h hour	n number of cases, nano (10^9)
H2AX H2A histone family member X	NaCl sodium chloride
H3/4 histone 3 or 4	NaOH sodium hydroxide
HAT histone acetyltransferases	ncRNAs non-coding RNAs
HCC hepatocellular carcinoma	NHEJ non-homologous end joining
HDACs histone deacetylases	NLS nuclear localization signal
HDMs histone demethylases	NoLS nucleolar localization signal
HDR homology-directed recombination	NPM1 nucleophosmin 1
HMTs histone methyltransferases	NRAS neuroblastoma RAS
HP1 heterochromatin protein 1	NUP98 Nuclear pore complex protein
HRP horseradish peroxidase, horseradish peroxidase	OASL oligoadenylate synthase-like
HSC hematopoietic stem cell	Oct-3/4 octamer-binding transcription factor 3 and 4
IC50 half-maximal inhibitory concentration	PAM protospacer adjacent motif
IDH-1/2 isocitrate dehydrogenase 1 or 2	PARP poly adenosine diphosphate-ribose polymerase
IFI6 interferon alpha-inducible protein 6	PBMC peripheral blood mononuclear cells
IL interleukin	PBS phosphate-buffered saline
Indels insertion or deletions	PBX3 pre-B-cell leukemia transcription factor 3
ITD internal tandem duplication	PCR polymerase chain reaction
K lysine	Pen Strep Penicillin/Streptomycin
kb kilobase, kilo base	PPi pyrophosphate
kDa kilo Dalton	pre-LSCs pre-leukemic stem cells
KI knockin	PRMTs arginine N-methyltransferases
KMT lysine methyltransferases	R arginine
KMT2 histone-lysine N-methyltransferase 2	R.I.N. RNA Integrity Number
KO knockout	REs repetitive elements
KRAS Kirsten rat sarcoma virus	RHA right homologous arm
l litre	RISC RNA induced silencing complex
LHA left homologous arm	RNA ribonucleic acid
LINEs long interspersed transposable elements	RNA-Seq RNA sequencing
lncRNAs long non-coding RNAs	RPKT reads per kilobase of transcript
m mili (10^3)	rpm rounds per minute
M molar	RT-qPCR Quantitative reverse transcription PCR
MALDI-TOF MS time-of-flight mass spectrometry	rv reverse
MASPIN mammary serine protease inhibitor	SAP shrimp alkaline phosphatase
me methylation	SCF stem cell factor
MECOM EVI1 complex locus protein EVI1	SD standard deviation
MeCP2 methyl CpG binding protein 2	SDS-PAGE sodium dodecyl sulfate-polyacrylamide gel electrophoresis
MEIS1 myeloid ecotropic viral integration site 1	sec second
min minute	secAML secondary acute myeloid leukemia
miRNAs microRNAs	SET Su(var)3-9, Enhancer-of-zeste and Trithorax
Mn1 meningioma	SFRP1 Secreted frizzled-related protein 1
MNCs mononuclear cells	
mRNA messenger RNA	

List of Abbreviations

SINEs short interspersed transposable elements
siRNA small interfering RNAs
SPRI solid-phase reversible immobilization
SR1 stem regenin 1
SSC side scatter
SV40 prom SV40 promoter

T thymine
TAE tris-acetate-EDTA
TBE tris-borate-EDTA
TBS-T Tris-buffered saline-Tween
TEMED N,N,N',N'-Tetramethylethylenediamine
TET2 tet methylcytosine dioxygenase 2
TF transcription factor
TGF- β transforming growth factor beta 1
TNF α tumor necrosis factor alpha

Tris-HCl tris(hydroxymethyl)aminomethane-hydrochloride
TSGs tumor suppressor genes

U uracil
UHRF1 ubiquitin like with PHD and ring finger domains 1
UNG uracil-N-glycosylase
UV ultraviolet

V volt

WT wild type

α alpha

Δ delta

Table of Contents

1	Summary	iii
2	Zusammenfassung	v
3	List of Abbreviations	vii
4	Introduction	1
4.1	Normal hematopoiesis.....	1
4.2	Malignant hematopoiesis.....	3
4.2.1	Myelodysplastic syndromes	3
4.2.2	Leukemia	5
4.2.3	Acute myeloid leukemia is a (epi)genetic disorder	6
4.3	Epigenetics in normal and malignant cells.....	11
4.3.1	Epigenetic mechanisms: DNA methylation, histone modifications and non-coding regulate gene expression	11
4.3.2	Gene expression controlled by DNA methylation	13
4.3.3	Regulation of gene expression by histone methylation	17
4.3.4	Cross-talk of DNMTs and KMTs	19
4.4	Therapy of MDS and AML patients.....	21
4.4.1	Overview of therapeutic strategies for MDS patients	21
4.4.2	Overview of therapeutic strategies for AML patients	22
4.4.3	Azanucleosides for the treatment of MDS and AML.....	22
4.4.4	Dual inhibition of DNMT1 and G9a by a reversible, first-in-class dual inhibitor..	23
4.5	Aim of the PhD thesis.....	26
5	Material and Methods	27
5.1	Equipment	27
5.2	Consumables	30
5.3	Chemicals and Reagents	32
5.4	Prepared buffer solutions	34
5.5	Kits.....	35
5.6	Prokaryotic cell line.....	36
5.7	Cytokines/ Inhibitors for cell cultivation.....	36
5.8	Media	36
5.9	Human eukaryotic cell lines	37

Table of Contents

5.10	Human primary AML samples	38
5.11	Epigenetic drugs	39
5.12	Antibodies	40
5.13	Primers	41
5.14	Templates and plasmids for molecular cloning.....	44
5.15	crRNAs	45
5.16	Software	45
5.17	Cell biology	45
5.17.1	Cell culture of eukaryotic cells.....	45
5.17.2	Drug treatment of cell lines and primary cells	47
5.17.3	Functional assays	47
5.18	Molecular Biology	50
5.18.1	Investigation mRNA expression of genes.....	50
5.18.2	Investigating protein expression of genes by western blot	52
5.18.3	Cytokine release analysis by Luminex.....	53
5.18.4	DNA methylation analyses	54
5.19	Generation of a recombinant THP-1 reporter cell line.....	58
5.19.1	Selection of the most suitable crRNA for HDR-based CRISPR/Cas9 editing at the SFRP1 gene site	59
5.19.2	Molecular Cloning of the SFRP1_mCherry_puro construct	61
5.19.3	HDR-based CRISPR/Cas9 KI of the SFRP1_mCherry_puro construct at the SFRP1 gene site of the THP-1 cell line	67
5.20	Validation of transfected THP-1 single cell clones	69
5.20.1	Genotyping of THP-1 reporter gene clones.....	69
5.20.2	High-throughput FACS screening and fluorescence microscopy to test the mCherry signal.....	69
5.21	Statistical analysis.....	70
6	Results	71
6.1	Potency of CM-272 tested on various leukemia cell lines.....	71
6.1.1	Dual inhibition of DNMT/G9a by CM-272 displays high cytotoxic potency across a broad range of MDS/AML cell lines.....	71

Table of Contents

6.1.2	Protein degradation of DNMT/G9a and reactivation of epigenetic silenced genes in MDS/AML cell lines by CM-272	74
6.1.3	CM-272 leads to apoptosis, cell cycle arrest, reduced colony formation and decreased proliferation without DNA damage of MDS/AML cell lines.....	76
6.2	Antitumor effect on patient-derived AML cells by CM-272	78
6.3	Transcriptional reprogramming by CM-272 in MDS/AML cell lines.....	80
6.3.1	Activation of an antiviral immune response of MDS/AML cell lines upon CM-272 treatment.....	82
6.3.2	Myelomonocytic differentiation of OCI-AML3 upon CM-272 treatment.....	84
6.3.3	CM-272 induces XPO1 downregulation, nuclear relocalization of NPM1c and decreased HOX gene expression in OCI-AML3	86
6.4	Generation of a suitable reporter gene cell line for screening of epigenetic agents	88
6.4.1	The SFRP1 gene can be used for epigenetic drug screening in AML.....	88
6.4.2	Identification of the optimal RNP targeting the SFRP1 gene.....	90
6.4.3	Molecular cloning of the SFRP1_mCherry_puro construct.....	92
6.4.4	THP-1 is a suitable AML reporter cell line for HDR-based CRISPR/Cas9 editing at the SFRP1 gene site	94
6.4.5	Validation of single cell clones of THP-1 by genotyping and FACS.....	96
6.5	Investigating the potential of DAC and CM-272 to reactivate SFRP1 in clone 7 and 15 by fluorescence microscopy and FACS	98
7	Discussion	100
7.1	CM-272 highly affected many different MDS/AML subtypes due to dual inhibition of G9a and DNMTs	100
7.2	DNA and histone demethylation had the strongest effect on OCI-AML3 harboring a DNMT3A and NPM1 mutation	102
7.3	Upregulated endogenous dsRNAs of LTR/ERVs could be linked to viral mimicry and anti-tumor effects in leukemia cells.....	103
7.4	Dual inhibition of DNMT/G9a led to myelomonocytic differentiation of OCI-AML3 through reduced HOX9/MEIS1 activity	104
7.5	CM-272 induced anti-neoplastic effects in primary AML blasts	105

Table of Contents

7.6	Generation of the SFRP1-specific reporter gene cell line as an epigenetic drug screening model for AML.....	106
7.7	The gold standard treatment of DAC and CM-272 was verified by the reporter cell lines THP-1 clone 7 and 15.....	108
8	Conclusion.....	110
9	Outlook.....	111
10	List of Figures.....	xvii
11	List of Tables.....	xix
12	Appendix.....	xxi
12.1	Sequence to analyze for MassARRAY.....	xxi
12.2	Sequence of SFRP1_mCherry_puro construct.....	xxii
12.3	Sequencing of PCR 1, 2, and 3 of clone 7 and 15.....	xxiii
13	Acknowledgement.....	xxiv
14	Bibliography.....	xxv

4 Introduction

4.1 Normal hematopoiesis

The term hematopoiesis describes cellular processes by which mature blood cells are formed. In mammals, this continuous mechanism starts early during embryonic development at the yolk sac, then proceeds transiently to the developing fetal liver and finally establishes at the adult stage within the bone marrow and thymus¹.

In adult humans, approximately one trillion (10^{12}) of hematopoietic and immune cells arise daily in the bone marrow to replenish the blood system, illustrating blood as a highly regenerative tissue.² The blood system is composed of various cell types that are organized in a specific phylogenetic hierarchy with hematopoietic stem cells (HSCs) at the top and terminally differentiated blood cells on the bottom of this lineage organization. HSCs are a rare cell population in the bone marrow and possess two very important fundamental properties. First, HSCs produce all myeloid or lymphoid lineage restricted progenitor cells, which are still immature blast cells that in turn proliferate and differentiate into all types of mature blood cells. Second, HSCs have the ability to durably self-renew, or generate daughter stem cells that sustain a certain pool of multipotent HSCs for a lifelong blood production.²

As a result of lineage commitment of hematopoietic progenitors, those cells gradually lose their potential to differentiate into alternative cell lineages. Common lymphoid progenitors can give rise to T, B, and natural killer cells, while common myeloid progenitors are developed in granulocytes (neutrophils, basophils, eosinophiles) and macrophages. Another cell type, dendritic cells can originate either from lymphoid or myeloid progenitors.³ (Figure 1)

At the mature stage, differentiated blood cells are released to the bloodstream where they take on a variety of different functions. Red blood cells or erythrocytes transport oxygen and carbon dioxide, maintain systemic acid/base equilibria and are equipped with an antioxidant system.⁴ White blood cells or leukocytes consist of lymphocytes (T and B cells), macrophages and granulocytes and contribute to innate and adaptive immune responses to injuries and pathogens⁵. Megakaryocytes, the third cellular component of blood, release platelets (also called thrombocytes) that facilitate blood clotting (coagulation) at sites of injuries, thus promoting wound healing⁶.

This hematopoietic homeostasis of HSC differentiation and self-renewal is tightly regulated by cell-intrinsic factors, such as transcriptional and epigenetic regulators and metabolic pathways. Cell-extrinsic signals influencing stem cell activity are comprised of long-range humoral and neural signals or local stimuli from the bone marrow microenvironment (also called stem cell niche). In case of (epi)genetically altered, malignant HSCs, excessive differentiation or insufficient self-

Introduction

renewal minimizes the number of HSCs whereas insufficient differentiation or elevated self-renewal leads to myeloproliferative diseases or leukemia.⁷

Therefore, understanding molecular mechanisms of normal hematopoiesis does not only provide a fundamental knowledge about this tightly regulated process, but also would help with deciphering neoplastic transformation and developing new therapies for hematopoietic malignancies such as leukemia.

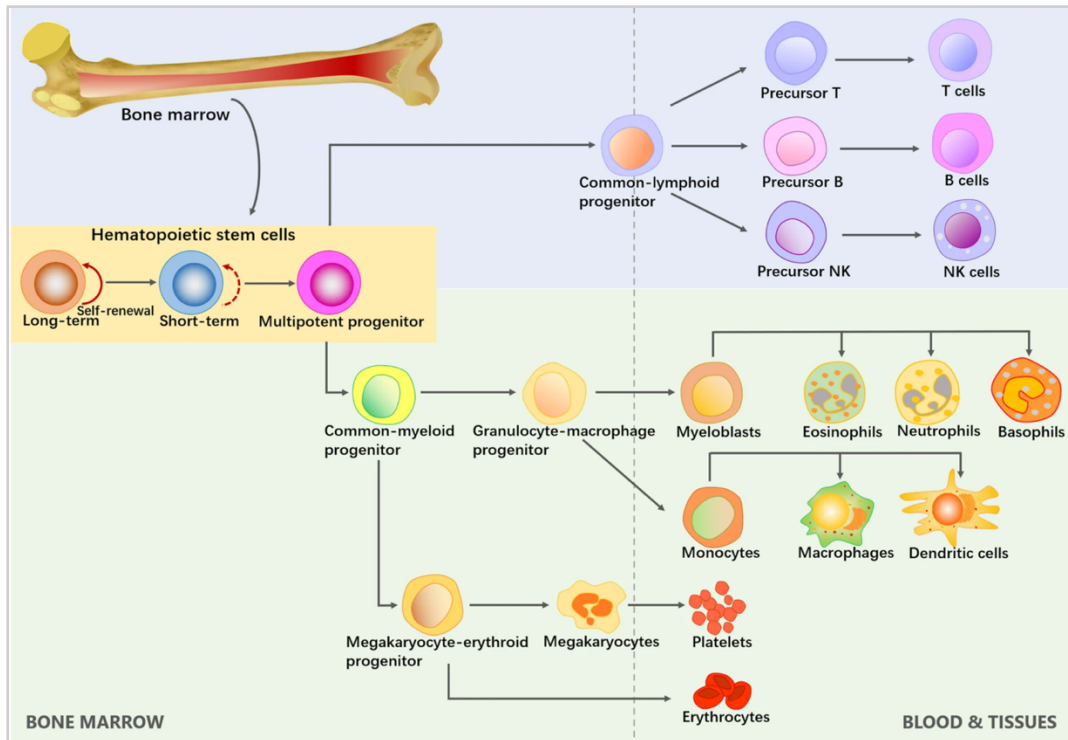


Figure 1: The hierarchical blood system from HSCs to differentiated blood cells.

HSCs are located in the bone marrow and give rise to all types of blood cells which are either myeloid or lymphoid origin. Additionally, HSCs have self-renewal potential to sustain a pool of multipotent cells. Hematopoietic cells of the lymphoid lineage are T, B, and NK cells while blood cells belonging to the myeloid lineage are granulocytes (eosinophiles, neutrophils, basophils), macrophages, megakaryocytes (platelets) and erythrocytes. Dendritic cells are allocated to both lineages.⁸

4.2 Malignant hematopoiesis

4.2.1 Myelodysplastic syndromes

Myelodysplastic syndromes (MDS) are a group of clonal hematopoietic stem cell disorders characterized by aberrant hematopoiesis⁹. More specifically, MDS is diagnosed in case of persistent and clinically unexplained cytopenia (reduction of mature blood cells), significant morphological dysplasia (abnormal cells) of hematopoietic cells and cytogenetic and/or molecular genetic changes causing loss of polyclonal hematopoiesis¹⁰. MDS patients are diagnosed with a bone marrow blast count of <20 % in contrast to acute myeloid leukemia (AML) with ≥ 20 % blast cells.

According to the latest population-based registry data, the annual age-adjusted MDS incidence reported for Germany and the United States is approximately 4/100.000 persons and rises with age. MDS is a disease of elderly with a median age of 70 years.^{11,12} Unfortunately, the overall 5-year survival rate has stagnated at ca. 31 %, which is a relatively poor probability despite the increasing number of new treatment options¹³.

In recent years, genome-wide next-generation sequencing has provided a more comprehensive overview of occurring mutations in MDS that are crucial for disease prognosis and therapy decision. Among the analyzed genes, 45 % of them were identified to be mutated in 85 % of all cases. These recurrent mutations are present in genes associated with DNA methylation, post-transcriptional chromatin modification, transcription regulation, the RNA spliceosome machinery, DNA cohesion complexes, and signal transduction^{14,15}. (Figure 2)

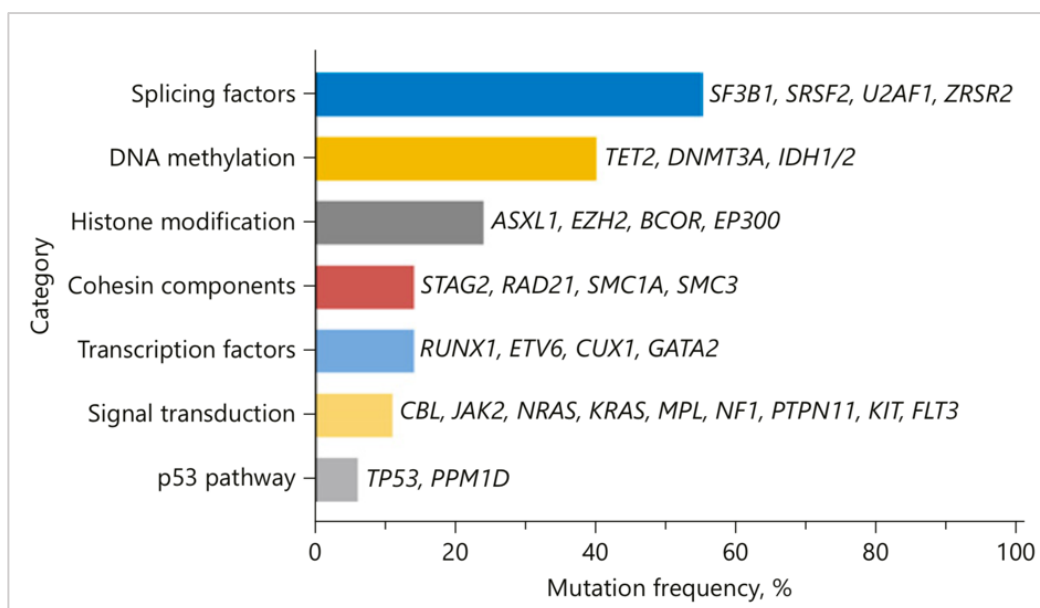


Figure 2: Frequency of mutated genes in MDS having prognostic and therapeutic significance.

Genome-wide next-generation sequencing data revealed mutated genes in MDS that are associated to different biological processes including splicing factors, DNA methylation, and histone modification.¹⁶

Introduction

Approximately one third of MDS cases eventually progress to a secondary acute myeloid leukemia (MDS-derived AML or secAML), which is classified as a distinct clinicopathologic entity termed “AML with myelodysplasia-related changes” (AML-MRC).¹¹ The transformation of a preleukemic state to an AML is associated with clonal evolution characterized by the expansion or emergence of a subclone with a unique set of mutations. Tumor burden and clonal evolution is monitored not only using blast count but also sequencing allowing early detection.¹⁷ (Figure 3)

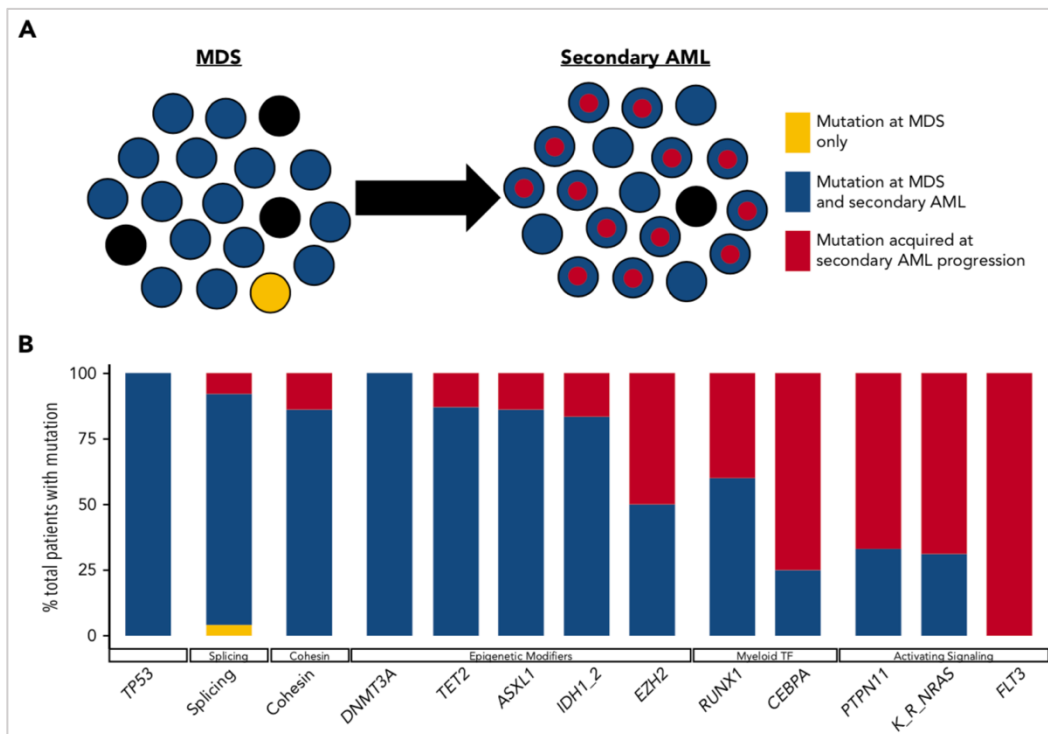


Figure 3: Transformation of MDS to secAML by clonal evolution.

(A and B) Mutated genes were assessed from paired MDS and secondary AML samples (n=60) obtained from different disease stages of the same patients in a longitudinal study. Early acquired mutations (blue) define a subclone which has the ability to expand to become the most abundant clone at MDS diagnosis. Additional mutations can be accumulated causing disease progression to secAML (blue and red).¹⁷

4.2.2 Leukemia

Leukemia or blood cancer is the 15th most commonly diagnosed cancer and 11th leading cause of cancer death worldwide. The incidence and mortality rate (cases per 100,000 people) of leukemia worldwide is slightly higher among males relative to females (6.1 and 4.2 for men; 4.3 and 2.8 for women).¹⁸

Leukemogenesis (the development of leukemia) is characterized by a step-wise neoplastic transformation model arising from HSCs. Within this model, the acquisition of pre-leukemic mutations in HSCs can form a small number of dominant HSC-derived clones that are prone to transform into leukemic cells. This process is termed Clonal Hematopoiesis of Indeterminate Potential (CHIP). These genetically altered HSCs, also called pre-leukemic stem cells (pre-LSCs), can still form healthy blood cells toward myeloid/lymphoid-lineage bias, however, additional mutations can result in the malignant expansion of aberrant progenitor cells by dysfunctional differentiation. Ultimately, LSCs produce an uncontrolled accumulation of undifferentiated blood cells, called “blast” cells that disrupts healthy hematopoietic cells leading to cytopenia and dysplasia.^{19,20} (Figure 4)

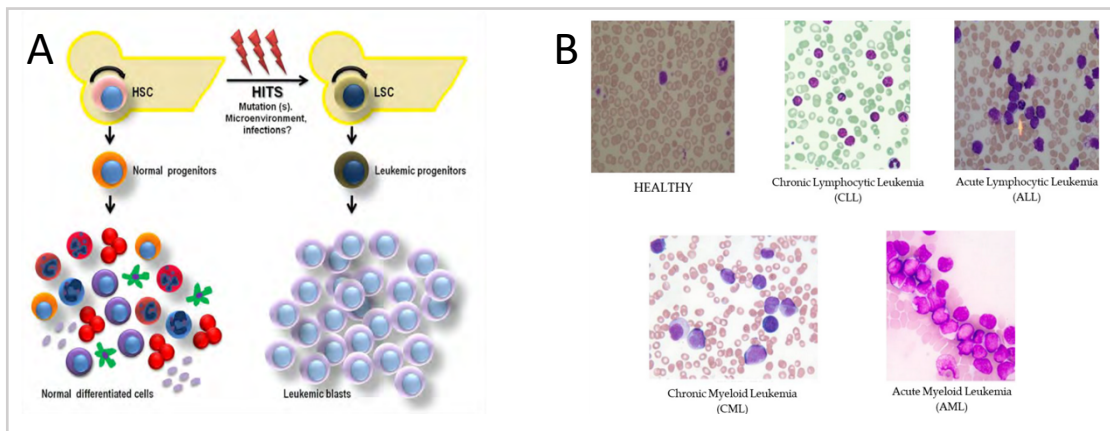


Figure 4: Normal hematopoiesis and different types of leukemia.

(A) HSCs give rise to all types of blood cells to replenish the blood system. Altered HSCs altered due to mutations, their microenvironment or infections can transform to LSCs generating poorly functional blast cells that replace healthy blood cells.²⁰ **(B)** Four different types of leukemia named chronic lymphocytic leukemia (CLL), acute lymphocytic leukemia (ALL), chronic myeloid leukemia (CML), and acute myeloid leukemia (AML) can be developed with distinct morphological features.²¹

Since dysfunctional proliferation of leukemic blasts can affect all types of leukocytes, leukemia is a very heterogeneous disease that is classified in different subtypes according to cell of origin (myeloid or lymphoid leukemias) and the degree of cellular differentiation blockade (acute and chronic leukemias). Acute leukemias develop quickly within one year from abnormal cells that are

undifferentiated and less mature. Immature, healthy blast cells normally make up 1 % - 5 % of bone marrow cells, however, in acute leukemias the number of blasts elevates having ≥ 20 % in the bone marrow as defined by the World Health Organization criteria.²² In contrast, chronic leukemias are characterized by a mix of mature and abnormal cells that lead to a slow onset of the disease with symptoms arising only after years without increased blast numbers.²³⁻²⁵ (Figure 4). The proportion of new cases among the four leukemia subtypes varies by sex and is illustrated in Table 1.

Table 1: Proportion of new cases of leukemia subtypes in women and men in Germany in 2015-2016. (¹Acute lymphoid leukemia, ²Chronic lymphoid leukemia, ³Acute myeloid leukemia, ⁴Chronic lymphoid leukemia, ⁵all others, including inaccurately designated forms of leukemia).²⁶

	<i>ALL</i> ¹	<i>CLL</i> ²	<i>AML</i> ³	<i>CML</i> ⁴	<i>Others</i> ⁵
Women	6 %	36 %	25 %	9 %	24 %
Men	6 %	39 %	22 %	8 %	25 %

Known risk factors associated with the development of leukemia are exposure to ionizing radiation, benzene and previous chemotherapy (alkylating agents and topoisomerase inhibitors).^{18,27,28} Additionally, viral infections (e.g. T-cell leukemia virus, Epstein Barr virus) can lead to subtypes of ALL. Several genetic syndromes (e.g. Down syndrome, Fanconi anemia, Bloom syndrome, Li-Fraumeni syndrome) are also linked to a higher risk to develop AML or ALL.²⁹⁻³¹ Nevertheless, other factors that might be responsible for leukemia onset remain under intense investigations. To diagnose leukemias, a complete blood count, liver function as well as a complete metabolic and coagulation panel are initially examined. In addition, peripheral blood smear, bone marrow aspiration and biopsies are often required followed by more detailed analyses (e.g. flow cytometry, cytogenetic testing) to distinguish between subtypes.³²

Standard treatment of leukemia include chemotherapy, but also radiation therapy, monoclonal antibodies, and stem cell transplantation.³³⁻³⁶ Moreover, a succeeding therapy is depending on the subtype of leukemia, cytogenetics and molecular findings, patient age, and comorbid conditions.³⁷

4.2.3 Acute myeloid leukemia is a (epi)genetic disorder

Altered HSCs and subsequent aberrant progeny were shown to carry either large chromosomal rearrangements, gene fusions or genetic mutations that define different AML subtypes. As such, two well-characterized chromosomal translocations are t(8:21) in core-binding factor AML (CBF-AML) or t(15:17) in acute promyelocytic leukemia (APL). Three AML types are characterized by a rearrangement involving the histone-lysine N-methyltransferase 2 (KMT2), MDS1 and EVI1

complex locus protein EVI1 (MECOM), and Nuclear pore complex protein (NUP98). KMT2 has more than 80 fusion partners with MLLT3 and MLLT10 being most common. However, recent advances in genomic studies displayed a normal karyotype in 97 % of AML cases harboring no large chromosomal abnormalities but only small molecular changes³⁸. Interestingly, *de novo* AML genomes have fewer mutations compared to other adult cancers, with an average of only 13 mutations found in genes³⁹. Based on extensive analyses of cohorts of AML patients, a two-hit model of leukemogenesis has been proposed which divides the various AML-associated mutations into two classes. Mutated genes of the class I induce pro-proliferative pathways and of class II are associated with a disturbed hematopoietic differentiation^{39,40-42}. Recently, a third class of mutations has been added to the original two-hit model, where the mutated gene class plays a role in epigenetic pathways. (Table 2) Importantly, mutations of different classes co-occur and promote disease progression synergistically. For example, the class II mutated gene nucleophosmin 1 (NPM1) has been associated with the class I mutation of FMS-like tyrosine kinase 3 (FLT3)-internal tandem duplication (ITD) or with mutations in the epigenetic genes DNA methyltransferase 3A (DNMT3A) and isocitrate dehydrogenase 1 or 2 (IDH1/IDH2) (class III mutations).³⁸ Ultimately, the interaction of different chromosomal rearrangements and somatic mutations have a dramatic impact on the pathogenesis of AML and are crucial for therapy decision and prognosis.

Table 2: Notable mutated genes, their classification and frequency in AML.³⁹

The genomic and epigenomic landscape of 200 clinically annotated adult cases of *de novo* AML were analyzed by whole-genome sequencing and whole-exome sequencing to identify driver mutations in AML and their frequency.

Identified mutated genes in AML: FMS-like tyrosine kinase 3 (FLT3), Kirsten rat sarcoma virus (KRAS), neuroblastoma RAS (NRAS), TP53, receptor tyrosine kinase (c-Kit), nucleophosmin 1 (NPM1), CCAAT enhancer binding protein alpha (CEPBA), DNA methyltransferase 3A (DNMT3A), tet methylcytosine dioxygenase 2 (TET2), isocitrate dehydrogenase 1 and 2 (IDH1/ IDH2)

Class I mutations (proliferation)				Class II mutations (differentiation)		Class III mutations (epigenetic regulation)		
FLT3	K/NRAS	TP53	c-Kit	NPM1	CEPBA	DNMT3A	TET2	IDH1/IDH2
28%	12%	8%	4%	27%	6%	26%	9%	20%

4.2.3.1 NPM1c and DNMT3A^{R882} are common AML-driver mutations

NPM1c: NPM1 also known as B23 is an abundant multifunctional phosphoprotein that resides in nucleoli. It takes part in many different cellular processes such as maintaining the genomic stability, mediating DNA-repair processes, and regulating gene transcription through chromatin condensation and decondensation. Based on its motifs and functional domains, NPM1 acts as a nuclear chaperone for both proteins and nucleic acids and shuttles between cellular compartments.⁴³ The nuclear localization signal (NLS) is responsible for the transport from the

Introduction

cytoplasm to the nucleoplasm and the nucleolar localization signal (NoLS) localizes the wild type NPM1 (NPM1wt) into the nucleolus. The nuclear export is mediated by the interaction of the nuclear export signals (NESs) with the nuclear exporter exportin 1 (XPO1).⁴⁴

Alterations of NPM1 are frequently seen in multiple malignancies including gastric, colon, ovarian, bladder and prostate cancer. In therapy-related MDS that often evolves to secAML, a partial or total loss of chromosome 5 is often observed where NPM1 is located (5q35 locus). About one third of the AML patients harbor NPM1 mutations. Mutations are almost exclusively found in exon 12 being unique for myeloid malignancies compared to solid tumors. Within the NoLS motif, the tryptophan residues 289 and 290 (or 290 alone) are lost and a new C-terminal NES is generated. Consequently, all mutated NPM1 proteins translocate from the nucleus to the cytoplasm via XPO1, thus called cytoplasmic NPM1 (NPM1c). These AML mutations are always heterozygous because NPM1wt is essential for cell survival. The dominant mutants form heterodimers with the NPM1wt causing a cytoplasmic delocalization and perturb its normal function.⁴⁵ (Figure 5) Extensive studies have shown that genomic stability is decreased, the function of tumor suppressor genes (TSGs) such as AFR and p53 is disturbed, apoptosis is decreased and the oncogene MYC is less degraded in NPM1-mutated cells. Moreover, NPM1-mutant AML exhibit higher HOX gene levels than NPM1wt AML. HOXA and HOXB genes are highly expressed in normal adult HSPCs but are physiologically silenced in mature blood cells. Elevated HOX expression in normal HSPCs leads to leukemic transformation and an undifferentiated cell state. It has been suggested that NPM1c causes a gain-of-function of HOX genes that maintains the leukemic state.⁴⁴ However, NPM1 mutations alone are insufficient to drive the leukemic transformation but additional mutations including FLT3 and DNMT3A are essential and synergize the AML development. (Figure 6)

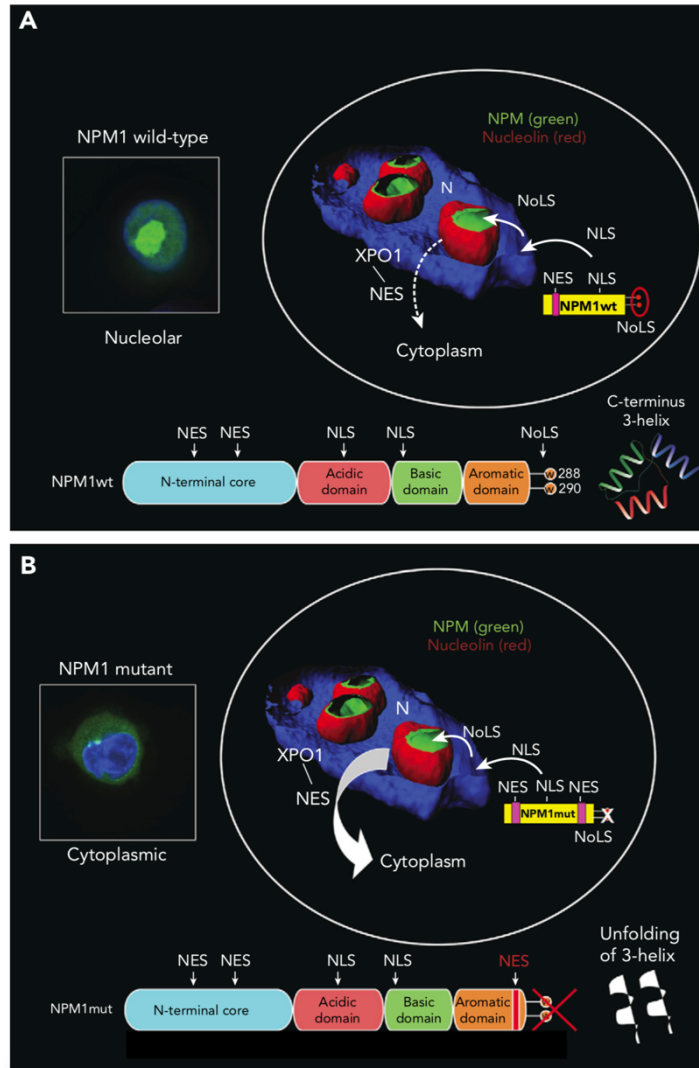


Figure 5: NPM1wt and NPM1c shuttle between cellular compartments.

(A) NPM1wt protein is composed of two motifs that lead to nuclear export (NESs) and motifs that dictate the localization within the nucleus (NLS) and nucleolus (NoLS). NPM1wt is predominantly found within the nucleolus due to weaker export than import signals. **(B)** In NPM1 mutant (NPM1c) AML, a third NES motif is inserted at the C terminus and the tryptophan-residues 288 and 290 are lost. This leads to an increased export to the cytoplasm via XPO1. Thereby, NPM1c forms heterodimers with NPM1wt and perturbs its function.⁴⁴

DNMT3A^{R882}: DNMT3A is one of three DNA methyltransferases responsible for *de novo* DNA methylation (see chapter 4.3.2). Dysregulated DNA methylation is also well-known to be associated with hematological malignancies such as MDS and AML⁴⁶. In fact, about 25-35 % of AML and 10 % of MDS patients carry mostly heterozygous DNMT3A mutations resulting in a loss of function. These data imply that mutated DNMT3A dramatically contributes to clonal hematopoiesis and increase the risk of disease progression.^{9,47} Importantly, 60 % of the DNMT3A mutations in AML are a point mutation of arginine 882 within the methyltransferase catalytic domain that is changed to histidine (R882H) or cysteine (R882C)⁴⁸. DNMT3A^{R882} mutant loses its methyltransferase activity while acting as a dominant negative mutant, minimizing the enzymatic activity of the wild-

Introduction

type DNMT3A by over 80 %⁴⁹. As a result of this mutation, DNA hypomethylation occurs and leukemic stemness genes, e.g. meningo gene (Mn1), homeobox A (HoxA) gene cluster and HOX cofactor Meis1 (myeloid ecotropic viral integration site 1) become activated. Moreover, DNMT3A^{R882} enhances the binding of active histone modifiers at the enhancer elements.⁴⁹⁻⁵¹

DNMT3A^{R882} with other mutations: Various studies reported that DNMT3A^{R882} induced DNA hypomethylation is an initiating event in AML development.^{52,53} HSCs containing DNMT3A mutations are in a pre-leukemic state favoring malignant transformation by acquiring additional genetic alterations, e.g. mutations in FLT3, NPM1, and IDH1⁴⁸. Other studies suggest that DNMT3A mutation can epigenetically synergize the leukemic transformation with other genetic alterations. Public datasets of AML patients showed a co-occurrence of DNMT3A, FLT3 and NPM1 mutations in many AML patients. Additionally, a KI mouse model with triple gene mutations (*Dnmt3a* mutation /*Flt3-Itid*/*Npm1c*) exhibited a fully penetrant leukemic phenotype. However, double mutation model (*Dnmt3a* mutation with either *Flt3-ITD* or *Npm1c*) displayed long latency and low penetrance.⁵⁴ Recently, Garg et al. reported that triple-mutant AML patient samples are characterized by high leukemic stem cell⁵⁵. (Figure 6)

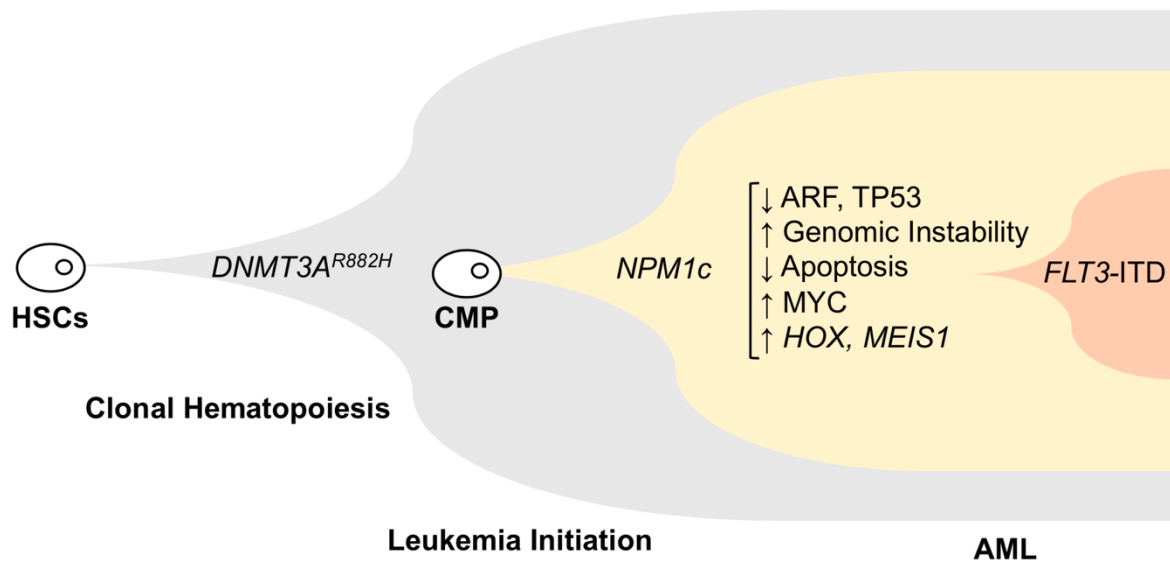


Figure 6: Mechanisms of leukemic evolution.

This figure shows the most common combination of mutations that cause the transformation of a HSC to a common myeloid progenitor (CMP) and an AML cell. Mutation of the DNMT3A gene is considered as an early event and additional mutations such as NPM1c and FLT3-IDT are often seen to co-occur at a later point.⁵⁶

4.3 Epigenetics in normal and malignant cells

4.3.1 Epigenetic mechanisms: DNA methylation, histone modifications and non-coding regulate gene expression

Gene expression can be turned on or off through genetic alterations such as mutations or chromosomal rearrangements which are inherited, irreversible transformations. In contrast, epigenetics describes the regulation of gene expression without changing the DNA code itself. Here, chemical tags are reversibly added or removed to DNA or histones in response to changes in the environment as a way of adaptation. These epigenetic marks are coded as information which are used as a type of transcriptional memory of the parent cell and can be passed on to the next cell generation(s) during cell division and proliferation. Ultimately, regulation of gene expression by epigenetics is important for the cell identity, lineage determination, regeneration and re-establishing of the next generation. DNA methylation, histone modifications, and non-coding RNAs are the three major molecular mechanisms of epigenetics.^{57,58}

DNA methylation: DNA methylation, the selective transfer of a methyl-group to a cytosine within a CpG (5'-deoxycytidine-phosphate-desoxyguanosine-3') dinucleotide, is associated with gene silencing. 5-methylcytosines (5mC) are formed by two types of DNMT (*de novo* and maintenance DNMTs) using a methyl-group donor such as S-Adenosyl-L-methionine (AdoMet or SAM). DNA demethylases such as TET2 remove this epigenetic mark by catalyzing the conversion of the modified DNA base 5mC to 5-hydroxymethylcytosine (5hmC). The 5hmC and its oxidized derivatives are subsequently replaced with an unmodified cytosine by base excision repair to achieve demethylation.

Histone modifications: DNA is packaged around a histone octamer containing pairs of the histone proteins H2A, H2B, H3, and H4 and form the basic unit of chromatin. All histones are subject to chemical modifications such as acetylation, methylation, ubiquitylation, and phosphorylation by specific enzymes. Chemical changes can either activate or repress transcription of genes depending on the type of modification and its location in the histone protein.

The most studied histone modifications are histone acetylation and histone methylation. Histone acetylation (ac) is associated with gene activation and occurs at N-terminal conserved lysine (K) residues of histone 3 (H3K9ac and H3K14ac) and histone 4 (H4K5ac, H4K8ac, H4K2ac, and H4K16ac) by histone acetyltransferases (HATs). The counterparts of HATs are histone deacetylases (HDACs). Histone methylation (me) frequently occurs on histone H3 and H4 on specific lysine and arginine (R) residues by lysine methyltransferases (KMTs) and protein arginine N-methyltransferases (PRMTs), respectively. A lysine residue can be mono-, di- or trimethylated, while arginine residues can be only mono- or demethylated. Depending on the location of a histone

Introduction

lysine methylation, it can lead to activation or inhibition of the gene transcription. H3K9me, H3K27me, and H4K20me are associated with gene repression whereas H3K4me and H3K36me are considered to be activation marks. Histone methyltransferases (HMTs) are counteracted by histone demethylases (HDMs).^{59,60}

Both DNA methylation and histone modifications determine the chromatin structure resulting in either loose, transcriptionally active euchromatin or dense, transcriptionally inactive heterochromatin. The open euchromatin state promotes gene expression by allowing transcription factors (TFs) and enzymes to interact with the DNA. The closed heterochromatin state suppresses the gene expression by preventing initiation of transcription.⁶¹ These different chemical changes of DNA and histones as well as the involved enzymes and other proteins are in close relationship and affect each other.⁶²

Non-coding RNAs: The third epigenetic mechanism is a cluster of different non-coding RNAs (ncRNAs) that also play a significant role in regulating gene expression at the transcriptional and post-transcriptional level. Small non-coding RNAs (sncRNAs) such as microRNAs (miRNAs) and small interfering RNAs (siRNA) or long non-coding RNAs (lncRNAs) are transcribed from DNA but not translated into proteins. miRNA mostly interact with the 3' untranslated region (3'UTR) of target mRNA to suppress expression.⁶³ siRNAs are double-stranded RNAs (dsRNAs) that incorporate into a RNA induced silencing complex (RISC) protein when targeting and cleaving a specific mRNA, thereby inhibiting gene expression⁶⁴. LncRNA are defined as RNAs longer than 200 nucleotides forming a large and highly heterogeneous group of transcripts that differ in their biogenesis and genetic origin.⁶⁵ In addition, ncRNAs regulate gene expression by a dynamic interaction with molecules involved in DNA methylation and histone modifications.⁶⁶ (Figure 7)

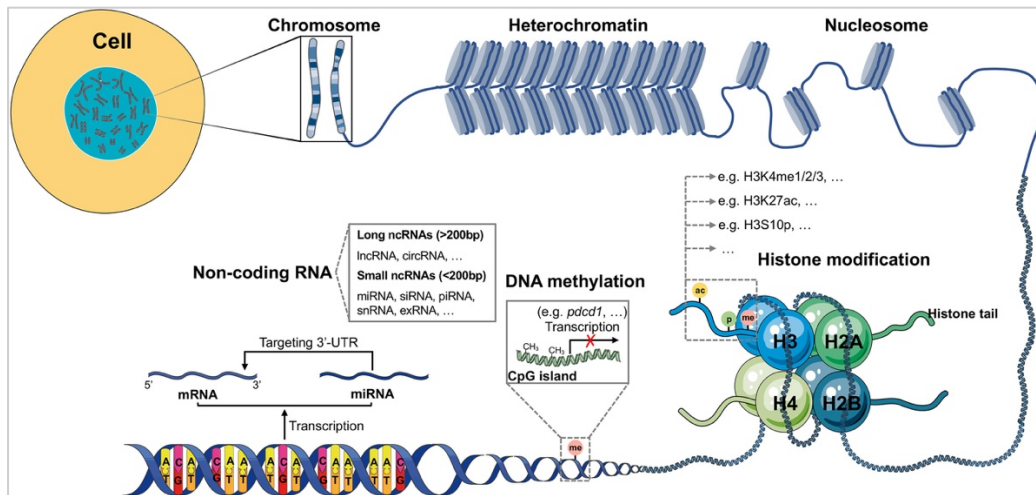


Figure 7: An overview of the epigenetic mechanisms: DNA methylation, histone modification and ncRNAs. Gene transcription and expression can be regulated by epigenetics that describe the mechanisms: DNA methylation (CpG dinucleotides), histone modifications (e.g. acetylation and methylation), and ncRNA (sncRNAs and lincRNAs). These mechanisms mediate either an activation or suppression of genes causing a cell type specific phenotype.⁶⁷

4.3.2 Gene expression controlled by DNA methylation

A typical epigenetic mark of heterochromatin is the covalent modification of DNA leading to 5mC. Gene silencing by DNA methylation plays an important role in maintaining the stability of the genome, genomic imprinting, inactivation of X-chromosome in females, regulation of transcription and developmental processes.⁶⁸ This kind of regulated gene suppression is found primarily in repetitive genomic regions (e.g. satellite DNA), within centromeres, and repetitive elements such as short interspersed transposable elements (SINEs) and long interspersed transposable elements (LINEs).

Methylation of the 5th carbon of cytosine residue occurs in the cytosine-guanine sequence in mammalian DNA strands, is established during early development, and is heritable.^{69,70} In humans, ca. 70 % of the CpG dinucleotides are methylated despite very low CpG frequency due to spontaneous deamination of methylated cytosines creating thymines (CpG suppression). CpG dinucleotides are unevenly distributed throughout the mammalian genome with a higher density within so-called CpG islands that have a length of 0.3 – 2 kb. These CpG islands overlap promoter regions of approximately 60-70 % of all human genes that are either protected from methylation and therefore active or repressed by methylation during differentiation in normal cells.^{71,72} (Figure 9)

DNMT1, one of three DNMTs, mainly plays a role in the maintenance of methylation from parent to daughter cell by methylating hemi-methylated cytosines in double-stranded DNA (dsDNA) molecules during DNA replication.

Unmethylated dsDNA can be methylated by DNMT3A and DNMT3B, enzymes that are associated with *de novo* methylation.⁷³⁻⁷⁶ Interestingly, DNMT1 can also have a *de novo* activity whereas DNMT3A/3B were observed to maintain symmetrical CpG methylation at distinct repetitive and single copy sequences in embryonic stem cells.⁷⁷

4.3.2.1 The role of DNMTs in hematopoiesis

For the last decades, scientists have shown that the DNA methylome undergoes extensive changes during hematopoietic development.⁷⁸⁻⁸⁰ Various studies revealed that DNA methylation plays a causative role in cell fate determination than being a consequence of hematopoietic differentiation.^{81,82}

The maintenance enzyme DNMT1 is important for HSC self-renewal, homing and suppression of apoptosis, and the regulation of myeloid/lymphoid lineage commitment.^{80,81,83-85}

Whereas, murine HSCs with a double KO *Dnmt3a* (HSC *Dnmt3a*^{-/-}) show enhanced hematopoietic regeneration by extensively repopulating in recipient mice (15 times more HSCs) compared to the recipients transplanted with normal HSCs. They also maintain their self-renewal capacity for at least 12 transplant generations in contrast to normal transplanted HSCs. Furthermore, *Dnmt3a*^{-/-} HSCs showed a higher *in vitro* colony-forming activity and a lower differentiation potential *in vivo*. On molecular level, *Dnmt3a*^{-/-} HSCs exhibit an aberrant DNA methylation pattern and a dysregulated expression of genes associated with differentiation and multipotency.

Despite only mild phenotypical changes of *Dnmt3b*^{-/-} HSCs *in vivo*, *Dnmt3b* seems to have a redundant, yet synergistic, role with *Dnmt3a* in HSCs in terms of CpG island hypermethylation.⁸⁶

These data have demonstrated that a disturbed activity of DNMTs can have dramatic outcomes for hematopoietic development.

4.3.2.2 Deregulated DNMT1 activity correlates with hypermethylated promoter of TSGs in AML

In various cancer types comprising both solid⁸⁷⁻⁹¹ and blood cancers⁹²⁻⁹⁴ including AML⁹⁵⁻⁹⁸, DNMTs have been shown to act as oncoproteins promoting tumorigenesis, cancer cell cycle progression, proliferation and immune escape. Over the last two decades, it has been reported that deregulated DNMT activity is associated with DNA hypermethylation at CpG islands in MDS and AML.⁹⁹ Promoter of TSGs harboring CpG islands are often affected by aberrant DNA hypermethylation. These genes are involved in either of the following crucial cellular signaling pathways: cell growth/cell cycle progression, cell proliferation, DNA repair mechanisms, and

apoptosis. Ultimately, silencing of TSGs by DNA methylation increases the risk of dysregulated cell growth and facilitates tumorigenesis¹⁰⁰. (Figure 9)

DNMT1, the most abundantly expressed DNMT in dividing cells, represents an important therapeutic target for methylation inhibition and re-expression of TSGs¹⁰¹. One of the most promising TSG affected by DNMT1 in AML is p15, a cyclin-dependent kinase inhibitor. DNMT1-mediated downregulation of p15 expression by promoter hypermethylation is observed in approximately 80% of AML patients and is associated with disease progression and aggressiveness¹⁰². Bone marrow cells from AML patients compared with healthy donors revealed a 5.3-fold upregulation of DNMT1 transcripts that correlated with a methylated p15 in 72% of AML patients. These data indicated that DNMT1 can induce hypermethylation and silencing of TSGs in AML.¹⁰³

4.3.2.3 The WNT-antagonist SFRP1 is a hypermethylated TSG in various cancers including AML

Secreted frizzled-related protein 1 (SFRP1) is one of five members of the secreted glycoprotein SFRP family (SFRP1-5).¹⁰⁴ The gene is located at position 8p11.21 and encodes 314 amino acids (35.4 kDa). The protein is composed of two independent structural domains namely the carboxy-terminal netrin domain and an amino-terminal cysteine-rich domain.¹⁰⁵ SFRP1 is an important WNT antagonist and thereby modulates the highly conserved WNT signaling pathway. This pathway is involved in the regulation of proliferation, cell-fate, migration, and cell polarity during developmental processes. The transcriptional coactivator β -catenin is stabilized through the ligand WNT and subcellular localized to orchestrate the transcription of various genes including MYC and Cyclin D1 (“on” state).

SFRP1 can directly bind to the WNT ligand antagonizing the signaling cascade. In the absence of WNT, a continuous phosphorylation of β -catenin is mediated by the destruction complex including the proteins casein kinase 1 α (CK1 α), axis inhibitor (AXIN), adenomatous polyposis coli (APC), and glycogen synthase kinase-3 beta (GSK3 β). This leads to a ubiquitination and proteasomal degradation of β -catenin (off state).^{106,107} (Figure 8)

The SFRP1 expression is highly downregulated in many human cancers which contributes to the dysregulation of cell proliferation, migration, invasion and eventually the formation of cancer. Therefore, SFRP1 is classified as a TSG in different cancer entities such as colorectal cancer (CRC), prostate cancer, and renal cell cancer. Promoter DNA hypermethylation of SFRP1 has been recognized as a common mechanism for its downregulation in cancer including CRC, bladder cancer, non-small-cell lung cancer, and gastric cancer. The downregulation of SFRP1 and its hypermethylation are also associated with poor survival among CRC patients.¹⁰⁸⁻¹¹²

For the maintenance of HSCs, the WNT signaling pathway plays an important role with β -catenin as the key molecule. Consequently, abnormal activation of the WNT signaling pathway through promoter hypermethylation contributes to the pathogenesis of AML. In addition, several studies could show that AML patients with elevated promoter methylation of SFRPs have lower survival outcome.¹¹³⁻¹¹⁵ These data suggest that hypermethylation of SFRP1 contributes to the disease progression in AML patients.

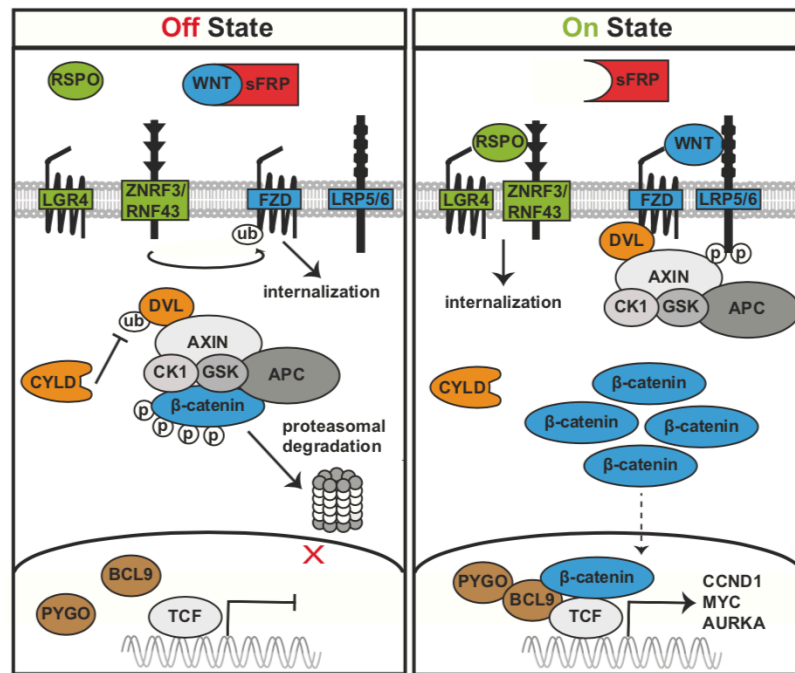


Figure 8: SFRP1 antagonizes the WNT signaling pathway.

In the “off” state of the WNT pathway (left), SFRP1 is bound to the ligand WNT leading to the formation of a destruction complex (CK1 α , AXIN, APC, and GSK3 β) for β -catenin and its continuous proteasomal degradation. During cellular development, the WNT pathway is switched on and WNT can bind to its receptor Frizzled (FZD). This mediates the disruption of the destruction complex allowing the stabilization and nuclear translocation of β -catenin. As a result, WNT target genes are transcribed.¹⁰⁷

4.3.2.4 Global DNA hypomethylation in cancer

While TSGs are hypermethylated in the course of carcinogenesis, the overall genome shows a hypomethylated DNA pattern (Figure 9). Global DNA hypomethylation is often associated with poor prognosis which can be explained by different plausible mechanisms.¹¹⁶⁻¹¹⁸ First, repetitive elements (REs) are hypomethylated in cancer, including the interspersed retrotransposon LINE-1, which accounts for approximately 17 % of the human genome.¹¹⁹ Hypomethylated REs are associated with chromosomal instability causing genetic alterations such as aneuploidy, chromosomal translocations, and copy number alterations.¹²⁰⁻¹²² Second, gene activation of proto-oncogenes, or cancer germline (CG) antigen gene may promote oncogenic phenotypes and/ or disease progression.¹²³⁻¹²⁷ (Figure 9) Third, hypomethylation also affects large heterochromatin

regions termed LOCKs and their nuclear organization, turning euchromatic in cancer. These large-scale hypomethylated blocks promote gene expression variabilities and have been associated with a selective growth advantage in cancer cells.¹²⁸

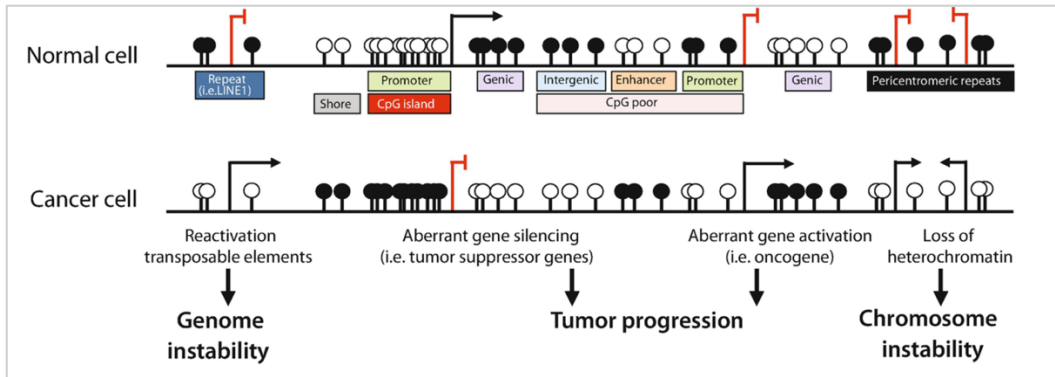


Figure 9: Gene regulation by DNA methylation of normal and cancer cells.

There is a distinct distribution of CpG methylation over the genome that provides regulated gene expression and intact genome integrity. During tumorigenesis, DNA methylation patterns are changed leading to genome and chromosome instability as well as tumor progression. White circle: unmethylated CpG; black circle: methylated CpG.¹²⁹

4.3.3 Regulation of gene expression by histone methylation

4.3.3.1 Histone 3 lysine 9 methylation (H3K9me) suppresses gene expression

Histone methylation, a dynamic process of transcription activation and repression, has been reported to influence the chromatin architecture, the recruitment of transcriptional factors, the interaction with initiation and elongation factors and RNA processing. It is catalyzed by several HMTs and takes place at either lysine or arginine residues on histone H3 or H4.

Lysines can be reversibly mono-, di- or trimethylated which causes gene activation (e.g. H3K4, H3K36, H3K79) or gene repression (e.g. H3K9 or H3K27) depending on the modification. In total, there are six major classes of KMT1-6.¹³⁰

The KMT1 enzyme family causes transcriptional repression by H3K9 methylation being catalyzed by one of five members: SUV39H1, SUV39H2, G9A, GLP, and SETDB1.¹³¹⁻¹³³ These enzymes seem to have distinct methylation preferences - SUV39H1 and SUV39H2 for example are primarily responsible for centromeric and pericentromeric heterochromatin by tri-methylation.¹³⁴ G9A and G9a-like protein (GLP) are specific to mono- and di-methyltransferases of H3K9 and are predominantly found associated with silenced genes in euchromatin.¹³⁵ SETDB1 catalyzes trimethylation of H3K9 to inactivate ERVs and the X-chromosome.^{136,137}

Moreover, these enzymes also contain binding sites specifically for the methylation marks that they create on chromatin facilitating a positive feedback loop.¹³⁸

4.3.3.2 G9a in healthy and malignant cells

G9a, also called EHMT2 (euchromatic histone-lysine N-methyltransferase 2), belongs to the Su(var)3-9 family (KMT class 1). G9a is composed of an automethylation site, nuclear localization signals, a catalytic active Su(var)3-9, Enhancer-of-zeste and Trithorax (SET) domain, as well as ankyrin repeats. (Figure 10A) The SET domain is responsible for histone methylation and the ankyrin repeats are involved in protein-protein interactions and recognition of mono- and dimethylated H3K9 marks. Consequently, G9a is a multipotent regulator of gene expression either causing gene silencing by histone methylation or gene activation by recruiting partner molecules on the chromatin.^{139,140} (Figure 10B)

G9a is responsible for reversible mono- and dimethylation of histone 3 lysine 9 (H3K9me1 or H3K9me2) and is predominantly found in a heterodimer complex with the KMT G9a-like protein (GLP). Methylated H3K9 is recognized by the heterochromatin protein 1 (HP1) and attracts DNMTs leading to transcriptional silencing.¹⁴¹ Emerging evidence illustrates that G9a has wide-ranging cellular functions comprising developmental processes, pluripotency, cellular differentiation and cell cycle regulation¹⁴⁰. For example, G9a is essential for the repression of developmental genes, the determination of cell specification and the maintenance of T-cell homeostasis¹³⁹.

Several studies revealed that G9a is upregulated in many cancers such as esophageal squamous cell carcinoma, hepatocellular carcinoma, aggressive lung cancer, brain cancer, multiple myeloma, and aggressive ovarian carcinoma. Patients with high levels of G9a show poor prognosis in these cancer entities. It could also be found a direct correlation between elevated G9a expression with higher methylation level causing inactivation of TSGs. For example, in breast cancer G9a overexpression leads to the repression of the metastasis suppressor genes desmocollin 3 (DSC3) and mammary serine protease inhibitor (MASPIN).¹³⁹ A G9a knockout (KO) mouse model of AML showed a significant delay of disease progression that was connected to the methyltransferase activity of G9a and its interaction with the leukemogenic TF HoxA9.¹⁴² Several studies revealed that inhibiting G9a expression decrease cancer cell proliferation¹⁴³, delays disease progression¹⁴² and reduces tumor metastasis¹⁴⁴.

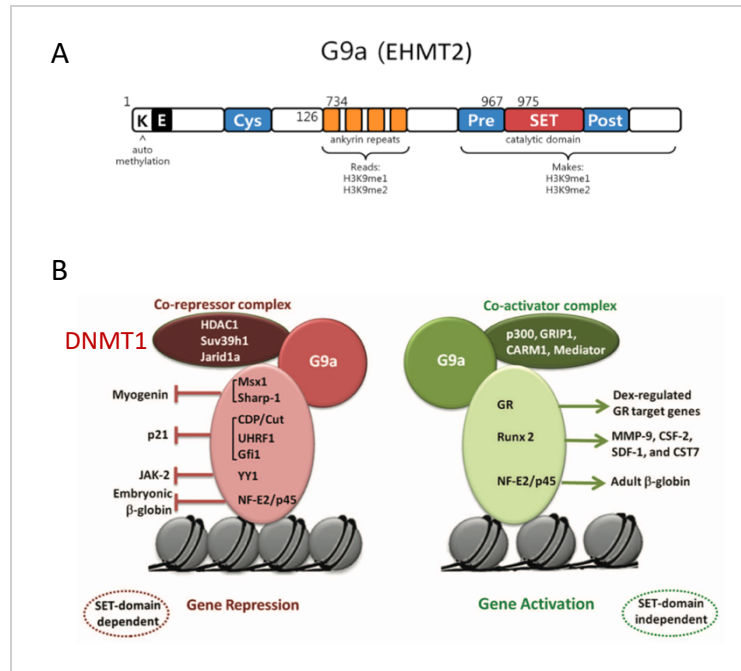


Figure 10: G9a is a multipotent regulator of gene expression.

(A) The gene G9a contains an automethylation region, ankyrin repeats and the catalytically active SET domain.¹³⁹ (B) Besides histone methylation, G9a also interacts with many molecules (e.g. DNMT1) causing gene repression or activation.¹⁴⁰

4.3.4 Cross-talk of DNMTs and KMTs

Gene regulation and genetic integrity are tightly regulated by many different types of epigenetic modifiers and molecules sensing epigenetic marks. Interestingly, recent studies have been gathering more and more evidence that these epigenetic modifications do not work separately from each other but are rather interrelated.

Specifically, the link between DNA methylation and histone modifications is mediated by a group of proteins with methyl-DNA binding activity such as methyl CpG binding protein 2 (MeCP2), methyl-CpG binding domain protein 1 (MBD1) and Kaiso (Zinc finger and BTB domain containing protein 33, ZBTB33). These DNA methylation binding proteins recognize methylated promoters causing the recruitment of other proteins including HDACs and HMT,^{74,145,146} for example, MeCP2 interacts with the HMT Suv39h1/2 triggering H3K9me.¹⁴⁷ These findings suggest that DNA methylation does not only act independently of other epigenetic processes but also through histone modifications. In general, it was shown that methylation of H3K4 (gene activation mark) is inhibited by DNA methylation while H3K9 methylation (gene repression mark) stands in linear correlation with DNA methylation.^{148,149}

In embryonic cells, a complex of enzymes including G9a and histone deacetylases are recruited which leads to the silencing of octamer-binding TF 3 and 4 (Oct-3/4), a TF important for

Introduction

embryonic development. Subsequently, DNMT3A and DNMT3B are recruited to the site of the promoter of Oct3/4 catalyzing *de novo* DNA methylation.¹⁵⁰

Another HMT called Suv39h1/2 mediates H3K9 trimethylation at the pericentric heterochromatin which seems to be required for the establishment of DNA methylation. This histone mark is bound by HP1 followed by an interaction with DNMT3A/B and DNA methylation at the H3K9-methylated heterochromatin.¹⁵¹

The interaction of the maintenance DNA methyltransferase DNMT1 with G9a is associated with the recruitment of UHRF1 (ubiquitin like with PHD and ring finger domains 1) and the H3K9me2/3 binding factor HP1. UHRF1 is known as a DNMT1 co-factor that binds preferentially to hemi-methylated DNA.^{152,153,154,155} Inhibition of DNMT1 and G9a reduces both DNA and H3K9 methylation levels, reactivates TSGs and inhibits cancer cell proliferation^{156,157}. (Figure 11)

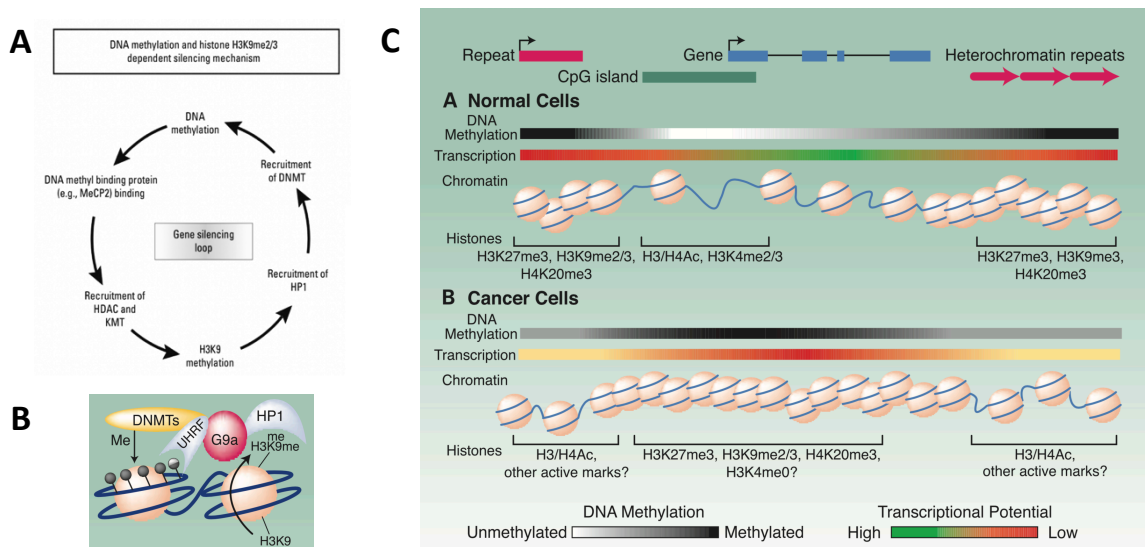


Figure 11: Gene downregulation by a cross-talk between DNA methylation and H3K9me2/3.

(A) DNA methylation is strongly associated with H3K9me2/3 directly by their epigenetic writers and indirectly through other proteins (DNA methyl binding proteins e.g. MeCP2 or heterochromatin protein HP1). **(B)** Physical interaction of G9a with DNMT1 is mediated by HP1 and the cofactor UHRF1 leading to a coordinately regulation of H3K9me2 and DNA methylation during DNA replication. **(C)** A dysregulated crosstalk between DNA and histone methylation can contribute to the development of cancer cells by changing the structure of hetero- and euchromatin and disturbing gene expression.^{158,154}

In conclusion, abnormal epigenetic patterns in cancer including MDS and AML play an important role for the disease progression. Therefore, targeting dysregulated epigenetic modifiers provides a very promising therapeutic approach for MDS and AML patients that is explained in the following chapter.

4.4 Therapy of MDS and AML patients

Hematologists or oncologists decide which therapy fits best to MDS and AML patients according to the patient's comorbidities as well as the biological/molecular assessment (e. g. blast count, cytogenetic and molecular abnormalities) of their disease (see chapter 4.2.1 and 4.2.2). Risk categories based on prognostic scoring determine the therapeutic approaches.

4.4.1 Overview of therapeutic strategies for MDS patients

Severity of the disease MDS is defined by the type of cytopenia, the bone marrow blast count, and cytogenetic aberrations. Based on the clinical findings, MDS patients are referred to lower-risk or higher-risk groups.^{159,160}

First-line therapy of lower-risk MDS patients includes erythropoietin (EPO) and thrombopoietin (TPO) analogues to treat common symptoms like anemia and thrombocytopenia^{161,162}. Younger patients that often show an activated immune response durably benefit from immunosuppressive therapy. Other treatment options of lower-risk MDS patients are inhibiting overactive transforming growth factor beta 1 (TGF- β) signaling and using vitamin C for MDS patients with mutated TET2 gene.^{163,164} Lenalidomide is approved in Europe for lower-risk MDS patients with a 5q deletion and facilitates ubiquitination and degradation of specific targets, which are important for the survival of malignant cells¹⁶⁵.

Higher-risk MDS patients show beneficial effects when treated with the inhibitor of the anti-apoptotic protein BCL-2 (B-Cell Leukemia/Lymphoma 2) called venetoclax¹⁶⁶ or immune checkpoint inhibitors that reverse immune system evasion of malignant cells¹⁶⁷. Other inhibitors recognizing janus kinase 1 and 2 (JAK1/2)¹⁶⁸, FLT3 as well as the BET (bromodomain and extraterminal) protein are applied to higher-risk MDS patients in clinical trials. Intensive chemotherapy and stem cell transplantation are used for high-risk patients too.¹⁶⁰ Moreover, DNMT inhibitors (DNMTi) including azacitidine (AZA, Vidaza) and decitabine (DAC, Dacogen) are approved by the Food and Drug Administration (FDA) and the European Medicine Agency (EMA) to treat higher-risk MDS patients¹⁶⁹. To improve the bioavailability of decitabine, a combination of decitabine and cedazuridine, a cytidine deaminase inhibitor is applied to patients¹⁷⁰. (see chapter 4.4.3)

4.4.2 Overview of therapeutic strategies for AML patients

Based on individual clinical and molecular information of AML patients, the first phase of treatment of standard chemotherapy so called “induction” therapy is applied to achieve complete remission with preferably no measurable residual disease¹⁷¹. Standard induction therapy follows the 7+3 regimen which means a continuous infusion of the chemotherapeutic cytarabine over 7 days with the addition of an anthracycline, typically daunorubicin, daily for the first 3 days. AML patients with favorable and intermediate risk based on their cytogenetics and molecular status have shown a complete response in up to 80 % or 50-60 % of the cases, respectively. However, only 40 % of patients with an adverse risk disease benefit of this treatment.¹⁷²

Additional targeted therapy to traditional 7+3 induction chemotherapy has been shown to improve patient’s outcome. Typical drugs for targeted therapy are gemtuzumab ozogomycin, which is a monoclonal antibody against CD33¹⁷³, or midostaurin being a tyrosine kinase inhibitor active in patients with a FLT3 mutation.¹⁷⁴ Decitabine and azacitidine have also shown efficacy in elderly patients with AML.¹⁷⁵ (see chapter 4.4.3)

Further treatment is called consolidation (post-remission therapy) which aims to prevent relapse of the disease. Treatment strategies to reach this goal are cytotoxic chemotherapies with or without targeted therapy or allogenic hematopoietic stem cell transplantation (Allo SCT) determined by unique risks and benefits provided by each treatment arm.¹⁷⁶

Allo SCT, a process by which stem cells are obtained from a donor other than the recipient, is applied to treat chemo-refractory MDS and AML patients by restoring normal hematopoiesis and is considered to be “last resort” therapy. By Allo SCT, the risk of relapse can be reduced while the risk of non-relapse mortality is increased. Non-relapse mortality can be caused by therapy itself or morbidity due to chronic graft versus host disease, secondary malignancies or infections from chronic immunosuppression.¹⁷⁷

4.4.3 Azanucleosides for the treatment of MDS and AML

Targeting proteins involved in epigenetic machinery represents a valuable alternative to traditional chemotherapy in AML and MDS, so far particularly in elderly and/ or medically not-fit patients.

The azanucleosides (AZN) DAC and AZA reverse DNA methylation by inhibiting DNMTs and thereby triggering the re-programming of tumor cells.^{178,179} After their cell uptake mediated by different nucleoside transporters, AZN are intracellularly metabolized and incorporated into DNA as cytidine substitutes during cellular replication (S-phase dependent drugs). DAC exclusively incorporates into DNA whereas AZA only at a rate of 10-20% into DNA, since the majority of AZA incorporates into RNA. At relatively low doses, these nucleoside-analogs are recognized and irreversibly bound by DNMT1 inducing a so called “suicide complex”, which undergoes

proteasomal degradation. The resulting DNA hypomethylation can restore gene transcription, in particularly TSGs involved in apoptosis, DNA repair, differentiation, and angiogenesis.¹⁸⁰ Recent publications also describe their impact on the immune response through activation of endogenous retroviruses^{181,182}. Despite convincing evidence of a beneficial outcome for MDS and AML patients, these FDA-approved hypomethylating agents have also two crucial limitations.

One limitation of these cytidine analogs is their short half-life of 35-40 min in the blood stream of patients, in contrast to about 10h in buffer at 37 °C and neutral pH. Reason for the short half-life is the activity of the cytidine deaminase that rapidly inactivates DAC and AZA.

The occurrence of resistance in patients is another drawback. One group of patients do not show any improvements after 4-6 cycles of treatment (primary resistance) and the second group initially responds but relapses after a couple of months (secondary resistance). Unfortunately, the exact mechanism has not been elucidated so far and more investigations are needed to improve the potential of nucleoside-based DNMTi in MDS and AML.

One promising direction is the development of reversible, non-nucleoside molecules targeting DNMTs and other epigenetic modulators without incorporating into the DNA, which avoids the change of the DNA sequence that might induce irreversible mutations.

4.4.4 Dual inhibition of DNMT1 and G9a by a reversible, first-in-class dual inhibitor

MDS and AML patients with poor-prognosis show clinical benefits when treated with DAC or AZA by reversing critical epigenetic events driving the cancer phenotype. Additionally, other inhibitors for epigenetic modifiers such as G9a, a histone lysine methyltransferase, are under investigations for drug development. As mentioned previously (see chapter 4.3.3.2), Overexpressed G9a seen in many tumors is associated with transcriptionally silencing of TSGs as well as tumor metastasis, increased proliferation, and disease progression.¹⁸³ Intriguingly, G9a and DNMT1 physically interact with each other to coordinate DNA and histone methylation during cell division reinforcing their repressive activity of gene transcription¹⁵³. (see chapter 4.4.3) Therefore, a combinational blockage of both enzymes could counteract their dysregulated activity and enhance the reprogramming of the transcriptome. And in fact, single or combinational treatments of an AML cell line (OCI-AML2) by inhibitors for G9a (A-366) and DNMT1 (DAC) induced a reduction of cell growth. A simultaneous inhibition of G9a and DNMT1 showed a more pronounced, synergistic effect on the proliferation of leukemia cells.¹⁸⁴

Recently, Jose-Eneriz et al. designed and discovered new first-in-class reversible dual small molecule inhibitors against G9a and DNMTs as an improved approach in cancer therapeutics.¹⁸⁴

The new dual inhibitors do not rely on DNA incorporation for activity as AZA and DAC, which

Introduction

implies many advantages over the conventional DNMTi. In a panel of human cancer cell lines, it could be shown that DAC had a 1000-fold variability of potency due to different incorporation of DAC into DNA. Applying non-incorporating compounds targeting DNMTs directly would offer a well-defined therapeutic window with optimal potency for DNA demethylation. Furthermore, it is assumed that DAC- and AZA-resistant tumor cells block the import, metabolization, and incorporation into DNA/RNA, which would be circumvented by non-nucleoside inhibitors.¹⁸⁵

Jose-Eneriz et al. developed substrate-competitive inhibitors of G9a and DNMT directing the substrate-binding groove (H3 and DNA, respectively) but not the SAM-binding pocket. (Figure 12) Furthermore, these compounds are highly selective against their specific targets and also inhibit DNMT3A, DNMT3B, and GLP. The effective dose is in the nanomolar (nM) range similar to their reference compounds for G9a (BIS-01294 and UNC0638) and DNMT (AZA and DAC). In addition, ADME studies (absorption, distribution, metabolism and excretion properties), cardiovascular safety and toxicity analyses lead to their multifactorial optimization.

With their lead compound CM-272, they could show an inhibition of cell proliferation and promotion of apoptosis in different hematological neoplasia including AML and ALL. CM-272 also induced interferon-stimulated genes, immunogenic cell death and prolonged survival of xenograft models of AML and ALL.¹⁸⁴ Further functional investigations of CM-272 were done in hepatocellular carcinoma (HCC) and bladder cancer. This compound inhibited the metabolic adaption of HCC cells to hypoxia, induced differentiated phenotype in HCC and fibrogenic cells and reactivated the metabolic tumor suppressor gene (TSG) fructose-1,6-bisphosphatase (FBP1), which is known to be transcriptionally silenced in HCC.¹⁸⁶ In bladder cancer, CM-272 caused apoptosis and immunogenic cell death¹⁸⁷.

In summary, a reversible inhibition of DNMTs and G9a could be an alternative therapeutic approach for MDS and AML patients that suffer from the drawbacks of the conventional DNMTi AZA and DAC.

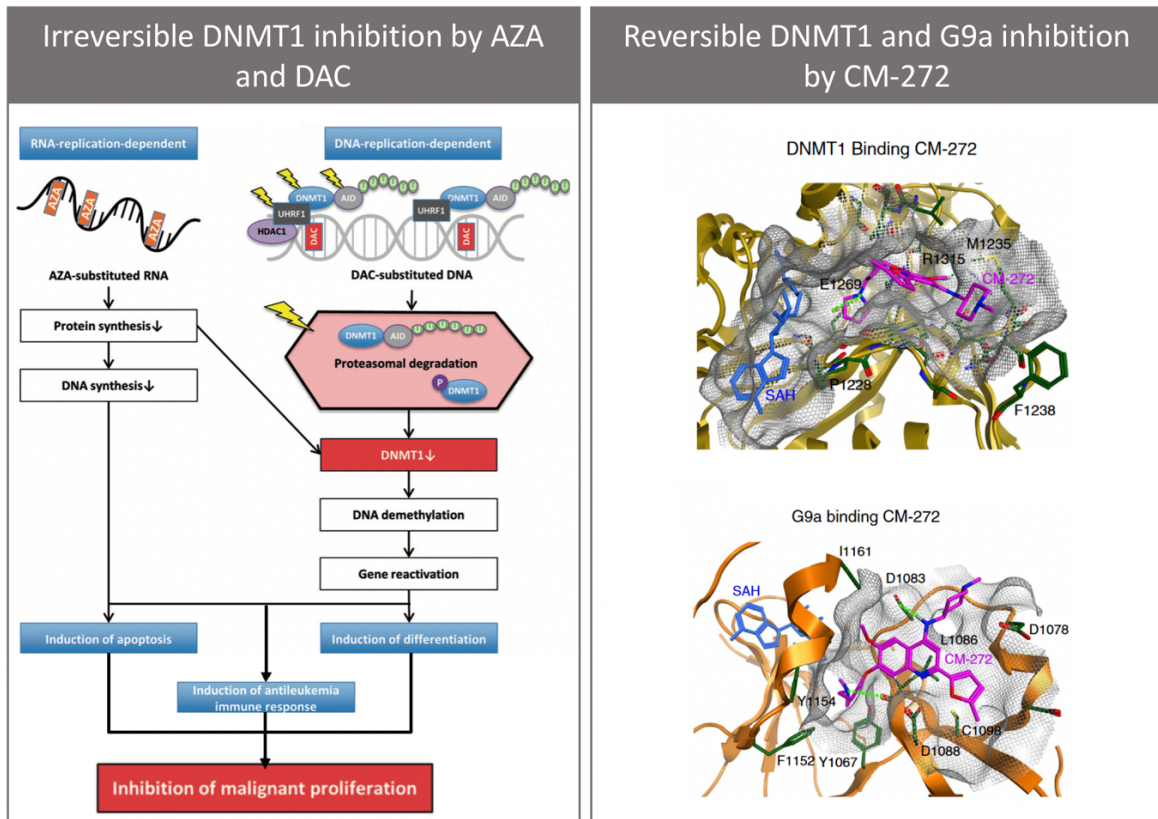


Figure 12: DNMTi AZA and DAC versus dual inhibitor CM-272.

Irreversible nucleoside-analogs, AZA and DAC incorporate into RNA or DNA, and thereby inhibit DNMT1 and mediate DNA demethylation. It is known that these drugs cause gene reactivation and inhibit malignant proliferation. (left picture modified from Pleyer et al. ¹⁸⁸) CM-272, a new compound that dually inhibit DNMT1 and G9a by reversible binding of both enzymes could be used as a promising alternative therapeutic strategy to treat MDS and AML patients.¹⁸⁴

4.5 Aim of the PhD thesis

The goal of this study is to identify AML-specific vulnerabilities that can be targeted by DNMT/KMT inhibitors in order to understand the molecular and functional consequences of therapeutic applications. Specifically, the aim is to investigate the effect of the reversible DNMT/G9a dual inhibition by the first-in-class small molecule CM-272 on various MDS/AML *in vitro* models and primary human AML cells with a heterogenous mutational background. Furthermore, mechanisms of the CM-272-specific anti-tumor effects should be analyzed by molecular biological methods including RNA sequencing. In addition, a recombinant AML reporter cell line should be generated as a screening tool for epigenetic drugs. Finally, the potential to reactivate an epigenetically silenced TSG by CM-272 compared to the conventional DNMTi decitabine should be examined with the new AML reporter cell line.

5 Material and Methods

5.1 Equipment

Table 3: General equipment.

Type	Model	Supplier
Aspirator	N2400-9000	Starlab
Autoclave	Systec V-100	Systec
Automated cell counter	Countess II FL	Thermo Fisher Scientific
Bacteria Shaker	Certomat SI	Sartorius
Biological safety cabinet	NU-440-601E	NuAire
	HERAsafe 12	Heraeus
	HERAsafe 18	Heraeus
Cell imaging system	EVOS FL Imaging System	Thermo Fisher Scientific
Centrifuge	Megafuge 1.0 R	Heraeus
Counting chamber	Countess II FL Hemacytometer	Thermo Fisher Scientific
Cytocentrifuge	Shandon Cytospin 4	Thermo Fisher Scientific
Erlenmeyer flasks	Duran 500 ml	DWK Life Science
Fluorometer	Qubit4	Thermo Fisher Scientific
Flow Cytometry	BD FACSCanto II	BD Biosciences
	BD LSR II-HTS	BD Biosciences
Freezer (-20°C)	Premium NoFrost	Liebherr
Freezer (-80°C)	Forma™ 900 Series	Thermo Fisher Scientific
Freezing container	CoolCell LX (1°C/min)	Corning
Fridge (4 °C)	Premium	Liebherr
Fridge-Freezer (4°C, -20°C)	Comfort NoFrost	Liebherr
Fume hood	2-543-GAND	Köttermann Systemlabor
		Thermo Fisher
Gel documentation chamber	UV solo TS	Biometra
Glass storage bottles	Kimax (500 ml, 1000 ml)	DWK Life Sciences
Heating block	Dry Bath System	Starlab
Horizontal electrophoresis system	Mini-Sub Cell GT	Bio-Rad
Ice flake machine	AF10	Scotsman

Material and Methods

Incubator shaker	Signature Incubating Rocker	VWR
Incubator with CO ₂ supply	HERAcell 150	Thermo Fisher Scientific
	HERAcell 240	Thermo Fisher Scientific
Inverted microscope	Primovert	Zeiss
Light cube	DAPI LED Cube	Thermo Fisher Scientific
	GFP LED Cube	
	Texas Red LED Cube	
Liquid nitrogen tank	ESPACE 151 GAZ	Air Liquide
Luminex instrument	Luminex Magpix	Luminex
Magnetic separator	MidiMACS Separator (columns)	Miltenyi Biotec
	DynaMag (1.5 ml)	Dynal
Magnetic stirrer	Hei-Mix L	Heidolph Instruments
Magnetic stirrer with heating	N2400-3010	Starlab
Magnetic stirring bars	∅ 6 mm (PTFE)	neoLab
MassARRAY	Sequenom, MALDI-ToF mass spectrometry	Agena
Measuring cylinders	250 ml, 500 ml, 1000 ml	Vitlab
Microliter centrifuge	Biofuge Fresco	Heraeus
	Heraeus Fresco 17 Centrifuge	Thermo Fisher Scientific
Microplate reader	FLUOstar Omega	BMG Labtech
Microscope	Primovert	Zeiss
Microvolume UV-Vis spectrophotometer	NanoDrop One	Thermo Fisher Scientific
Microwave	R-26ST-A	Sharp
Mini centrifuge	SU1550	Sunlab
Mini vortex mixer	SU1900	Sunlab
Monitor	U32R594CWU	ALSO/ Zehnbaauer
Multichannel pipette	8 and 12-channel pipette (10- 300 µL)	Starlab
Nucleofector	Nucleofector 2b	Lonza
Objectives	4x, 10x, 20x, 40x, 60x, 100x	Thermo Fisher Scientific
pH electrode	LE409	Mettler Toledo
pH meter	FiveEasy	Mettler Toledo

Material and Methods

Pipettors	Pipetus PipetBoy2	Hirschmann Laborgeräte Integra
Power supply for blotting and electrophoresis	PowerPac Basic	Bio-Rad
Precision balance	EW 620-3NM	Kern
Pyrosequencer	Pyrosequencer Pyromark Q96	Qiagen
Real-time PCR system	QuantStudio 3	Applied Biosystems (Thermo Fisher)
Refrigerator (4°C)	Economy	Liebherr
Rocker	IKA	Th. Geyer
Rotator mixer	RM-Multi 1	Starlab
Scoops	6 ½ inch	Sigma-Aldrich
Single channel pipettes	ErgoOne	Starlab
Thermal Cycler	T100 Thermal Cycler Biometra T3	Bio-Rad Biometra
Tube roller	N2400-7010 SRT9	Starlab Stuart Equipment
Vacuum Prep Tool	Pyrosequencing Vacuum Prep Tool	Qiagen
Vertical electrophoresis and clotting system	Mini-PROTEAN Tetra Cell -Mini Trans Blot Cell -Color-coded cassettes -electrodes	Bio-Rad
Vortex Mixer	VF2	Janke & Kunkel IKA Labortechnik
Water bath (large)	F12-ED Refrigerated/ Heating Circulator	Julabo
Water bath (small)	SUB Aqua Pro 5 L	Grant
Water purification system	Astacus	membraPure
Western blot and gel documentation system	iBright CL1000 Imaging System	Thermo Fisher Scientific
Western blot foam pads	Foam pads	Biorad

5.2 Consumables

Table 4: Consumables.

Type	Model	Supplier
3 ml syringe	3 ml Syringe, sterile, individual pack	Santa Cruz
96-well plates for IC50	Black 96-well clear F-bottom plates	Greiner Bio One
Blunt end needles	Blunt End Needles 16 g	Stem Cell Technologies
Aluminum foil	Rotilabo	Carl Roth
Aspirating pipettes	Falcon (2 ml)	Corning
Cardboard boxes for freezers	81 place Cardboard boxes for freezers	Sigma
Cartridge	PyroMark Q24 Cartridge for pyrosequencing	Qiagen
Cell culture flasks with filter cap	CytoOne (75 cm ² , 225 cm ²)	Starlab
Cell culture plates (suspension and adherent)	Cellstar (96 Well, 24 Well, 12 Well, 6 Well) Meniscus-free 6-well plates	Greiner Bio-One StemCell technologies
Conical centrifuge tubes	Falcon (15ml, 50 ml)	Corning
Cord blood collection bags	Cord blood collection bags	Macopharma
Counting chamber	Countess II FL Hemacytometer	Thermo Fisher Scientific
Counting chamber slides (disposable)	Countess Counting Chamber Slides	Thermo Fisher Scientific
Cryovials	2.0 ml with internal threaded cap	Corning
Filter Paper for western blot	Filter Paper 8x10.5cm	Thermo Fisher Scientific
Filtration bottles	CytoONE Bottle Top Filtration Unit (250 ml, 500 ml)	Starlab
Glass bottles	100 ml, 250 ml, 1000 ml	Neolab
Gloves	Starguard Nitril Gloves Small	Starlab
Graduated Pipettes, sterile pack	5 ml, 10 ml, 25 ml, 50 ml	Greiner
Magnetic bead column	LS + Columns	Miltenyi

Material and Methods

Microreaction strips	Fast Reaction 8 strip caps	Thermo Fisher Scientific
Microreaction tubes	1.5 ml, 2 ml	Eppendorf
	0.6 ml	Starlab
Microcentrifuge tubes	Axygen (1.7 ml)	Corning
Parafilm	4" x 250'	American National Can
PCR plates	- 96well PCR plate for pyrosequencing	Applied Biosystem
	- Sample plate low for pyrosequencing	Qiagen
	- MicroAmp Fast 96-Well Reaction Plate (0.1 ml) for qPCR	Applied Biosystems (Thermo Fisher)
PCR tubes	0.2 ml 12-Strip PCR tubes	Starlab
Pipette tips	TipOne (10 μ l, 200 μ l, 1000 μ l)	Starlab
Pipette filter tips	TipOne Filter Tip (10 μ l, 20 μ l	Starlab
	200 μ l, 1000 μ l)	
Pipetting reservoirs	25 ml	Argos Technologies
Polystyrene round-bottom tubes with 35 μ L cell strainer cap	Falcon (5ml)	BD
Pre Stained Ladder	iBright Pre Stained Ladder	Thermo Fisher Scientific
PVDF transfer membrane	0.45 μ m, 26.5 cm x 3.75	Thermo Fisher Scientific
SepMate PBMC Isolation Tubes	SepMate-50 tubes	StemCell Technologies
Serological aspirating pipettes	Serological aspirating pipettes, sterile, no filter	Greiner
Sterile filter units	Millex-HV (0.45 μ m, 33 mm)	Merck Millipore Ltd.
Smart dish for CFU	SmartDish (6-well plates)	STEMCELL Technologies
Strainer	40 μ M, 70 μ M, 10 μ M	Neolab, Greiner
Syringe needles	BD Microlance 3	BD
Syringes	Norm-Ject (10 ml)	Henke Sass Wolf
Transfer pipettes	Falcon (3 ml)	Corning
Weighing boats	89 mm x 89 mm x 25 mm	neoLab
Weighing paper	Whatman (B-2, 3 inch x 3 inch)	GE Healthcare
Western Blotting filter paper	8 cm x 10.5 cm	Thermo Fisher Scientific

5.3 Chemicals and Reagents

Table 5: Chemicals and reagents.

Product	Supplier
ACK Lysis Buffer	Thermo Fisher (Gibco)
Agarose NEEO Ultra-Quality	Carl Roth
Ammonium persulfate (APS)	Bio-Rad
Ampicillin	Sigma-Aldrich
Annealing buffer for pyrosequencing	Qiagen
BD FACS Clean Solution	BD Bioscience
Binding buffer for pyrosequencing	Qiagen
β -Mercaptoethanol	Carl Roth
Bovine Serum Albumin (BSA)	Sigma-Aldrich
Caspase Glo 3/7 Assay	Promega
Cell Titer Glo Cell Viability	Promega
4',6-diamidino-2-phenylindole (DAPI)	Carl Roth
Dimethyl sulfoxide (DMSO)	Sigma-Aldrich
6X DNA Loading Buffer	Thermo Fisher Scientific
DNase I	Th.Geyer
dNTPs Mix (100 mM)	Thermo Fisher Scientific NEB
DPBS	Thermo Fisher (Gibco)
Ethanol (70 %) for pyrosequencing	Applichem
Ethanol	Carl Roth
FACSFlow™	BD Bioscience
FBS Heat Inactivated	Thermo Fisher (Gibco)
Ficoll	Sigma-Aldrich
GelGreen Nucleic Acid Gel Stain	Biotium
GeneRuler 100 bp Plus DNA Ladder, 100 - 2000bp	Thermo Fisher Scientific
Giemsa	Carl Roth
Glycerol	Sigma-Aldrich
4X Laemmli Sample Buffer	Bio-Rad
LB-media (Bacto Yeast Extract/ Bacto Tryptone/ Bacto Agar)	BD Bioscience
May-Grünwald staining	Carl Roth

Material and Methods

Methanol	Thermo Fisher Scientific
20X MOPS Running Buffer	Biorad
Optimem	Gibco
N,N,N',N'-Tetramethylethylenediamine (TEMED)	Bio-Rad
No Stain Protein Labeling Reagent	Thermo Fisher Scientific
Nuclease-free water	Qiagen
PageRuler Plus Prestained Protein Ladder, 10-250 kDa	Thermo Fisher Scientific
Penicilin/ Streptomycin (Pen/Strep)	Thermo Fisher (Gibco)
Pierce ECL Western Blotting Substrate	Thermo Fisher Scientific
Pierce Universal Nuclease for Cell Lysis	Thermo Fisher Scientific
Pierce RIPA Buffer	Thermo Fisher Scientific
Phosphate buffered saline (PBS) sterile	Sigma-Aldrich
Protease inhibitor cocktail	Cell Signaling
Rinse Solution	BD Bioscience
RNaseZap	Sigma-Aldrich
Sepharose beads for pyrosequencing	GE Healthcare
Shutdown Solution	BD Bioscience
Skim milk powder	Serva
Sodium chloride (NaCl)	Carl Roth
Sodium dodecyl sulfate (SDS)	Carl Roth
Sodium hydroxide (NaOH)	Carl Roth
NaOH denaturation buffer for pyrosequencing	Qiagen
10X TBE Electrophoresis Buffer	Thermo Fisher Scientific
Tris(hydroxymethyl)aminomethane (Tris)	Carl Roth
Tris(hydroxymethyl)aminomethane- hydrochloride (Tris-HCl)	Carl Roth
Trypan Blue Stain, 0.4%	Thermo Fisher Scientific
Tween 20	Carl Roth

5.4 Prepared buffer solutions

Table 6: Prepared buffer solutions.

Buffer type	Compositions
Blotting buffer (10X stock)	480 mM Tris 390 mM glycine 0.375 % SDS 950 ml dH ₂ O Titrated to pH 9.19 with 10 M NaOH Filled to 1000 ml with dH ₂ O
Blotting buffer (1X working solution)	100 ml 10X blotting buffer 200 ml methanol 700 ml dH ₂ O
Blocking buffer	5 % skim milk powder in TBS-T 5 % BSA in TBS-T
TBS (10X stock)	152 mM Tris-HCl 46 mM Tris 1.5 M NaCl Filled to 1000ml with H ₂ O
TBS-T (1X working solution)	100 ml 10X TBS 1 ml Tween 20 899 ml dH ₂ O
FACS buffer	PBS 3 % FBS 2 mM EDTA
RIPA lysis buffer	1x Protease inhibitor cocktail 0.01 Nuclease RIPA buffer

5.5 Kits

Table 7: Kits.

Product	Supplier
Apoptosis, DNA damage, Cell Proliferation kit	BD Biosciences
CD34 MicroBead Kit UltraPure, human	Miltenyi Biotec
Cell fractionation kit	Cell Signaling
Cell line Nucleofector Kit V	Lonza
DNA purification SPRI Magnetic Beads kit	Canvax Biotech
EZ DNA methylation kit	Zymo Research
FastStart High Fidelity PCR System	Sigma-Aldrich
Higher Purity DNA Purification SPRI Magnetic Beads	Biotrend/Canvax Biotech
Hot Start Taq DNA Polymerase	New England Biolabs
Human Custom ProcartaPlex 16-plex	Thermo Fisher Scientific
Mix2Seq kit-overnight	Eurofins Genomics
NEBuilder HiFi DNA Assembly Cloning Kit	New England Biolabs
NucleoSpin Gel & PCR clean-up kit	Macherey-Nagel
NucleoSpin Tissue, Mini kit for DNA from cells and tissue	Macherey Nagel
OneTaq DNA polymerase	New England Biolabs
Pierce BCA Protein Assay Kit	Thermo Fisher Scientific
PowerUp SYBR Green Master Mix	Thermo Fisher Scientific
PureLink RNA Mini Kit	Thermo Fisher (Invitrogen)
Q5 High-Fidelity DNA Polymerase	New England Biolabs
QIAprep Spin Miniprep kit	Qiagen
Qubit RNA Broad Range	Thermo Fisher Scientific
qScript cDNA Synthesis Kit	Quantabio
Shandon Kwik-Diff	Thermo Fisher Scientific
SuperSignal West Pico PLUS Chemiluminescence Substrate	Thermo Fisher Scientific
Surveyor Mutation Detection Kit for Standard Gel Electrophoresis	Transgenomic Inc Omaha, NE, USA
TGX FastCast Acrylamide kit	Bio-Rad

5.6 Prokaryotic cell line

Table 8: Prokaryotic cell line.

Prokaryotic cell line	Supplier
NEB 10-beta Competent <i>E.coli</i> High Efficiency	New England Biolabs

5.7 Cytokines/ Inhibitors for cell cultivation

Table 9: Cytokines/ Inhibitor for cultivating MDS/AML cell lines and primary AML cells.

Cytokine/ Inhibitor	Manufacturer
SR1 (aryl hydrocarbon receptor inhibitor)	Biozol (Selleck)
Recombinant FLT3-L	Miltenyi Biotec/Tebu Bio (Peprotech)
Recombinant G-CSF	Peprotech
Recombinant GM-CSF	Peprotech
Recombinant IL-3	Peprotech
SCF	Miltenyi Biotec
EPO	Peprotech

5.8 Media

Table 10: Media.

Medium	Supplier
DMEM (1X) with Glutamax	Thermo Fisher Scientific (Gibco)
IMDM	Thermo Fisher Scientific (Gibco)
Methocult H4230	StemCell Technologies
RPMI 1640 with Glutamax	Thermo Fisher Scientific (Gibco)
Stem Span	Miltenyi Biotec

Table 11: Supplements for Methocult media for Colony Forming Unit (CFU) assay.

Methocult Media	
50 ng/ml	SCF
10 ng/ml	IL-3
10 ng/ml	GM-CSF
3 U/ml	EPO

5.9 Human eukaryotic cell lines

Table 12: Media composition of eukaryotic cell lines.

Culture media always contained 1 % Penicillin-Streptomycin (Pen-Strep).

Cell line	Culture medium	Cell type	Key Mutations	Reference
F-36P	RPMI + 20 % FBS + 10 ng/ ml GM-CSF	secAML	KMT2A TP53	189
K-562	RPMI + 10 % FBS	CML	BCR-ABL TP53	190
Kasumi-1	RPMI + 20 % FBS	<i>de novo</i> AML	AML1-ETO KIT TP53	191
KG1a	RPMI 1640 + 20% FBS	<i>de novo</i> AML	TP53 NRAS	192
MDS-L	RPMI + 10 % FBS + 40 ng/ ml GM-CSF	MDS	TP53 CEBPA NRAS	193
MOLM13	RPMI + 10 % FBS	secAML	MLL-AF9 FLT3 ITD KMT2A	194
NB4	RPMI + 10 % FBS	<i>de novo</i> AML	TP53 PML-RARA	195
OCI-AML2	RPMI + 10 % FBS	<i>de novo</i> AML	DNMT3A ^{R635W} FLT3 ^{A680V}	196
OCI-AML3	RPMI + 10 % FBS	<i>de novo</i> AML	DNMT3A ^{R882C} NPM1c	196
PC3	RPMI + 10 % FBS	prostate cancer	TP53	197
SKM-1	RPMI + 20 % FBS + 1 ng/ml GM-CSF	secAML	EZH2 TET2	198
THP-1	RPMI + 10 % FBS	<i>de novo</i> AML	NRAS TP53	199
UoCM1	90% McCoy's 5a + 10% FBS	<i>de novo</i> AML	KMT2A	200

5.10 Human primary AML samples

Table 13: Primary AML samples.

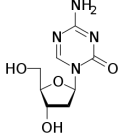
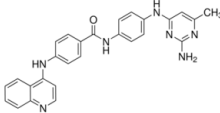
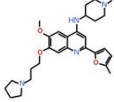
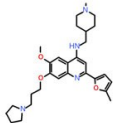
UPN #	Key mutations	Source
# 1	FLT3-ITD; NPM1c; DNMT3A ^{R882}	Bone marrow
# 2	FLT3-ITD; NPM1c	Bone marrow
# 3	FLT3-ITD; NPM1c	PBMC
# 4	FLT3-ITD; NPM1c; DNMT3A ^{R882}	PBMC
# 5	FLT3-ITD; NPM1c	Bone marrow

Table 14: Supplements for SpemSpan media for primary AML culturing.

StemSpan media	
1 %	Pen-Strep
1 μ M	SR1
100ng/ml	SCF
50ng/ml	FLT3-L
20ng/ml	IL-3
20ng/ml	G-CSF

5.11 Epigenetic drugs

Table 15: Epigenetic drugs.

Drug	Inhibition	Manufacturer
<p>Decitabine</p> 	<p>Cytosine-substitute</p> <p>Indirect DNMT</p>	<p>Sigma</p>
<p>SGI-1027</p> 	<p>Direct DNMT</p>	<p>Sigma</p>
<p>CM-272</p> 	<p>Direct DNMT and G9a</p>	<p>Axon Medchem</p>
<p>CM-579</p> 	<p>Direct DNMT and G9a</p>	<p>Hölzel Diagnostika</p>

5.12 Antibodies

Table 16: Antibodies for flow cytometry.

Antibody	Channel	Dilution	Experiment	Manufacturer
CD14	PE	1:400	differentiation	Biolegend
CD11b	APC	1:100	marker	Thermo Fisher Scientific
Cleaved PARP	PE	1:100	apoptosis, DNA	BD
H2AX (pS139)	APC (Alexa Fluor 647)	1:100	damage and	BD
BrdU	PerCP-C5.5	1:100	cell proliferation	BD

Table 17: Primary antibodies for western blot.

Prim. Antibody	Species	Dilution	Size	Manufacturer
DNMT1	rabbit	1:1000 in BSA	200 kDa	Cell Signaling
DNMT3A	rabbit	1:1000 in BSA	120 kDa	Cell Signaling
DNM3B	rabbit	1:1000 in BSA	96 kDa	Cell Signaling
G9a	rabbit	1:1000 in BSA	160 and 180 kDa	Cell Signaling
SFRP1	rabbit	1:1000 in BSA	35 kDa	Cell Signaling
cMYC	rabbit	1:2000 in milk	50-60 kDa	Proteintech
Total β -catenin	mouse	1:2000 in BSA	90 kDa	BD Bioscience
Active β -catenin	rabbit	1:1000 in BSA	90 kDa	Cell Signaling
NPM1c (mutant)	rabbit	1:500 in BSA	33 kDa	Thermo Fisher Scientific
β -tubulin	mouse	1:10,000 in milk	50 kDa	Sigma Aldrich
GAPDH	mouse	1:10,000 in milk	35 kDa	Thermo Fisher Scientific
Vinculin	rabbit	1:1000 in BSA	132 kDa	Cell Signaling
LaminB1	rabbit	1:1000 in milk	66-70 kDa	Proteintech

Table 18: Secondary antibodies for western blot.

Secondary antibody	Species	Dilution	Dilution buffer	Manufacturer
IgG-HRP-conjugate	Goat anti-mouse	1:3000	5% milk in TBS-T	Bio-Rad
IgG-HRP-conjugate	Goat-anti-rabbit	1:3000	5% BSA in TBS-T	Bio-Rad

5.13 Primers

Table 19: Primers for RT-qPCR.

Gene name	Primer pair	Sequence (5' – 3' direction)	Origin
b2M	Forward	CCAGCAGAGAATGGAAAGTC	AG Kühn
	Reverse	GATGCTGCTTACATGTCTCG	
WNT5A	Forward	CACCAGAGCAGACAACCTATTT	AG Guezuguez
	Reverse	CATCACAACACGGAGGAATCA	
DKK1	Forward	ATGCGTCACGCTATGTGCTGCC	AG Guezuguez
	Reverse	GACAGACCTTCTCCACAGTAACAACGCTG	
SFRP1	Forward	GAAATCTGAGGCCATCATTGAACATC	AG Guezuguez
	Reverse	GACAATCTTCTTGTCGCCATTTTC	
	Reverse	AGATCAGCTCCCCGACATACTCGCAG	
IFI6	Forward	TTCTCTCCTCCAAGGTCTAGTG	AG Guezuguez
	Reverse	CAAGTGAAGAGCAGCAGGTAG	
OASL	Forward	GACTGCGGAGCCCATCAC	AG Guezuguez
	Reverse	TCAGGCTCACATAGACCTCAG	
FOSB	Forward	GCCGAGTCTCAATATCTGTCTTCG	AG Guezuguez
	Reverse	CACGAAGGAACCGGGCATTTC	
EGR2	Forward	CTTTGACCAGATGAACGGAGTGG	AG Guezuguez
	Reverse	ATGGAGAAGTGGCCATGTAAGTG	
PBX3	Forward	CAAGTCGGA GCCAATGTG	AG Kühn
	Reverse	ATGTAGCTCAGGGAAAAGTG	
MEIS1	Forward	TCGCGCAGAAAAACCTCTAT	AG Kühn
	Reverse	CCAAGAGGGCTGGTCAGTTA	

Table 20: Primers for pyrosequencing.

Primer name	Sequence (5'-3' direction)	Sequence to analyze	Localization	T _m (°C)	Ref.
SFRP1.fw	GTTAGTAGTAAG	TTYGYGAYGTYGGGGTTGTT	chr8:413091	50	region from 201
	TTTAGGGTTGT				
SFRP1 Rv-Bio	CTTTTATCCCCAAA	TTYGTYGTTTTTYGYG	80-41309246		
	ATCCCTAAAAATTTA	YGYGTTTTGTYGTAAT			
SFRP1 Sq	GGTTTTGAGTTTTGTT	TTTAGGGATTTT			

T

Table 21: Primers for MassARRAY.

Primer name	Sequence (5'-3' direction)	Sequence to analyze	localization	Tm (°C)
SFRP1.fw	GTTTTATTTTGG GGTTTGGAGGTTT	Sequence in appendix	chr8:4116578 6-41167175	60
SFRP1.rv	ACAACAAACCAACA ACTAAATACCCCTACT			
LINE-1.fw	TTTATATTTTGGTATG ATTTTGTAG	TTTACATTTTGGCATGATTTT GCAGCGGCTGGTACCGTT GTTCCTTTCCATGTTTAGCG		56
LINE-1.rv	TTTATCACCACCAAAC CTACCCT	CTTCCTTCAGGAGCTCTTTTA GGGCAGGCCTGGTGGTGAC AAA		

Table 22: Primers for Surveyor assay.

Primer name	Sequence (5'-3' direction)	Tm (°C)
SFRP1-5'UTR-S1N.for	CAACGCTGGGGACTGCGCCTTTTG	68
SFRP1-exon1-S1N.rev	GGCAGCACCATCTTCTTGTAGCCCACG	

Table 23: Primers for molecular cloning.

Frag- ment	Primer name	Sequence (5' – 3' direction)	Tm (°C)	Size (bp)
F0/FL	F0/1-SFRP1-LHA.fw	CACCCAGCCCCGAGCGCCGCCTC	68	765
	F0/5-SFRP1-RHA.rv	GAGCCAGCGACACGGGTAGATGGG		
F1	F0/1-SFRP1-LHA.fw	CACCCAGCCCCGAGCGCCGCCTC	72	359
	F1-SFRP1-LHA.rv	GTTAGTAGCTCCGCTTCCGCTTGCCGAGCCCACG GCCAGAAGCGCC		
F2	F2-P2A-mCherry.fw	GGAAGCGGAGCTACTAACTTCAGCCTGCTGAAGC AGGCTGGAGACGTGGAGGAGAACCCTGGACCTA TGGTGAGCAAGGGCGAGGAGGAT	67	924
	F2-mCherry-SV40polyA.rv	GGAGCCTGGGGACTTTCCACACCATAAGATACAT TGATGAGTTTGGACAAACCACAAGTGAATGCAG TGAAAAAATGCTTTATTTGTGAAATTTGTGATGC TATTGCTTTATTTGTAACCATTATAAGCTGCAATAA ACAAGTTTTACTTGTACAGCTCGTCCATGCCGCC		
F3	F3-SV40prom.fw	GGTGTGGAAAGTCCCCAGGCTCC	67	348
	F3-SV40prom_puro.rv	CGCACCGTGGCTTGTACTCGGTCATTTTGC AAAAGCCTAGGCCTCCAAAAAAGCC		
F4	F4-puro.fw	ATGACCGAGTACAAGCCCACGGTGCGCC	71	740
	F4_puro-SV40PolyA.rv	AAGCTCACGTAGTCGTAAGTCAAGATAC ATTGATGAGTTTGGACAAACCACAAGTGAATGCAGTGA GAATGCAGTGAATAAATGCTTTATTT GTGAAATTTGTGATGCTATTGCTTTATTTGTAAC CATTATAAGCTGCAATAAACAAGTTTTAGGC ACCGGGCTTGCGGGTCATG		
F5	F5-SFRP1-RHA.fw	GAGTACGACTACGTGAGCTTCCAGTCGGAC	68	302
	F0/5-SFRP1-RHA.rv	GAGCCAGCGACACGGGTAGATGGG		

Table 24: Primers for sequencing of SFRP1_mCherry_puro construct in pcDNA TOPO-vector.

Primer name	Sequence (5' – 3' direction)
Seq-mCherry.p645.fw	CGTGGAACAGTACGAACGCGCCGAG
Seq-puro-p166.rv	GCGTGAGGAAGAGTTCTTGCAGCTCG
T7 promoter.fw	TAATACGACTCACTATAGGG
BGH.rv	TAGAAGGCACAGTCGAGG

Table 25: Primers for genotyping of the expected size for WT/KO/KI alleles of SFRP1.

PCR	Primer name	Sequence (5' – 3' direction)	Size
1	F0/1-SFRP1-LHA.for	CACCCAGCCCGCAGCGCCGCCTC	765 bp
	F0/5-SFRP1-RHA.rev	GAGCCAGCGACACGGGTAGATGGG	
2	F0/1-SFRP1-LHA.for	CACCCAGCCCGCAGCGCCGCCTC	757 bp
	mCherry.p669.rev	CTCGGCGCGTTCTGACTGTCCACGATGG	
3	seq.puro.p497.for	GCAACCTCCCCTTCTACGAGCG	673 bp
	F0/5-SFRP1-RHA.rev	GAGCCAGCGACACGGGTAGATGGG	

5.14 Templates and plasmids for molecular cloning

Table 26: Templates and plasmids for molecular cloning.

Templates	Usage	Kindly provided by/ purchased from
gDNA of OCI-AML3	Template for SFRP1	AG Guezguez
pJF001 plasmid (pRS41K-mCherry-sfGFP from Addgene)	Template for mCherry	AG Wölfel
pCMB-HmB plasmid	Template for SV40 prom	AG Schuppan/ Bockamp
pMX-puro-DEST plasmid	Template for puromycin	AG Wölfel
pcDNA™3.1/V5-His TOPO® TA plasmid	SFRP1_mCherry_puro construct inserted	Thermo Fisher Scientific

5.15 crRNAs

Table 27: crRNA candidates for HDR-based CRISPR/Cas9 editing of the SFRP1 gene.

crRNA name	Strand	Sequence (5'-3' direction)	PAM location (5'-NG ₃ ' in exon 1)
crRNA #1	+	GACATCGGCCCGTACCAGAGCGG	460
crRNA #2	+	AGTGTGACAAGTTCCCCGAGGGG	803
crRNA #3	-	GCTCACGTAGTCGTACTCGCTGG	407

5.16 Software

Table 28: Software.

Software	Purpose	Developer
EndNote X9	bibliographic management software	Clarivate
FlowJo	FACS analysis	BD Bioscience
Geneious	Molecular biology and sequence analysis	Geneious
GraphPad Prism	Graphing, statistical analysis	Biozol (Selleck)
iBright Analysis Software	Western blot analysis	Thermo Fisher Scientific
Microsoft Office	Word, Excel	Microsoft Corporation
QuantStudio Design & Analysis Software	RT-qPCR analysis	Thermo Fisher Scientific (applied biosystems)
Pyro Q-CpG 1.0.9 Software	Pyrosequencing	Qiagen

5.17 Cell biology

5.17.1 Cell culture of eukaryotic cells

5.17.1.1 Freezing and thawing of eukaryotic cells

Accumulation of alterations, outgrowth of clones within the population or contamination can occur due to extensive cultivation, which affects cell function. Therefore, a proportion of MDS/AML cells were cryopreserved during cell cultivation in order to have access to earlier cell passages. All MDS/AML cell stocks used in experiments were verified for cell authentication using SNP typing service (Multiplexion, DKFZ, Heidelberg). MDS/AML cells were washed in PBS and cryopreserved in 1 ml freezing media containing 90% FBS and 10% DMSO by a controlled-rate freezing system. Cryovials were inserted in freezing containers called CoolCell LX with a freezing

rate of 1 °C/ min. After one night at -80 °C, the cells were transferred to a liquid nitrogen tank for long-term storage.

For recultivation, cryovials were quickly thawed for ca. 2 min in a water bath at 37 °C. Subsequently, the cell solution was dissolved in 5 ml culture media for cell lines or 40 ml IMDM media + 100 µg/ ml DNase I for primary cells. After one centrifugation step at 1,500 rpm for 5 min, cells were resuspended in their specific media and cultivated. (Table 12)

5.17.1.2 Culturing of eukaryotic cells

All MDS/AML cell lines and primary cells were stored in cell culture suspension flasks or plates in an incubator at 37 °C and CO₂ content of 5 %. Depending on the cell line, cells were cultured in their culture media with a cell density between 0.1 – 3.0 Mio cells/ ml before the next passaging and media change. (Table 12) Passaging was done twice a week under sterile conditions in a safety cabinet. Briefly, cells were counted, split, washed in PBS and resuspended in new media or used for experiments.

5.17.1.3 Determination of cell number and cell viability

To determine the cell density and viability, cells were mixed with 4 % trypan blue, a dye that is absorbed by dead cells with disrupted cell membrane. 10-20 µl of the cell suspension was added either in a hemocytometer or in counting chambers. Blue stained, dead cells could be distinguished from transparent, live cells under a light microscope and manually counted. Cells within the four corner squares were counted and the mean value of the cell number was multiplied by the factor 10⁴ and the dilution factor to determine the cell concentration (cells/ml) of viable and dead cells. The automated cell counter Countess II FL measured the percentage and concentration of live and dead cells and included a dilution factor of 2. The required cell number was obtained by resuspending the cells into the appropriate volume of media and seeding into cell culture dishes.

5.17.1.4 Isolation of MNCs and HSPCs from umbilical cord blood

HSPCs can be obtained from different sources such as peripheral blood, umbilical cord blood or bone marrow. Due to higher frequency of HSPCs (0.1-0.5 %) in umbilical cord blood compared to peripheral blood with only 0.05-0.2 %²⁰², blood was collected in umbilical cord blood collection bags directly after a Cesarean-section in the Gynecology department, University Medicine Center Mainz. To isolate mononuclear cells (MNCs) and HSPCs, the Ficoll density centrifugation following the SepMate protocol was carried out. Additionally, 2-5 ml of ACK lysis buffer was added to the cell pellet, incubated at room temperature (RT) and frequently mixed for 20 min to remove erythrocytes.

CD34-depletion via magnetic separation was performed to obtain HSPCs from MNCs. Here, the CD34 MicroBead kit with LS columns from Miltenyi was used following the manufacture's instructions.

5.17.2 Drug treatment of cell lines and primary cells

Cell lines of MDS and AML were always seeded at a cell concentration of 0.5-1.0 Mio/ml in 96 well-plates, 6 well-plates or T25 cell culture flasks depending on the downstream experiment and the cell number that was needed. DAC was applied daily while SGI-1027, CM-272 and CM-579 only once on the day of cell plating when not stated differently.

Frozen aliquots of primary AML cells were thawed in IMDM, 20 % FBS and 1 µg/µl of DNase I. Only samples with a proportion of >80 % viable cells evaluated by 0.4 % trypan blue, were used for the CM-272 treatment. Cells were plated in a 12 well plate with a cell density of 1 Mio/ml in 2 ml StemSpan media supplemented with small molecules and cytokines. (Table 14) On the same day, the cells were treated with 30nM, 100nM, 300nM, 500nM, or 1000nM CM-272 or vehicle (DMSO) for 72 h.

5.17.2.1 Dose-response curve and IC50 determination of drugs:

Cells were plated in opaque-walled 96 well-plates at a density of 50,000 cells per well in 85 µl of media for DAC treatment or 95 µl of media for CM-272 treatment. On the day of plating, cells were treated with nine different concentrations that were serially diluted 2-fold from 0,039 µM to 10 µM and one vehicle control (DMSO). CM-272 was applied once and DAC daily for 72 h before the cell viability assay was carried out. CellTiter-Glo Luminescent Cell Viability Assay was performed according to the manufacturer's description. The luminescence was measured in the FLUOstar Omega microplate reader. Percentage of cell viability for each drug concentration was determined by normalizing treated samples to DMSO control. The IC50 values for each cell line and drug were computed by GraphPad Prism software.

5.17.3 Functional assays

5.17.3.1 Colony-forming assay

After 72 h incubation with CM-272, 10,000 viable primary patient cells and 500 viable cell line cells were plated in 1 ml Methocult in meniscus-free 6-well plates. Methocult was supplemented with IMEM and cytokines (Table 11) and 1% Pen/Strep. The assay was performed according to the manufacturer's description (StemCell Technologies). After another 8 days of culturing, colonies

(defined as an accumulation of > 10 cells) were counted. Images of colonies were captured using an EVOS M5000 imaging system with a 20x objective.

5.17.3.2 Morphological examination: Cytospins and stainings

Drug-treated primary AML patient samples and OCI-AML3 were harvested after 48 h and their phenotypical changes were investigated. After one PBS washing step, 100,000 cells were concentrated on glass slides by centrifugal force using a cytospin centrifuge with cytofunnels, filter cards and cytoclips. After 10 min air drying, samples were either wrapped in aluminum foil and stored at -20 °C until use, or directly stained. Primary cells were stained according to the Kwik-Diff kit instructions. Cell lines were incubated in the May-Grünwald staining for 4 min followed by a 4 % Giemsa staining for 4 min. Next, the cells were washed in AquaDest and dried overnight. Stained cells were sealed with a cover slip and mounting media. Pictures of cells were taken by the EVOS M5000 imaging system with 60x or 100x oil objectives.

5.17.3.3 Flow cytometry to investigate apoptosis, DNA damage, cell cycle, proliferation, and differentiation marker CD14 and CD11b

Flow cytometry, also called fluorescence-activated cell sorting (FACS), is a technology that is used for a multi-parametric analysis of single cells in solution. Flow cytometers provide lasers as light sources to generate both scattered and fluorescence light signals which are read by detectors. By converting them into electronic signals, cell populations can be analyzed and/ or purified based on their fluorescence or light scattering properties.²⁰³

Mature circulating monocytes are characterized by the expression of the surface marker CD14 and CD11b. To investigate their expression on OCI-AML3 after CM-272 treatment, flow cytometry was used. After 72 h treatment, 100,000 cells were harvested, counted and washed with PBS twice before they were incubated with the antibodies anti-CD14 and anti-CD11b for 30 min on ice covered with aluminum foil (Table 16). Afterwards, the cells were washed twice and resuspended in FACS buffer containing DAPI (1 µg/ ml) to discriminate viable from dead cells. At the BD Canto II machine, lymphocytes (FCS-A vs. SSC-A) → single cells (FCS-A vs FCS-H) → live cells (DAPI negative cells, Pacific Blue vs. SSC-A) → CD14 vs. CD11b were gated. CM-272 treated OCI-AML3 were compared to the DMSO control.

The BD kit Apoptosis, DNA Damage and Cell Proliferation for flow cytometry was used to investigate functional changes of MDS-L, F-36P and OCI-AML3 cells upon CM-272 treatment compared to their DMSO control. The assay was performed according to the kit instructions. This kit contains fluorescence-labeled antibodies specific for cleaved poly(ADP-ribose)-polymerase

(PARP), phosphorylated H2A histone family member X (H2AX), and incorporated bromodeoxyuridine (BrDU). PARP is a cellular apoptosis marker because it is cleaved by Caspase-3 resulting in inactivation of PARP and the inability of cells to repair DNA damage. Phosphorylated H2AX promotes DNA repair and maintains genomic stability and can be used as a marker for DNA damage. The gating strategy was similar to the procedure described above. BrDU is a synthetic nucleoside analogue similar to thymidine that incorporates into DNA of actively cycling cell fractions. Together with DAPI (4',6-Diamidino-2-phenylindol), which stains the nucleus of all cells, BrDU can be used to investigate proliferation and cell cycle of cells. BrDU positive cells are referred to S phase. G2 phase cells are BrDU-negative and contain twice as much as DAPI due to their doubled chromosome set compared to G1 phase cells. The different phases of cell cycle were distinguished by a certain gating strategy depicted below (Figure 13).

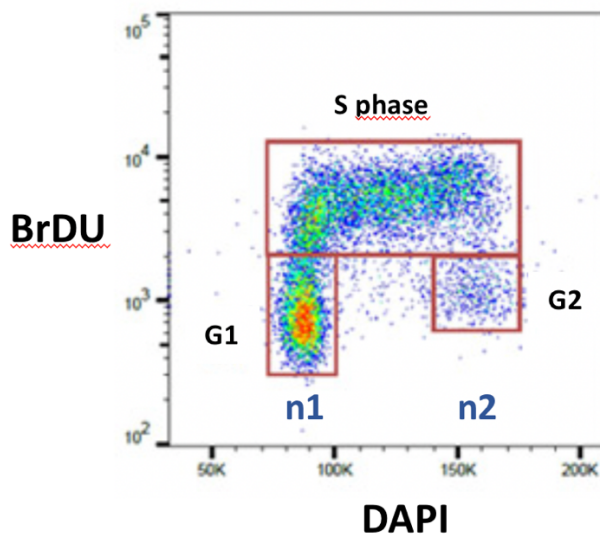


Figure 13: Cell cycle analysis by DAPI and BrDU staining.

Scatter plot of BrDU and DAPI stained cells to investigate cell cycle and proliferation by the BD kit “Apoptosis, DNA Damage and Cell Proliferation” and FACS. Depending on the staining, cells of different cell cycle states can be discriminated (**G1**: BrDU negative and low DAPI levels, **G2**: twice as much DAPI as G1 phase cells, **S**: only BrDU or double positive).

5.17.3.4 Apoptosis assay by Caspase 3/7 activity

Caspase 3/7 activity of CM-272 treated primary AML cells was investigated by the Caspase-Glo 3/7 assay following the manufacturer’s instructions (Promega). For each sample, 100 µl was mixed with the assay solution. The luminescence was measured in the FLUOstar Omega microplate reader. To analyze only the Caspase 3/7 activity of viable cells, the cell viability assay CellTiter-Glo was performed simultaneously. Luminescence signals of the Caspase 3/7 assay were normalized to the luminescence signal of CellTiter-Glo. Drug treated samples were normalized to the DMSO control to determine the percentage of viable cells affected by CM-272.

5.18 Molecular Biology

5.18.1 Investigation mRNA expression of genes

5.18.1.1 RNA isolation and quantification/ qualification of RNA

Total RNA was isolated using the PureLink RNA Mini Kit for downstream experiments including quantitative polymerase chain reaction (qPCR) and RNA sequencing (RNA-Seq). Samples for RNA-Seq were treated with an extra on-column DNase I digestion step. RNA for qPCR was quantified by the spectrophotometer NanoDrop that measures purity of nucleic acids by their absorbances. Wavelengths of 260 nm and 280 nm are specific for nucleic acids and proteins respectively, and a ratio of 2.0 is generally accepted as “pure” for RNA. The fluorometer Qubit was used for RNA-Seq samples providing a more precise concentration determination. RNA integrity was examined using the Agilent Bioanalyzer while only samples with R.I.N. (RNA Integrity Number) ≥ 7.0 were used for RNA-Seq.

5.18.1.2 RNA sequencing and Gene set enrichment analysis

RNA sequencing (RNA-Seq) is still a relatively new tool in molecular biology developed more than a decade ago. It is often used to determine quantitative changes in expression levels between experimental groups described as the differential gene expression (DGE).²⁰⁴ In this thesis, the whole transcriptome of MDS-L, F-36P, and OCI-AML3 was investigated regarding their response to CM-272 treatment compared to DMSO control after 72 h. In total, three biological replicates of each group were investigated.

RNA-Seq assay and bioinformatics data analysis were done at the Bioinformatics Core Facility at the Institute of Molecular Biology (IMB) Mainz. As previously described, the quality of isolated RNA was analyzed regarding its quality by the fluorometer Qubit and the Agilent Bioanalyzer at this institute. The core facility provided the messenger RNA (mRNA) and dsRNA expression data including reads per kilobase of transcript (RPKM), significance, and fold-changes of control versus CM-272 samples for this project.

Additionally, gene set enrichment analysis (GSEA) was performed to detect specific molecular signatures of CM-272-treated OCI-AML3 cells using the RNA-Seq gene list. Using the MSigDB database of the Broad institute, the normalized RNA-Seq gene lists for each replicate were analyzed by the DESeq2 method. Probes are ranked by signal-to-noise ratio and statistical significance determined by 1000 gene set permutations. Gene set permutation was used to enable direct comparisons between control and CM-272 results of OCI-AML3 (3 biological replicates each). Minimum gene set size was set to 10; median of probes was used to collapse multiple probe sets/genes. P value cut-off was set to 0.01 and false discovery rate to 0.01. This computational

method was used to determine whether gene classes are significantly altered in the treatment sample. Furthermore, altered gene sets were analyzed regarding their association with specific biological processes and a certain phenotype.

5.18.1.3 Quantitative reverse transcription PCR

A polymerase chain reaction (PCR) is a procedure in which a specific nucleic acid sequence is synthesized *in-vitro*. dsDNA becomes single stranded by denaturation so that the specific forward and reverse oligonucleotides (primer) can anneal to the strands at a lower temperature. A thermostable DNA polymerase elongates the primer in 5'-3' direction generating two double strands that will be used as new templates in the following cycles. These three steps are repeated for several cycles whereby the specific DNA section is exponentially amplified so that the PCR efficiency is theoretically 2.

One type of PCR is the quantitative reverse transcription PCR (RT-qPCR), by which absolute or relative mRNA expression levels of single genes are explored. Thereby, mRNA needs to be transcribed into complementary DNA (cDNA) by a reverse transcriptase (cDNA synthesis or RT-PCR) followed by a quantitative real time PCR (qPCR). This RT-qPCR method is a highly sensitive technique that tracks amplified cDNA after every cycle by fluorescence signals of the cyanine dye SYBR Green I. The number of cycles for a fluorescence level above a background of the unbound dye is called Ct value (threshold cycle). This value represents the mathematical unit for the measurement of the used DNA concentration. It is inversely proportional to the logarithm of the initial cDNA amount.²⁰⁵

mRNA of 500-2000ng total RNA was converted into cDNA by qScript cDNA SuperMix in a T100 Thermal Cycler as described in the user manual (Quantabio). To amplify cDNA and quantify gene expression, the PowerUp SYBR Green Master Mix containing a dual-lock *Taq* DNA-polymerase, optimized buffer, UNG (uracil-N-glycosylase) and dUTPs (deoxyuridine 5-triphosphate), and dNTPs (deoxynucleotide triphosphates) was used. The assay was performed in a QuantStudio 3 instrument. The gene B2M (beta-2-microglobulin) was always amplified as a reference gene to calculate the relative gene expression by the $\Delta\Delta C_t$ -method²⁰⁵. The sequences of forward (fw) and reverse (rv) primers of the analyzed genes and the reference gene are listed in Table 19. Data were reported as fold-changes of treated samples versus DMSO control. The qPCRs were performed according to the manufacturer's description (Thermo Fisher Scientific).

5.18.2 Investigating protein expression of genes by western blot

In 1979, protein blotting was introduced by Towbin et al. and became a routine tool for research laboratories. A protein mixture is separated by gel electrophoresis and subsequently transferred to a membrane. During immunodetection, the proteins of interest are visualized and identified with specific antibodies. From a protein pool, single proteins together with their molecular weight and quantity can be investigated. Additionally, different isoforms, altered processing products, and other post-translationally modified forms can be explored.²⁰⁶

5.18.2.1 Protein isolation and quantification

Cells were lysed in RIPA lysis buffer (1x Protease inhibitor cocktail and 0,01x Nuclease in RIPA buffer). After an incubation on ice for 10 min, sample solution was mixed at 4 °C for 20 min using a rotator mixer set at 25 rpm. Next, lysates were spun down at 4 °C and 13,000 rpm for 15 min. The supernatants containing the proteins were carefully transferred into fresh 1.5 ml reaction tubes. The proteins were directly used for western blot or stored at -80 °C.

The protein amount was determined by the Pierce BCA Protein Assay kit which is based on a standard of known protein concentrations producing a linear response curve. A highly sensitive and selective colorimetric staining according to the protein concentration could be detected at 562 nm using the FLUOstar Omega microplate reader. Absorbance of unknown protein amounts were interpolated into the formula ($y=a*m+b$) for the linear plot of the standard and computed by Excel.

5.18.2.2 Cell fractionation of proteins

In this thesis, the subcellular localization of the mutated NPM1c within OCI-AML3 cells after DMSO or CM-272 treatment (72 h) should be defined. Therefore, the cell fractionation kit by Cell Signaling was used to separate cells into the distinct fractions: cytoplasmic, membrane/organelle, and nuclear/cytoskeletal according to the manual description. The kit uses different isolation buffers specific for the cytoplasmic, membrane, and cytoskeletal/nuclear fractions. A whole cell lysate was investigated as well. Importantly, the normalization of the amount of protein in each compartment was done by the No-Stain protein labeling reagent which was applied to the gel. As additional loading controls, vinculin (whole cell lysate/cytoplasmic) and lamin B1 (nuclear) were examined.

After cell fractionation, the standard protocol for western blotting was performed as described below.

5.18.2.3 SDS-PAGE, blotting, Ab-staining and detection

Identical protein amounts (10-25 µg) were separated by sodium dodecyl sulfate–polyacrylamide gel electrophoresis (SDS-PAGE). Samples were diluted with 4x Laemmli buffer and nuclease-free water (total 15 µl), boiled at 100 °C for 5 min, quickly spun down and loaded on a 10 % polyacrylamide gel made by a TGX FastCast Acrylamide Kit. The PageRuler Plus Prestained Protein Ladder (5 µl) served as a protein marker. The gel was run in 1x XT MOPS running buffer at 150 V for 50 min in a Mini-PROTEAN Tetra Vertical Electrophoresis Cell.

Next, a 0.45 µm PVDF membrane primed in 100 % methanol for 2 min was used to transfer the sample proteins from the gel to the membrane. The transfer was also done in a Mini-PROTEAN Tetra electrophoresis system that contained a Mini Trans-Blot cell with color-coded cassettes and electrodes. The gel was inserted into a mini trans-blot cell with the primed PVDF membrane together with a foam pad and filter papers at both sides. The tank with the cassette was filled with ice-cold blotting buffer and an ice pack to keep it cold. Under stirring, a voltage of 100 V was applied for 1 h.

After protein transfer, the membrane was blocked with tris buffered saline with 0.1 % tween 20 (TBST) containing 5 % skim milk to prevent the nonspecific binding of antibodies. For the detection of specific proteins, primary antibodies against certain protein epitopes were chosen. (Table 17) The membrane was incubated 60-90 min or overnight under constant mixing in the antibody solution (5% skim milk in TBS-T or 5 % BSA in TBS-T). After three washing steps for 5 min in TBS-T, an anti-species secondary antibody linked to a horseradish peroxidase was diluted in the same solution as the primary antibody and applied to the membrane for 1 h. (Table 18)

The membrane was washed three times for 5 min before the protein could be visualized by a SuperSignal West Pico PLUS. Those protein bands were detected by the iBright™ CL1000 Imaging System and the signals were quantified by densitometry using the iBright Analysis Software.

5.18.3 Cytokine release analysis by Luminex

The Luminex assay (ProcartaPlex) is based on a Multi-Analyte Profiling technology enabling simultaneous detection and quantification of multiple secreted proteins (cytokines, chemokines, and growth factors) by combining different antibody-linked beads in a single 96 well-plate. These beads are comprised of a magnetic core and an internal dye with precise proportions of red and infrared fluorophores enabling a feasible workflow and precise target detection.

In this thesis, the used Human Custom ProcartaPlex 16-plex covered up to 16 secreted proteins. Based on standard concentrations (pg/ml) of the targets provided by the kit, a standard curve could be generated which was subsequently used for the concentration determination of the interleukins

(IL) IL-4, IL-8, and the tumor necrosis factor alpha (TNF α). These analytes were investigated on supernatants of MDS-L, F-36P, and OCI-AML3 cells treated with CM-272 or DMSO for 48 h. Briefly, 200-1000 μ l of the cell suspension was harvested and washed as usual. The supernatant was spun down at 12,000 g for 5 min to separate debris from liquid and stored at -20 °C. The assay was performed according to the manual instructions (Thermo Fisher Scientific). At the working group Clausen, the assay was performed with technical support of Dr. Ronald Backer using a Luminex Magpix.

5.18.4 DNA methylation analyses

5.18.4.1 DNA Isolation of genomic DNA from eukaryotic cells

Genomic DNA (gDNA) of human cell culture cells or tissue (placenta) was isolated using the NucleoSpin Tissue, Mini kit, following its instruction (Macherey-Nagel).

gDNA was eluted in 50 μ l of elution buffer and quantified using the NanoDrop for DNA methylation analysis or Qubit for molecular cloning.

5.18.4.2 Agarose gel electrophoresis

Using the agarose gel electrophoresis, DNA fragments are separated by size while the percentage of agarose determines the size of pores in the gel matrix. Small fragments are separated in higher percentage gels with smaller pores and larger fragments vice versa. DNA has a negatively charged phosphate backbone and migrates from the negative to the positive electrode when applying voltage.

Here, 1-2 % agarose gels were used to investigate DNA fragments after PCR and for their purification. Agarose was mixed with 1x tris-borate-EDTA (TBE) or 1X tris-acetate-EDTA (TAE) buffer and completely dissolved in a microwave. GelGreen, a stable and green fluorescent dye staining nucleic acid was added (1:10,000 dilution) before liquid agarose was poured in a chamber containing an appropriate comb. Next, the polymerized gel was inserted into an electrophoresis chamber filled with 1X TBE or TAE. Samples mixed with a 6x Loading dye and 100 bp or 1 kb DNA ladder containing DNA fragments of defined size were loaded on the gel. A DNA ladder contains DNA fragments of defined length to determine sample size. The agarose gel was run at 100 V for 40-60 min depending on the fragment size. Imaging was done using the iBright CL1000 Imagine System.

5.18.4.3 Bisulfite conversion of DNA for MassARRAY and pyrosequencing

To distinguish methylated and unmethylated CpG sites, bisulfite conversion is often applied. Thereby, unmethylated cytosines (C) are chemically converted into uracil (U) by a sodium bisulfite treatment of the DNA. However, methylated CpG dinucleotides-associated cytosines are resistant and remain unchanged. Consequently, two single-stranded DNA templates are generated that have changed their sequence being not complementary anymore. By PCR using (un)methylation-specific primers, a specific gene region is amplified while C-to-U changes are recognized as thymines (T). In this thesis, isolated gDNA was treated with the EZ DNA methylation-Gold Kit according to the instruction manual (Zymo Research) and used for MassARRAY and pyrosequencing.

5.18.4.4 MassARRAY

In a MassARRAY assay, methylated and unmethylated cytosines are discriminated based on their different weight analyzed by matrix-assisted laser desorption/ionization time-of-flight mass spectrometry (MALDI-TOF MS). It allows high-throughput quantitative DNA methylation analysis of multiple CpG sites. After bisulfite conversion of gDNA, the examined gene region is amplified by PCR with tagged primers (Table 21), *in vitro* transcribed into RNA and base-specifically cleaved by an endoribonuclease. The exact weight of the fragments differs according to bisulfite-treatment-induced variations in the DNA sequence. In the end, the size ratio of the cleaved products is determined and the proportion of methylated and unmethylated CpG sites of the analyzed gene regions can be assessed.²⁰⁷

The MassARRAY assay was performed in collaboration with AG Plass/Weichenhan at the DKFZ Heidelberg. The DNA methylation status of the promoter region of SFRP1 and LINE-1 of different MDS/AML cell lines (MDS-L, F-36P, MOLM13, KG1a, SKM-1, UoCm1, and OCI-AML3) was compared to healthy cells (placenta and MNC). The placenta tissue was obtained after a Cesarean-section at the Gynecology department, University Medicine Center Mainz. For SFRP1, three fragments containing five different CpG sites were investigated while three separate CpGs of LINE1 were analyzed. The retrotransposon LINE-1 (Long Interspersed Nuclear Elements) is frequently used as a surrogate marker for global hypermethylation as it occupies about 17% of the human DNA and is inactivated by hypermethylation.²⁰⁸ The average DNA methylation level of the examined CpGs of SFRP1 and LINE1 was plotted.

The experiment started with a bisulfite treatment of gDNA as described in chapter 5.18.4.3. 500 ng of DNA was used for the conversion and eluted 2x in 20 µl of M-Elution buffer (12.5 ng/µl DNA). 6,25 ng/µl of DNA were amplified with a Hot-Start *Taq* polymerase by specific PCR programs for SFRP1 (annealing temperature of 60 °C) and LINE1 (annealing temperature of 56 °C). The program was set according to the guidelines under “PCR using Hot Start *Taq* DNA

Polymerase” by NEB. (see below in Table 29, Table 30) A quality check of the PCR products was performed using a 2 % gel electrophoresis.

Table 29: PCR program with a Hot Start *Taq* polymerase for a MassARRAY assay.

PCR step	Temperature	Time	
Initial Denaturation	94 °C	15 min	
Denaturation	95°C	30 sec	
Annealing	56 / 60 °C	30 sec	45 cycles
Elongation	72 °C	60 sec	
Elongation	72 °C	5 min	
End	10 °C	hold	

Table 30: Components and concentrations of a PCR for the MassARRAY assay.

Component	7 µl reaction	Final Concentration
10X Standard Reaction Buffer	0.7 µl	1X
10 mM dNTPs	0.056 µl	1X
Hot Start <i>Taq</i> Polymerase	0.056 µl	1.25 units/ 50 µl
10 µM forward/reverse primer each	0.14 µl	0.5 µM each
Template DNA (6,25 ng/µl)	2.0 µl	3.5 ng
Nuclease-free water	4 µl	

Next, any ligation of the amplicons was inhibited by removing the phosphorylated ends of DNA using the shrimp alkaline phosphatase (SAP). 5 µl of the PCR product were mixed with 0.3 µl of SAP and 1.7 µl of water and incubated for 20 min at 37 °C. Afterwards, the reaction was inactivated at 85 °C for 5 min. During an all-in-one step, the SAP-treated PCR products were converted in RNA by the T7 polymerase and cleaved by the RNase A for 3 h at 37 °C. (see below in Table 31)

Table 31: Components for RNA conversion and cleavage.

Component	7 μl Reaction
water	3.21 μ l
5x buffer	0.89 μ l
T7 cleavage mix	0.22 μ l
DTT (dithiothreitol)	0.22 μ l
T7 polymerase	0.4 μ l
RNase A	0.06 μ l

The cleavage reaction of 7 μ l was desalted with 20 μ l of water and 6 mg resin (per well in a 96-well plate). The plate was shaken for 10 min and then spun down at 3,000 rpm for 5 min. Finally, the samples were spotted on a chip and run in a MALDI-TOF MS system (Sequenom, Agena). Data analysis was done in the AG Plass/ Weichenhan and final results were provided.

5.18.4.5 Pyrosequencing

Pyrosequencing is another DNA methylation method and was used to verify the results of the MassARRAY. It was performed at the Institute for Human Genetics, University Medicine Center Mainz. This assay is based on the principle of “sequencing by synthesis” of bisulfite converted DNA. By the detection of one incorporated nucleotide at a time, ssDNA is sequenced during its synthesis using a DNA-polymerase and sequencing primer. When a nucleotide complements the first unpaired base of the template, a pyrophosphate is released which produces a chemiluminescence signal. More precisely, the adenosine triphosphate (ATP) sulfurylase converts pyrophosphate (PP_i) to ATP in the presence of adenosine 5' phosphosulfate (APS). ATP is used as a substrate for the luciferase-mediated conversion of luciferin to oxyluciferin. Emission of visible light is proportional to the number of nucleotides and can be detected by a camera. The enzyme apyrase degrades any unincorporated nucleotides and ATP so that the reaction can restart with another nucleotide.²⁰⁹

To analyze the DNA methylation level of SFRP1 in healthy cells (MNC, placenta) and MDS/AML cell lines (MOLM13, UoCM1, KG1a), pyrosequencing-specific primers were designed (Table 20). The analyzed promoter region was already investigated by Reins et al., but the primer design was optimized using the Pyro Q-CpG 1.0.9 Software.

After DNA isolation, 500 ng DNA was converted by bisulfite treatment as described above (chapter 5.18.4.3). Next, the region of interest was amplified in a 25 μ l reaction mix using the FastStart High Fidelity PCR System (Sigma-Aldrich). The Thermal profile A for fragments up to 3 kb was used and adjusted to an annealing temperature of 50 °C for SFRP1 and LINE1. One primer

was biotinylated to generate biotinylated DNA fragments. 1.5 µl of PCR products were checked by 2 % gel electrophoresis before starting the pyrosequencing assay.

For the pyrosequencing assay, 40 µl of binding buffer, the PCR product, and 3 µl of sepharose beads were added to a 96-well PCR plate. The plate was sealed and mixed to allow the binding of biotin to streptavidin on the sepharose beads. Using a vacuum prep tool, components were mixed and washed in the following steps. Under vacuum, the hand tool was cleaned with Millipore water for 20 sec. Next, the sepharose beads with PCR products were sucked and attached to the pins of the hand tool. The suction head was placed into a 70 % ethanol pan for 5 sec followed by a pan filled with denaturation buffer for 5 min to form ssDNA. As a result, only biotinylated single strands bound to the beads remained on the pins and were washed for 5 sec in washing buffer. In the meantime, a pyro plate was prepared with 1.6 µl of sequencing primer and 40 µl of annealing buffer. The suction head was held over the pyro plate, the vacuum was switched off and the pins were dipped into the plate. The components (biotinylated ssDNA with primer and annealing buffer) were mixed by smooth shaking. To avoid secondary structures, the pyro plate was heated up to 80 °C for 2 min. A cleaned and dried cartridge was filled with the enzymes, substrates and nucleotides whereby the volume of each could be taken from the Pyro Q-CpG 1.0.9 Software. The cartridge and the pyro plate were finally placed into the Pyrosequencer Pyromark Q96 for analysis of the DNA methylation. Data of the CpG dinucleotide status could be exported as excel files after the experiment.

5.19 Generation of a recombinant THP-1 reporter cell line

A construct called “SFRP1_mCherry_puro” was designed to generate a recombinant AML reporter cell line. Upon treatment with epigenetic drugs, the epigenetically silenced SFRP1 promoter should be reactivated, which was detected by the reporter gene mCherry. The selection of crRNAs, molecular cloning, and the transfection of cancer cells was conducted in collaboration with the working group Wölfel at the University Medicine Center Mainz. The software Geneious was used for the design of the construct.

5.19.1 Selection of the most suitable crRNA for HDR-based CRISPR/Cas9 editing at the SFRP1 gene site

5.19.1.1 Identification of three crRNA candidates for HDR-based CRISPR/Cas9 editing of SFRP1

The CRISPR (clustered regularly interspaced short palindromic repeats)/ Cas9 (CRISPR associated protein 9) technology originates from fundamental research on microorganisms by the Noble Prize winners Jennifer Doudna and Emmanuelle Charpentier. This new molecular biological method is based on an adaptive immune defense mechanism of bacteria and archaea against foreign genetic material that has integrated into their genome. The CRISPR system is comprised of a CRISPR RNA array (crRNA array) encoding different guide RNAs (gRNA) and the trans-activating crRNA (tracrRNA) processing crRNA array into discrete units²¹⁰. These single guide RNAs (sgRNAs) containing a 20nt guide sequence form a complex with the Cas9 protein deriving from *Streptococcus pyogenes*. This complex scans the DNA for protospacer adjacent motif (PAM) associated with the targeted DNA that is complementary to the crRNA sequence. Once the complex has recognized this site, the Cas9 protein cleaves the DNA that leads to double-strand breaks. In human, they are repaired by the host repair mechanisms nonhomologous end joining (NHEJ) or homology-directed repair (HDR). By NHEJ, insertions or deletions (indels) can occur resulting in frameshift mutations and premature stop codons which inactivate genes²¹¹.

The SFRP1_mCherry_puro construct was supposed to be integrated into the first exon of the SFRP1 gene by the homology-directed recombination (HDR)-based CRISPR/Cas9 editing technology (see chapter 5.19.3.2). Before the SFRP1_mCherry_puro construct could be designed and generated, a suitable crRNA recognizing exon 1 of the SFRP1 gene needed to be selected first. Three crRNA candidates (crRNA #1, #2, #3 listed in Table 27) with only a low probability of off-targets were identified by web-based crRNA designing tools (IDT, benchling, broad institute, CHOPCHOP, CRISPOR).

5.19.1.2 Electroporation of PC-3 cells with ribonucleoprotein particles (RNPs) containing crRNA #1, #2, or #3

The three crRNA candidates were tested using the prostate cancer cell line PC3 endogenously expressing SFRP1 to identify the most suitable crRNA. 1 Mio PC3 cells per sample were harvested and washed in PBS. Cells were treated and electroporated according to the Cell line Nucleofector V kit. Electroporation is a physical transfection method using an electrical pulse to create temporary pores in cell membranes. Substances such as nucleic acid can pass into cells which is a highly

efficient technology to introduce foreign DNA into many cell types. However, it also leads to high cell death caused by high voltage pulses and only partially successful repair of the membrane.

To electroporate PC-3 cells, 82 μl of nucleofector solution was added to 18 μl of supplement solution (120 pmol) and given to the cell pellet in a 1.5 ml tube on ice. The CRISPR/Cas9 reagents (200 μM crRNAs, 200 μM traceRNA, 61 μM Cas9 endonuclease, 100 μM Cas9 electroporation enhancer) were reconstituted in IDTE (1X TE solution), aliquoted and stored at $-80\text{ }^{\circ}\text{C}$. To form a crRNA:traceRNA duplex, 2.5 μl of crRNA #1, #2, and #3 were mixed with 2.5 μl of traceRNA and heated up at $95\text{ }^{\circ}\text{C}$ for 5 min. Ribonucleoprotein particles (RNP) were made by incubating 1.7 μl of Cas9 with 1.2 μl of crRNA:traceRNA duplex and 2.1 μl of Optimem for 15 min at RT. Next, 5 μl of RNP of crRNA #1, #2, and 3# as well as a 2 μg of GFP-vector (0.5 $\mu\text{g}/\mu\text{l}$) were mixed with 1 μl of electroporation enhancer and 100 μl of cells and pipetted into a cuvette. Cells were electroporated using the pre-designed program T013 of the Nucleofector 2b device and subsequently incubated at $37\text{ }^{\circ}\text{C}$ for 15 min. Finally, the samples were transferred into a T25 flask for adherent cells containing 4 ml of prewarmed media. An untreated cell sample was used as a negative control for transfection.

The Cas9 guided by either of the three crRNAs was supposed to cleave the SFRP1 gene specifically at the crRNA complementary sequence. Consequently, the cleavage would cause double strand breaks that were supposed to be repaired by the error-prone cellular repair mechanism non-homologous end joining (NHEJ). By this process, small insertions or deletions so called Indels are generated resulting in a KO of SFRP1. The targeting of SFRP1 was examined by western blot (see chapter 5.18.2) and the surveyor assay (see chapter 5.19.1.3).

5.19.1.3 Surveyor assay of crRNA #3-specific CRISPR/Cas9 transfectant

The Surveyor Mutation Detection Kit was used to check for a SFRP1-specific targeting and cleavage by the crRNA #3-specific HDR-based CRISPR/Cas9. The key component of the kit is an endonuclease (S1N) that cleaves DNA with high specificity at sites of base-substitution mismatch and other distortions. Therefore, this S1N was used as a tool for mutation detection at the crRNA #3-specific cutting site of SFRP1 caused by the repair mechanism NHEJ.

Primers were designed ~ 100 bp upstream and ~ 200 bp downstream of the crRNA #3 binding site to generate DNA fragments of different size after S1N-mediated cleavage (primer sequence see Table 22). Using a WT PC3 reference sample (C) and the crRNA #3 sample (#3), the 300 bp sequence was amplified by PCR (PCR program and pipetting scheme see Table 33, Table 34). Gel electrophoresis of the PCR product was performed, the specific band was cut out and purified by the NucleoSpin Gel & PCR clean-up kit. Next, the amplicon of the control, the crRNA #3 sample, and a GC control (included in the kit) were used for a specific hybridization procedure at slowly

decreasing temperature (Table 32). Thereby, ssDNA of WT cells can hybridize with transfected cells of the heterogenous crRNA #3 sample forming heteroduplexes of dsDNA. The GC control served as a check-up for the nuclease activity. For the hybridization assay, 800 ng DNA were mixed with 4 μ l of MgCl₂ (0.15 M), 4 μ l of 10x Optimase buffer and nuclease-free water for a total volume of 38 μ l.

Table 32: Hybridization procedure with slowly decreasing temperature to form heteroduplexes.

Temperature	Time	Temperature Ramp
95 °C	10 min	
95 °C to 85 °C		(-2.0 °C/ sec)
85 °C	1 min	
85 °C to 75 °C		(-0.3 °C/ sec)
75 °C	1 min	
75 °C to 65 °C		(-0.3 °C/ sec)
65 °C	1 min	
65 °C to 55 °C		(-0.3 °C/ sec)
55 °C	1 min	
55 °C to 45 °C		(-0.3 °C/ sec)
45 °C	1 min	
45 °C to 35 °C		(-0.3 °C/ sec)
35 °C	1 min	
35 °C to 25 °C		(-0.3 °C/ sec)
25 °C	1 min	
4 °C	Hold ∞	

After hybridization, all three samples were split to treat one half with the S1N and the other half were kept untreated. 18 μ l of DNA were mixed with 1 μ l of S1N and 1 μ l of enhancer before the samples were incubated at 42 °C for 60 min. The stop solution (2 μ l) was added in the end. Finally, the samples were loaded on a 2 % agarose gel to check the result.

5.19.2 Molecular Cloning of the SFRP1_mCherry_puro construct

5.19.2.1 Design of the SFRP1_mCherry_puro construct

The design of the SFRP1_mCherry_puro construct was based on the CRISPR/Cas9-specific cutting site of crRNA #3 within exon 1 (schematic representation of construct see Figure 14). CRISPR/Cas9-mediated HDR was used to integrate the construct template into the SFRP1 gene site. Therefore, the designed DNA fragment needed to consist of a left and a right homologous arm (LHA and RHA) of the SFRP1 gene sequence being a prerequisite for the HDR mechanism.

Material and Methods

gDNA of OCI-AML3 served as a template for the homologous arms of SFRP1. (primer sequence see Table 23 and template description see Table 26)

Downstream of the SFRP1 promoter region, the mCherry gene encoding for a fluorescence protein was cloned in frame with the SFRP1 sequence. Thereby, the mCherry expression could be regulated by the SFRP1 promoter activity. The mCherry sequence derived from the pJF001 plasmid and the SV40 polyA tail was inserted by the “F2-mCherry-SV40polyA.rev”-primer. A SV40 polyA tail includes the sequence motif AAUAAA which promotes both polyadenylation and termination. It is recognized by the RNA polymerase II complex to process precursor mRNA, enhances stability of the mature mRNA, and increases efficiency of mRNA translation in eukaryotic cells.²¹²

Between the homologous arm LHA of SFRP1 and mCherry, the self-cleaving protein P2A was inserted to prevent peptide bonds between the Proline and Glycine at the C-terminal of 2A peptide. This caused the transcription of two separated proteins and not one fusion protein. The primer “F2-P2A-mCherry.for” provided the sequence for it.

Downstream of SFRP1 and mCherry, the puromycin-resistant gene was designed with its own promoter to be constitutively active independently of the SFRP1 promoter activity. Its permanent activation enabled an efficient selection by the puromycin antibiotic to obtain only positive cells bearing the construct. The sequence for the puromycin-resistant gene derived from the pMX-puro-DEST plasmid and the sequence for its SV40 promoter (SV40 prom) came from the pCMB-HmB plasmid. The sequence for its SV40 polyA tail was added by the primer “F4_puro-SV40PolyA.rev”. In the following steps (chapter 5.19.2.2), five DNA fragments were amplified by PCR and ligated to create the 2,673 bp full-length (FL) fragment that was inserted into a pcDNATM3.1/V5-His TOPO[®] TA plasmid. Subsequently, the SFRP1_mCherry_puro fragment was integrated at the SFRP1 gene site by HDR-based CRISPR/Cas9 editing (chapter 5.19.3).

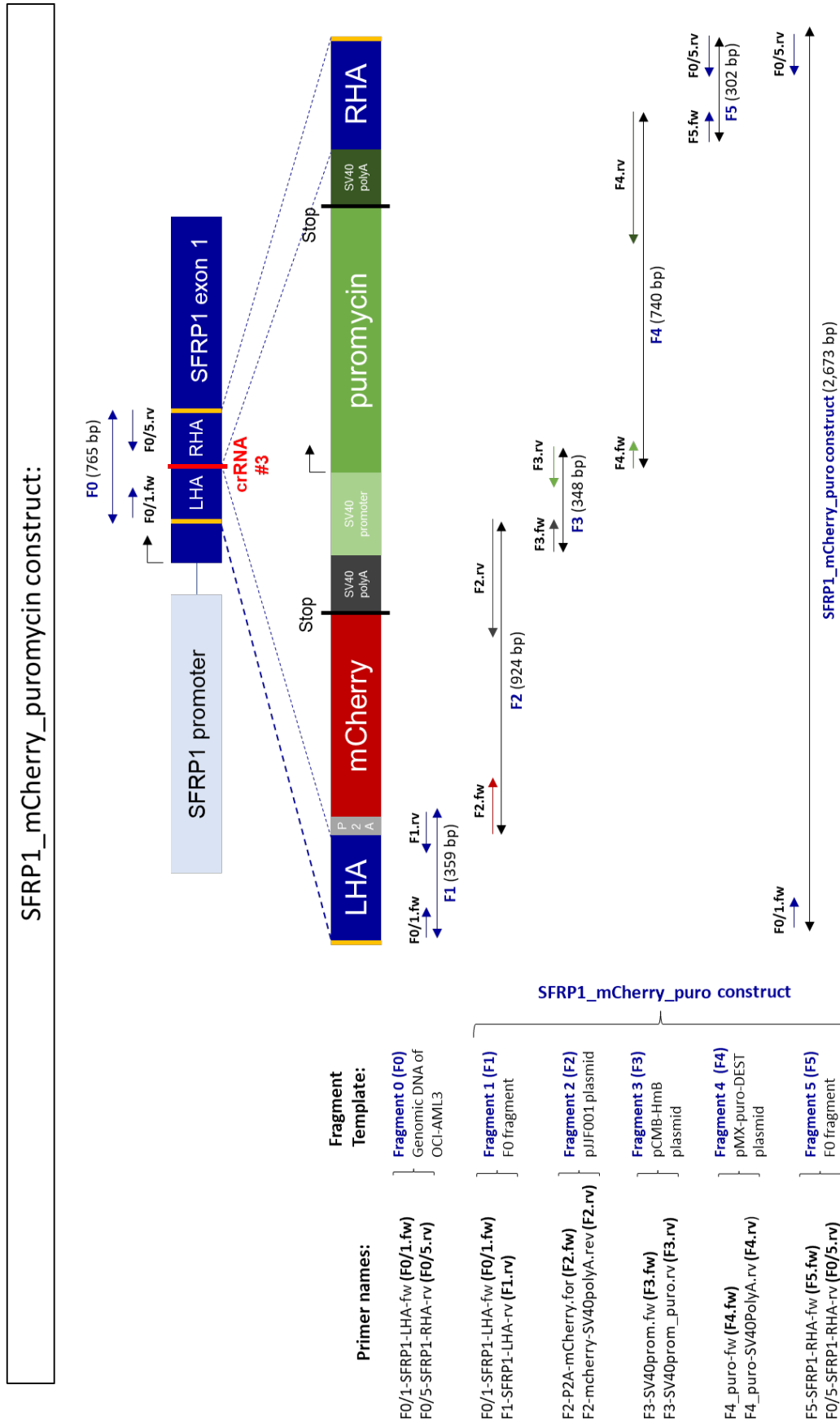


Figure 14: Schematic overview of the SFRP1_mCherry_puro construct.

5.19.2.2 Generation of construct fragments by PCR amplification

A PCR was performed to amplify five fragments for molecular cloning of the SFRP1_mCherry_puro construct. For highly precise amplification of the templates, the Q5 High-Fidelity DNA polymerase was used that has a ~280 times higher fidelity amplification capacity than the traditional *Taq* polymerase. Therefore, it provides amplicons with ultra-low error rates. However, it does not generate A-overhang compared to the *Taq* polymerase. The PCR program as well as the component and their concentrations for the Q5 polymerase-specific reaction can be seen below in Table 33, Table 34. Sequence of the primers are listed in Table 23.

Table 33: PCR program for Q5 polymerase.

Step	Temperature	Time
Pre-heating	98 °C	hold
Initial Denaturation	98 °C	3 min
Denaturation	98°C	10 sec
Annealing	see Table 23	20 sec
Elongation	72 °C	30 sec/ kb
Elongation	72 °C	3 min
End	4 °C	hold

Table 34: Component and concentrations for a standard PCR reaction.

Component	25 µl Reaction	Final Concentration
5X Q5 Reaction Buffer	5 µl	1X
5X GC enhancer	5 µl	1X
10 mM dNTPs	0.5 µl	200 µM
10 µM forward/reverse primer each	1.25 µl each	0.5 µM each
Template DNA (100 ng gDNA, 5 ng plasmid DNA or F0-Fragment)	1.0 µl	
Q5 polymerase	0.25 µl	0.02 U/µl
Nuclease-free water	to 25 µl	

5.19.2.3 Seamless assembly, TA-cloning and transformation

The five PCR products were run in a gel electrophoresis and purified using the Monarch DNA Gel Extraction kit following the manual instructions. The DNA was eluted in 6 µl of elution buffer and the concentration was determined by the fluorometer Qubit using the Qubit dsDNA BR Assay kit. The assembly of the five amplified DNA fragments was done by the NEBuilder HiFi DNA Assembly Cloning Kit. According to the fragment size, all fragments with an equimolar concentration of 0.5 pmol were added to a total volume of 5 µl, mixed with 10 µl of NEBuilder HiFi DNA assembly master mix and 5 µl of deionized water. The solution was incubated for 2 h at 50 °C in a thermocycler. Next, 10 µl of the assembled DNA fragments were amplified by PCR (Table 33, Table 34) using the flanking primers of the FL fragment (F0/1.fw and F0/5.rv, Table 23). Gel electrophoresis with the loaded amplicon was done to remove all compounds of the PCR. The correct band was cut out under UV-light and the DNA fragment embedded in agarose was purified using the Monarch DNA Gel Extraction kit.

This FL fragment was inserted into a pcDNA3.1/V5-His-TOPO-vector, which is based on TA-cloning. To generate A-overhangs, 500 ng of the insert was treated with 4 µl of One *Taq* polymerase mix containing ATP for 10 min at 68 °C. Next, 4 µl of PCR product, 1 µl of salt solution, and 1 µl of TOPO-vector were mixed and incubated for 30 min at RT following the manual description of the pcDNA 3.1/ V5-His TOPO TA expression kit.

Chemically competent 10-beta *E. coli* were used for the transformation of the TOPO-vector containing the construct. These *E. coli* bacteria were previously treated with calcium chloride to facilitate attachment of the plasmid DNA to the competent cell membrane. For the transformation, 4 µl of TOPO cloning reaction from the previous step were added to 25 µl of *E. coli* and incubated for 30 min on ice. After a heat shock step at 42 °C for 30 sec in a water bath, the cells were put back on ice. Next, the bacteria were mixed with 125 µl of SOC medium and were shaken at 37 °C for 1 h, before the suspension was spread on prewarmed selective plates with ampicillin and incubated overnight at 31 °C. On the next day, 6 colonies were picked.

5.19.2.4 Colony-PCR of *E. coli* clones

A quick Colony-PCR was performed to investigate the correct assembly and integration of the SFRP1_mcherry_puro insert in the pcDNA 3.1/ V5-His TOPO vector. Single transformed *E.coli* colonies were picked with a pipette tip under the microscope. The tip was transferred into a 0.5 ml tube that contained 100 µl LB-amp and mixed for a few seconds. Then, 10 µl of the LB-amp-colony mix was pipetted into a PCR-tube and spun down for 10 min at 10,000 rpm. After removal of the supernatant, the bacteria pellet could be used for the Colony-PCR. (Table 35, Table 36)

Table 35: Components and volume of Colony-PCR.

Components	Volume
2x Master Mix One Taq	10 μ l
10 μ M Forward (F0/1)	1 μ l
10 μ M Reverse (F0/5)	1 μ l
Nuclease-free water	8 μ l

Table 36: PCR-Program of Colony-PCR.

Step	Temperature	Time
Initial Denaturation	94 °C	3 min
Denaturation	94 °C	20 sec
Annealing	65 °C	20 sec
Elongation	68 °C	2.5 min (1 min/ kb)
Final Elongation	68 °C	5 min
End	4 °C	hold

5.19.2.5 Overnight culture of *E. coli* and plasmid isolation

E. coli colonies containing the TOPO-vector with the FL fragment were cultured in 6 ml LB-medium at 31 °C overnight in a bacteria shaker. On the next day, 750 μ l of the bacteria suspension + 250 μ l of 60 % Glycerol (in water) were frozen down and stored at -80 °C for long-term storage. The rest of the cultured *E. coli* were used to isolate plasmid DNA by the QIAprep Spin Miniprep kit according to the manufacturer's instructions. The centrifugation was done at 4,000 rpm for 10 min and the DNA was eluted in 30 μ l.

5.19.2.6 Sequencing of cloned SFRP1_mCherry_puro fragment

The cloned SFRP1_mCherry_puro construct was sequenced using the Mix2Seq kit-overnight to investigate whether it has the correct sequence according to our virtually designed construct. The performed sequencing method applies a so-called "Cycle Sequencing technique" which is a modified Sanger-Sequencing method with a thermostable DNA-polymerase. Before the DNA samples were sent to Eurofins, a small amount (1 μ l) of DNA was checked by agarose gel electrophoresis. 15 μ l of DNA (5 ng/ μ l) was mixed with 2 μ l of sequencing primer (10 pmol, Table 24) and water for a total volume of 17 μ l. The results could be downloaded from the Eurofins webpage and were analyzed using sequence information from the GenBank NCBI and the software Geneious.

5.19.3 HDR-based CRISPR/Cas9 KI of the SFRP1_mCherry_puro construct at the SFRP1 gene site of the THP-1 cell line

After the generation of the SFRP1_mCherry_puro construct, this dsDNA fragment of ~2,7 kb needed to be integrated into an AML cell line that contains an epigenetically silenced SFRP1 and highly efficiently repairs DNA breaks by the HDR repair mechanism. The THP-1 cell line fulfilled these criteria so that the HDR-mediated CRISPR/Cas9 KI of the SFRP1_mCherry_puro fragment could be done.

5.19.3.1 DNA enrichment and purification of the FL fragment

The SFRP1_mCherry_puro fragment needed to be purified and enriched using the DNA purification SPRI Magnetic Beads kit which is based on solid-phase reversible immobilization (SPRI) paramagnetic bead technology specific for PCR amplicon purification. The beads reversibly bind to carboxyl-coated paramagnetic particles allowing a high recovery of DNA. A PCR (Table 33, Table 34) with flanking primers (F0/1.fw and F0/5.rv, Table 23) was performed with a 25 µl PCR reaction mix containing 50 ng plasmid DNA (TOPO vector + construct). To increase the amount of amplified DNA, 500 µl of total PCR reaction mix was prepared and aliquoted into 20 PCR tubes. After the PCR run, the entire volume of the newly synthesized amplicon was mixed with 500 µl of bead solution in a 1.5 ml tube. The assay was carried out on a Magnetic Separation Rack for 1.5ml reaction tubes following the instructions of the kit. The air-drying step was done for 20 min and the DNA was eluted in 30 µl of elution buffer.

5.19.3.2 HDR-based CRISPR/ Cas9 KI of SFRP1_mCherry_puro

To generate a THP-1 reporter cell line, the SFRP1_mCherry_puro fragment has to be specifically integrated at the binding region of crRNA #3 within exon 1 of SFRP1 by a double strand break and the repair mechanism HDR. Therefore, THP-1 cells were electroporated and transfected with the purified SFRP1_mCherry_puro fragment according to the optimized protocol provided by Amaxa ("Cell Line Nucleofector Kit V for THP-1). As described above in chapter 5.19.1.2, 3 Mio cells were transfected and edited by the CRISPR/Cas9 technology. Instead of the electroporation enhancer, 8 µg DNA was added to the cells. An HDR-enhancer (1:100) was applied to the cells in order to increase the HDR efficiency. After 24 h, the medium was changed to remove dead cells and the remaining reagents in the sample.

5.19.3.3 Selection, subcloning, and expansion of transfected cells

Cells successfully transfected with the SFRP1_mCherry_puro construct were resistant against puromycin so that positive cell clones could be selected using puromycin antibiotic starting four days post transfection. After 10-12 days of puromycin selection, the remaining positive cells were subcloned by limiting dilution of the cell suspension to obtain single cell clones. Cells were plated in a 96-well plate at different concentrations (0.3/well and 0.1/well) in 100 μ l of media containing puromycin (Table 37). When the media of the cell clones turned yellow (after 2-3 weeks), 20 clones were picked from the highest dilution (D9, 0.1 cells/well). The clones were transferred in a T25 flask with 5 ml medium and expanded under puromycin selection. Avoiding long culture times, cell clone stocks were frozen down to liquid nitrogen as early as possible.

Table 37: Limiting dilutions for subcloning.

Step	Dilution			Cells per 100 μ l in a 96-well
D1	10 ⁵ cells/ml initial cell suspension			10,000
D2	1.5 ml of D1	+	13.5 ml medium	1,000
D3	1.5 ml of D2	+	13.5 ml medium	100
D4	5 ml of D3	+	10 ml medium	30
D5	5 ml of D4	+	10 ml medium	10
D6	5 ml of D5	+	10 ml medium	3
D7	5 ml of D6	+	10 ml medium	1
D8	5 ml of D7	+	10 ml medium	0.3
D9	5 ml of D8	+	10 ml medium	0.1

5.20 Validation of transfected THP-1 single cell clones

The THP-1 single cell clones were further validated regarding their genotype of the two SFRP1 alleles and their mCherry expression. Treatments with either a DMSO control or epigenetic inhibitors were used to investigate the mCherry expression of these cells.

5.20.1 Genotyping of THP-1 reporter gene clones

Single cell clones of THP-1 were investigated regarding their construct integration by PCR. Clones were kept under constant puromycin selection, therefore one can assume that all of the cells contained at least one KI allele with an intact puromycin gene and had either of the following three genotypes: SFRP1^{WT/KI}, SFRP1^{KO/KI}, SFRP1^{KI/KI}.

Primer pairs (Table 25) for three different PCRs (PCR #1, #2, #3) were designed examining both alleles and the transition site of SFRP1 LHA/ mCherry and puro/ SFRP1 RHA (see chapter 5.19.2.1 and Figure 14).

PCR #1 contained primers binding ~350 bp up- and downstream of the cutting site of crRNA #3. The Elongation time was set to 30 sec (enough for 1 kb) to specifically detect only WT or KO alleles and to avoid amplification of the integrated construct (~2.7 kb). The KI allele was explored by PCR #2 for the LHA/ mCherry region and PCR #3 for the puromycin/ RHA region. Additionally, these PCR products were sequenced using the Mix2seq kit (see chapter 5.19.2.6).

5.20.2 High-throughput FACS screening and fluorescence microscopy to test the mCherry signal

The gene mCherry encodes for a red fluorescent protein originally isolated from Cnidarians (jellyfish, sea anemones and corals) and has its excitation maximum at 587 nm and its emission maximum at 610 nm. Therefore, the reporter cell line could be investigated by fluorescence microscopy and FACS analysis in the TxRed channel.

The mCherry activity of the puromycin-resistant single clones was investigated by fluorescence microscopy using the EVOS imaging system. The basal mCherry expression as well as the response to the epigenetic inhibitors DAC and CM-272 were examined on cells in cell culture.

For a more precise quantification of mCherry positive, live cells and to measure the signal intensity, all clones were analyzed by FACS using the LSR II HTS at the core facility for flow cytometry (CFFC) at the Paul-Klein-Zentrum für Immunintervention (PKZI). Clones were treated with DMSO, DAC or CM-272 in a U-shaped 96-well plate enabling a high-throughput analysis of the basal mCherry activity and its potential for signal enhancement by the inhibitors. On the day of analysis, cells were washed once with PBS and resuspended in FACS-buffer containing DAPI (1

$\mu\text{g/ ml}$). At the LSR II HTS, cells were gated for lymphocytes (FSC-A vs. SSC-A) \rightarrow single cells (FSC-A vs FSC-H) \rightarrow live cells (BV421 vs. SSC-H) \rightarrow mCherry cells (PE-TxRed vs. PerCP-A). WT THP-1 cells served as a negative control of mCherry expression. Further drug screening experiments were carried out in the same manner.

5.21 Statistical analysis

The mean \pm standard deviation was calculated and displayed in the graphs of all data. Statistical significance between two groups was determined using the Student's t-test. One-way ANOVA was conducted to determine statistical significance between more than two groups. A p-value of < 0.05 was considered significant (****, $p < 0.0001$; ***, $p < 0.001$; **, $p < 0.01$; *, $p < 0.05$) and 'ns' indicated not significant. Statistical analysis was performed using GraphPad Prism software (version 7).

6 Results

The effect of the simultaneous inhibition of DNA and histone methyltransferases was investigated in MDS/AML cell line models and patient-derived AML blasts. MDS and AML patients are currently treated with the FDA- and EMA-approved cytosine analogs, AZA and DAC, that irreversibly inactivate DNMTs, counteract abnormal epigenetic pattern and induce anti-tumor processes.^{188,213} Recently, first-in-class reversible dual small molecule inhibitors against G9a and DNMTs were discovered showing higher potency to inhibit tumor growth in a variety of hematological malignancies (AML, ALL, and diffuse large B-cell lymphoma) than targeting DNMTs alone.¹⁸⁴ Therefore, the leading compound of the recent publication, CM-272 was also explored further in various molecular, functional and cell biological assays in this thesis. Additionally, a recombinant THP-1 reporter cell line was generated to screen for epigenetic drugs with high potency to reactivate the epigenetically silenced TSG SFRP1.

6.1 Potency of CM-272 tested on various leukemia cell lines

6.1.1 Dual inhibition of DNMT/G9a by CM-272 displays high cytotoxic potency across a broad range of MDS/AML cell lines

First of all, the apoptotic and anti-proliferative response of MDS/AML cell lines to different doses of CM-272 were examined. Furthermore, MDS-L, F-36P, and OCI-AML3 were used to compare CM-272 to three other methyltransferase inhibitors including DAC, SGI-1027, and CM-579. Thereby, the therapeutic window of CM-272 for these leukemia cell lines was identified and the cytotoxic effect of CM-272 could be compared to other representative drugs.

Cytotoxicity assays under specific cell culture conditions were performed to identify working concentrations of CM-272 for different MDS/AML *in vitro* models. To assess the latency of drug effects, a great variety of MDS/AML cell lines were treated once with different CM-272 concentrations for 24 h and 72 h. Dose-response curves of CM-272 with one MDS (MDS-L), three MDS-derived AML (MOLM13, F-36P, SKM-1), and six *de novo* AML cell lines (OCI-AML2, OCI-AML3, NB4, THP-1, Kasumi, KG1a) were generated. The inhibitory concentration at which 50 % of the cells are dead or inactivated (IC₅₀) could be determined using a dose-response curve. After 24 h, the IC₅₀s ranged among the cell lines between 0.197 μ M (OCI-AML2) and 8.772 μ M (MDS-L) while F-36P and KG1a had not reached an IC₅₀ yet after this short time indicated by arbitrary values (\sim). CM-272 became more potent after 72 h seen by overall lower IC₅₀ values which were between 0.089 μ M (OCI-AML2) and 4.787 μ M (KG1a). After 96 h, the IC₅₀ did not change significantly (data not shown). All cell lines responded to the treatment in a dose- and time-

Results

dependent manner with different sensitivity. However, OCI-AML2, MOLM13, and OCI-AML3 responded the most while KG1a was only minimally affected after 72 h. (Figure 15A)

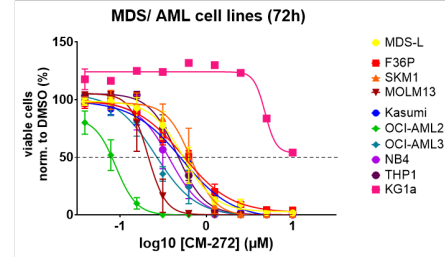
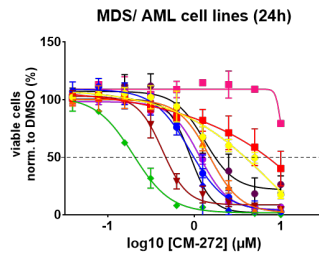
Next, CM-272 was compared to three other epigenetic drugs including the nucleoside-analog DAC, one of the first non-nucleoside DNMTi SGI-1027²¹⁴ as well as CM-579, a sister compound of CM272. Three cell lines representing the malignancies MDS (MDS-L), MDS-derived AML (F-36P), and *de novo* AML (OCI-AML3) were treated for 72 h. MDS-L contains the AML-driver mutations NRAS and TP53 while F-36P harbors mutations in the lysine methyltransferases 2a gene (KMT2A) and TP53. OCI-AML3 was selected due to its AML-specific mutations DNMT3A and NPM1. Due to the short half-life of DAC, it was applied daily whereas the other three drugs were given once. The dose-response curves revealed IC50s in nM range for all cell lines except F-36P (SGI-1027: 7.5 μ M and DAC: no toxicity). In all three cell lines, CM-272 showed the highest toxicity and potency to inhibit proliferation or to induce cytotoxicity while CM-579 was slightly less potent than CM-272. Compared with the sister compounds CM-272 and CM-579, higher concentrations were needed to reach an IC50 for DAC and SGI-1027. Interestingly, DAC only moderately induced cell death with any of the concentrations. DAC treated F-36P cells did not show any sign of toxicity or reduced proliferation. The sigmoid curve of SGI-1027 revealed a steep drop in viability particularly in OCI-AML3 providing only a very small range of effective concentrations with moderate toxicity. (Figure 15B)

For all subsequent experiments, MDS/AML cells were treated according to the determined IC50-values for each cell line and drug at 72 h under the specific culture conditions.

Results

A

Cell lines	IC50 24h (μM)	IC50 72h (μM)
MDS-L	8.772	0.537
MOLM13	0.429	0.209
F36P	~6315	0.537
SKM-1	1.497	0.667
OCI-AML2	0.197	0.089
OCI-AML3	0.897	0.256
NB4	1.145	0.375
THP-1	1.315	0.458
Kasumi	0.884	0.527
KG1a	~9.798	4.787



B

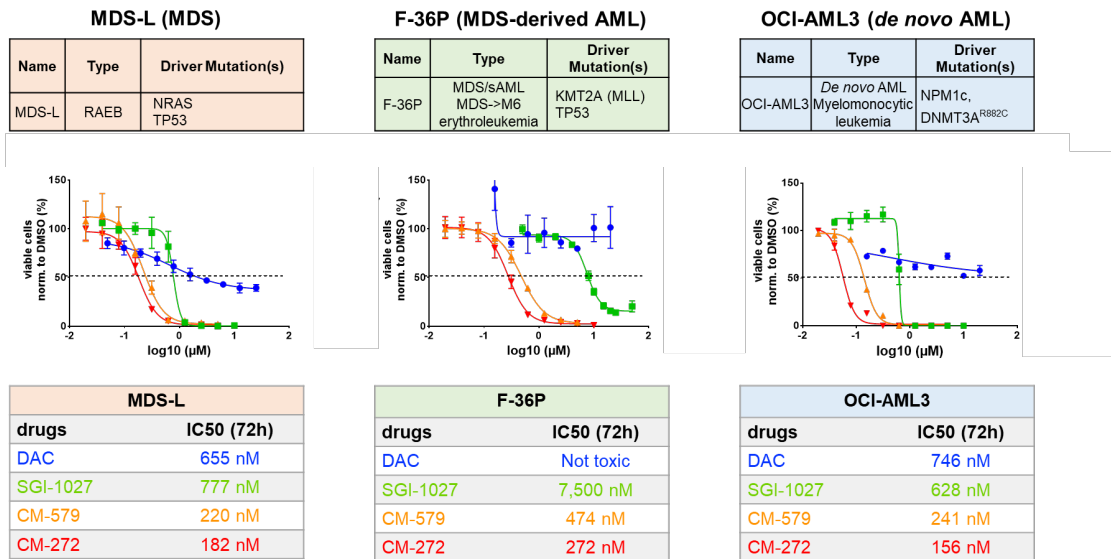


Figure 15: Cytotoxicity assays of MDS/AML cell lines treated with hypomethylating drugs.

(A) MDS/AML cell lines were treated with nine different concentrations of CM-272 in a single dose. After 24 h and 72 h, IC50s were determined by a cytotoxicity assay (n=3). Drug treatments were normalized to DMSO values. The IC50s were listed in a table categorizing MDS (orange), MDS-derived AML (green) and *de novo* AML (blue) cell lines. (B) MDS-L, F-36P, and OCI-AML3 were used to compare CM-272 to three other epigenetic inhibitors. After 72 h treatment with DAC (daily application), SGI-1027, CM-579, and CM-272 (single dose of all three drugs), IC50s were determined (n=3).

6.1.2 Protein degradation of DNMT/G9a and reactivation of epigenetic silenced genes in MDS/AML cell lines by CM-272

Protein and mRNA expression of DNMTs, G9a, and WNT-antagonists upon DAC, CM-272, and CM-579 treatments were further examined. SGI-1027 showed the highest IC₅₀ values with a very narrow therapeutic window being difficult to effectively treat cells without excessive cell death. Therefore, SGI-1027 was excluded from further analyses.

The protein levels of the methyltransferases DNMT1, 3A, 3B, G9a and the epigenetically silenced TSG SFRP1 as well as the G9a-specific histone mark H3K9me_{2/3} were investigated after drug treatment using western blot. MDS-L, F-36P, and OCI-AML3 were treated with the vehicle control DMSO or the compounds DAC, CM-579, and CM-272 for 72 h. All drugs led to a protein degradation of at least one DNMT in each of the three cell lines. Overall, G9a was less affected by the inhibitors than DNMTs. Interestingly, DAC seemed to inhibit DNMTs the most compared to CM-579 and CM-272. DAC had an impact on G9a degradation but the dual inhibitors showed a much higher inhibitory effect on G9a.

In MDS-L, the DNMTs were highly and similarly degraded upon DAC and CM-272 treatment whereas CM-579 showed a weak impact on the protein levels. CM-272 mediated the highest G9a degradation compared to the other two drugs in this cell line. In F-36P, DNMTs were highly degraded by DAC treatment while less pronounced by CM-272. CM-579 affected none of DNMTs. G9a remained unchanged upon all drug treatments. In OCI-AML3, DAC showed the strongest impact on the DNMTs leading to complete degradation. CM-579 and CM-272 similarly affected the DNMT protein level while DNMT3B was reduced the most followed by DNMT1 in OCI-AML3. Furthermore, CM-272 and CM579 treatment caused a reduction of the epigenetic mark H3K9me_{2/3} compared to the DMSO control and DAC in OCI-AML3. Controversially, the dual inhibitors did not change or even increase the histone modification of lysine 9 in MDS-L and F-36P.

A single dose of CM-579 and CM-272 was enough to upregulate the SFRP1 protein compared to three higher doses of DAC in all three cell lines after 72 h. (Figure 16A)

The transcripts of the WNT-antagonists WNT5A, DKK1, and SFRP1 were significantly re-activated upon CM-272 application in F-36P and OCI-AML3. In MDS-L cells, none of the transcripts could be detected and analyzed (data not shown). (Figure 16B)

These results indicated that CM-272 is a potent dual inhibitor of DNMTs and G9a in all three cell lines resulting in protein degradation. However, OCI-AML3 most sensitively responded to the treatment. The dual inhibitor showed comparable effects to the FDA-approved DNMTi DAC. In addition, this compound was able to re-activate epigenetically silenced genes seen in western blot and RT-qPCR.

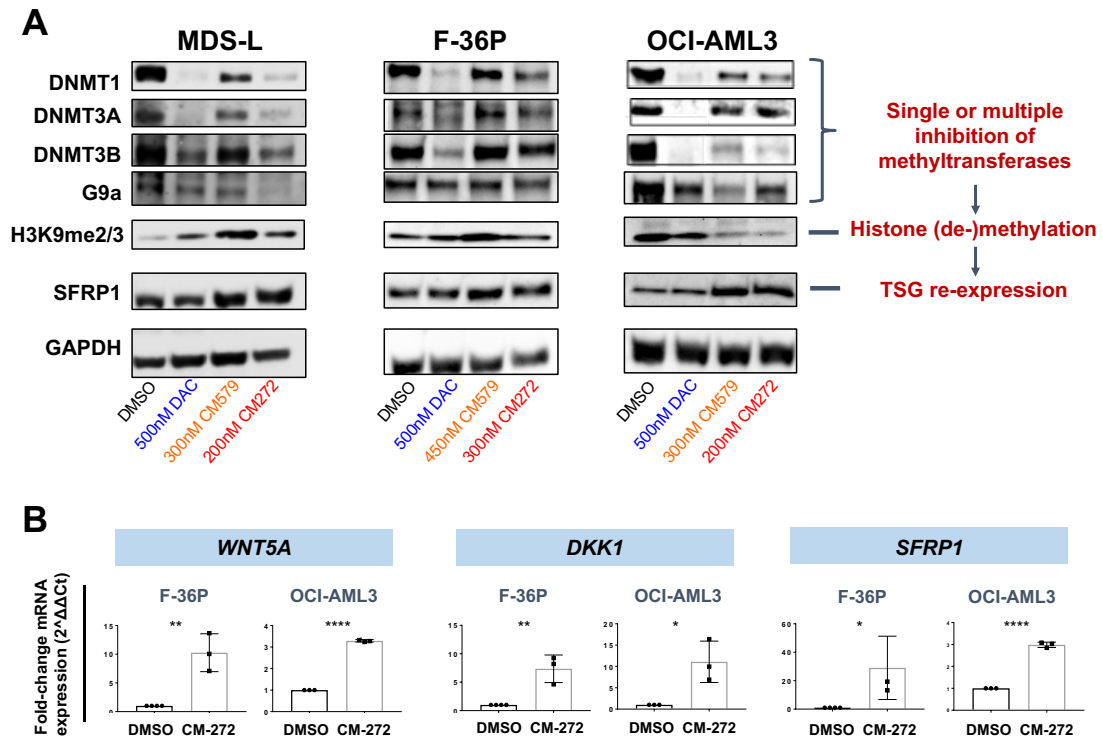


Figure 16: Impact of epigenetic inhibition on DNMTs, G9a, WNT antagonists, and H3K9me2/3.

(A) MDS-L, F-36P, and OCI-AML3 cells were treated with DAC (daily), CM-579, and CM-272 (both once) and DMSO for 72 h. By western blot, the impact of the drugs on the proteins DNMT1, DNMT3A, DNMT3B, G9a, and SFRP1 as well as the histone mark H3K9me2/3 were investigated. Two biological replicates showed similar results so that representative pictures were used here. (B) By RT-qPCR analyses, the mRNA of the WNT antagonists WNT5A, DKK1, and SFRP1 were detected in F-36P and OCI-AML3, not in MDS-L (data not shown). Fold-changes of CM-272 treatments versus DMSO was determined by the $2^{-\Delta\Delta CT}$ method using the housekeeping gene b2M. Statistical evaluation was done using the unpaired t-test. Mean with \pm SD of at least three biological replicates and two technical replicates were measured. p-values: > 0.05 (ns); \leq 0.05 (*); \leq 0.01 (**); \leq 0.001 (***) ; \leq 0.0001 (****)

6.1.3 CM-272 leads to apoptosis, cell cycle arrest, reduced colony formation and decreased proliferation without DNA damage of MDS/AML cell lines

Next, we wanted to understand the phenotypic effect on MDS-L, F-36P, and OCI-AML3 cells after CM-272-specific DNMT and G9a inhibition. Therefore, biological processes including proliferation, apoptosis, DNA damage, cell cycle, and tumor colony-formation were investigated. Cleaved PARP indicates the degree of apoptosis and phosphorylated H2AX represents a marker for DNA damage in cells, which were analyzed by FACS. All three cell lines showed elevated apoptosis without DNA damage upon drug treatment compared to DMSO control. (Figure 17A and B)

Using BrdU and DAPI in FACS, proliferation and the phases of cell cycle distribution could be investigated. Interestingly, CM-272-treated OCI-AML3 cells highly significantly reduced their proliferation and predominantly stayed in the G0/G1 phase (quiescence stage). The proportion of G0/G1 phase cells in the drug-treated MDS-L cells also increased while their proliferation decreased. In F-36P cells, the proliferation and the cell cycle phases changed only slightly towards cell quiescence. (Figure 17C, D)

The colony-forming potential upon dual inhibition of DNMTs/G9a by CM-272 in the three cell lines were reduced significantly. More concrete, the colony size/cell number of a single colony as well as the number of total colonies was lowered in the drug-treated samples and was dose-dependent at nM. (Figure 17E)

In summary, CM-272 seemed to predominantly affect the cell cycle of OCI-AML3 cells by trapping the cells in the G0/1 phase and reducing their proliferation. However, it did not induce DNA damage. This CM-272 blockage effect translated downstream by induction of apoptosis and reduction of tumor-growth potential.

Results

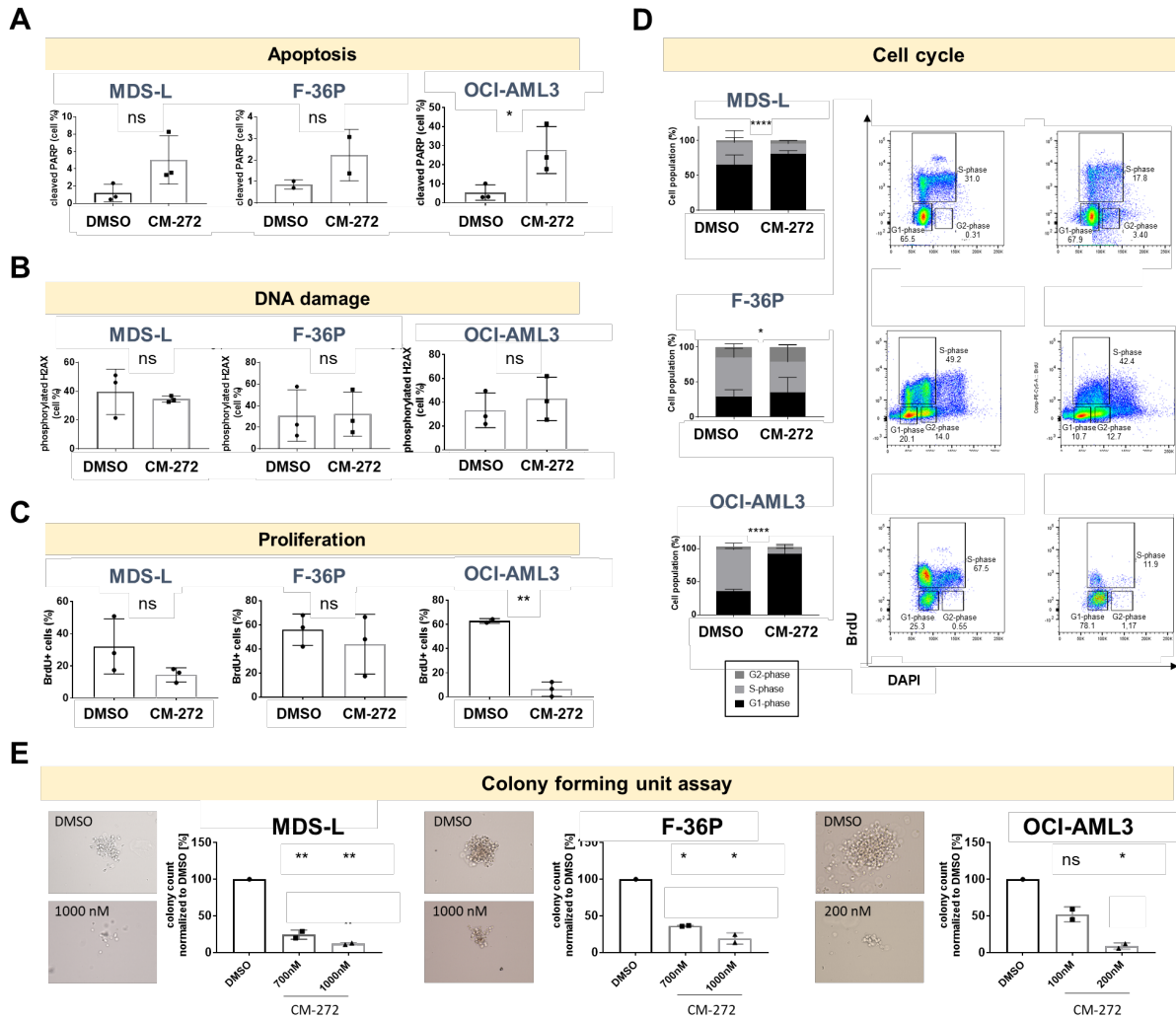


Figure 17: Functional assays with MDS/AML cell lines upon CM-272 treatment.

MDS-L, F-36P, and OCI-AML3 cells were treated with CM-272 or DMSO for 72 h and further analyzed by FACS (A-D) and Matrigel culturing (E). (A) Apoptosis, (B) DNA damage, (C) proliferation, and (D) cell cycle of live cells (DAPI-excluded cells) were investigated and means with \pm SD of biological and technical triplicates were measured. By DAPI and BrdU staining, different cell populations of the cell cycle phases G1, S, and G2 could be discriminated as depicted in the scatter plot examples. (E) CFU assays were performed in two biological replicates of all three cell lines. RGB pictures of the colonies were taken with a 20x objective. FACS data were statistically analyzed by unpaired t-test and the CFU assays by the one-way ANOVA. p-values: > 0.05 (ns); ≤ 0.05 (*); ≤ 0.01 (**); ≤ 0.001 (***) ; ≤ 0.0001 (****)

6.2 Antitumor effect on patient-derived AML cells by CM-272

In the next part, the promising results of the MDS/AML cell line models were verified by patient-derived AML cells. Since CM-272 was highly potent in OCI-AML3 harboring the most common AML mutations (DNMT3A, NPM1c), five different patient samples from different tissue of origin with AML-driver mutations were examined. They harbored a combination of FLT-ITD and NPM1c, or FLT-ITD, NPM1c, and DNMT3A-R882 mutations and were derived from the peripheral blood (PBMC) or directly from the bone marrow (Figure 18A). In contrast to previous cell line treatments, these more fragile, cryopreserved cells were treated with very low concentrations of CM-272 (30nM, 100nM, and 300nM, patient 2: additionally 500 nM, 1000nM) to investigate its specific anti-tumor effects. After 72 h of treatment, cytotoxicity, apoptosis, CFU assays, and cell morphology experiments were performed. (Figure 18B)

Despite of the low doses of CM-272, all patient samples responded strongly by showing a drop of cell viability in a dose-dependent manner. Patient 3 (mutated FLT-ITD and NPM1c, from PBMC) reacted most sensitively to the treatment. (Figure 18C-E)

Caspases are essential protease enzymes which are involved in programmed cell death. The activity of the caspase 3/7, so called executioner caspases were highly significantly increased in 4 out of 5 samples indicating an increase in apoptotic activity. (Figure 18D)

A significantly reduced colony number and smaller colony diameter of blast cells were observed in 3 out of 4 specimens by CFU, which was dose-dependent. Patient 4 cells did not survive the CFU experiment so these data could not be included in the evaluation. (Figure 18E)

Additionally, a May-Grünwald + Giemsa staining revealed morphological changes of the drug-treated cells towards myeloid differentiation. Typically, the cytoplasm-to-nucleus ratio increased and the nucleus was detected to be invaginated. (Figure 18F)

These results confirmed previous findings with OCI-AML3 regarding elevated apoptosis and cell differentiation.

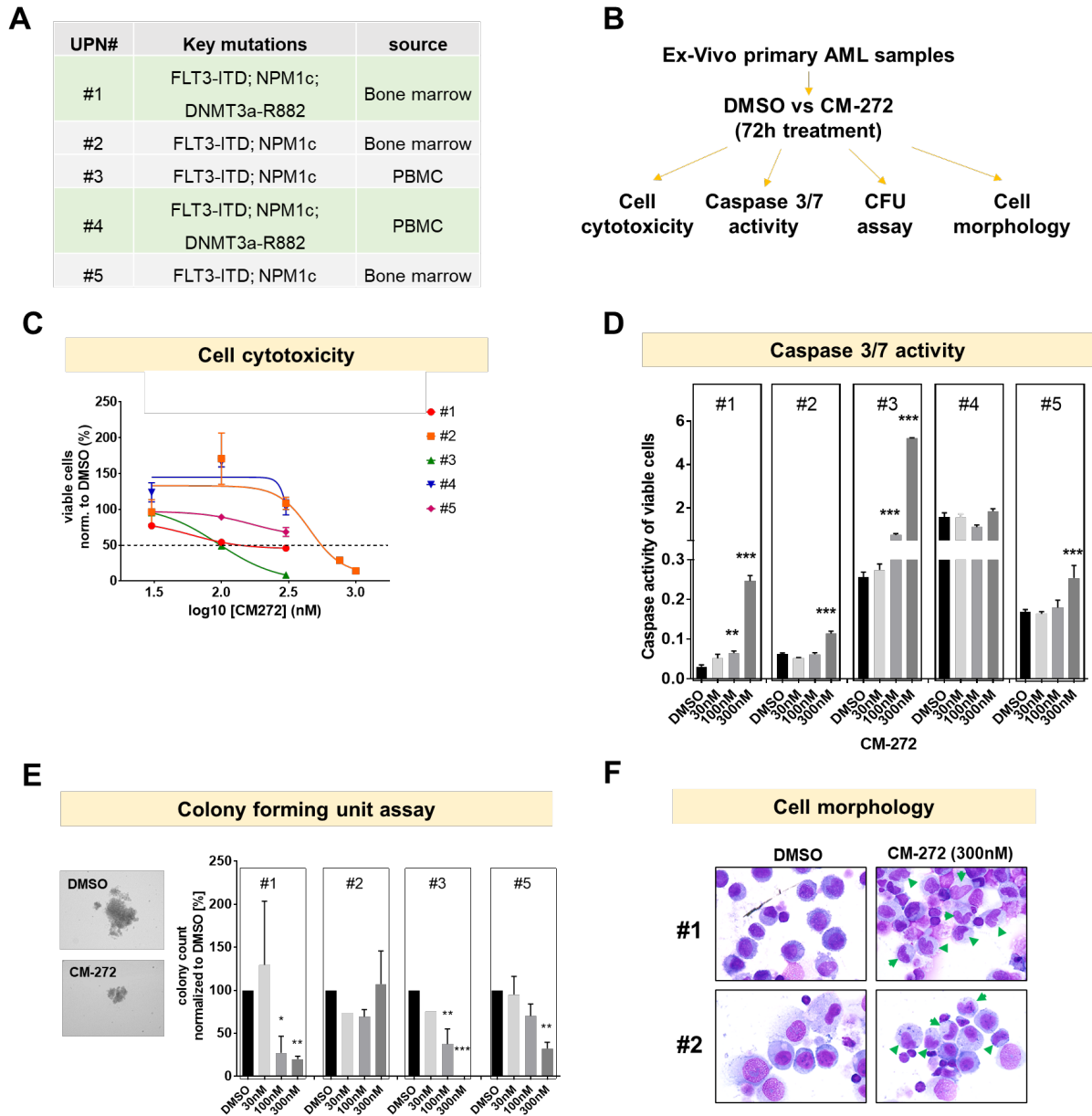


Figure 18: Functional assays with CM-272 treated patient-derived AML blasts.

(A) The potency of CM-272 were tested on five different patient-derived AML samples of different origin and genotype. (B) All performed assays are schematically depicted. After 72 h CM-272 treatment, their cell viability, Caspase 3/7 activity, CFU potential and cell morphology were investigated and compared to DMSO control. (C) Cytotoxicity and Caspase 3/7 activity assays were performed in triplicates. (E) CFU assays were carried out in technical duplicates and examined with a 20x objective in the Trans-channel. One-way ANOVA was performed to test statistical significance. (F) Cells were stained by a Kwik-Diff stain kit and analyzed with an 60x objective in the RGB channel. p-values: > 0.05 (ns); ≤ 0.05 (*); ≤ 0.01 (**); ≤ 0.001 (***); ≤ 0.0001 (****)

6.3 Transcriptional reprogramming by CM-272 in MDS/AML cell lines

Previous results showed an upregulation of the genes WNT5A, DKK1, and SFRP1 due to dual inhibition of DNMTs/G9a by CM-272 (see 6.1.2, Figure 16B). Functional assays also indicated a reprogramming of CM-272 treated MDS/AML cells. (see 6.1.3 and 6.2)

By RNA-Seq, the whole transcriptome of a bulk cell population treated with CM-272 could be investigated more broadly and affected genes and their corresponding signaling pathways could be identified. MDS-L, F-36P, and OCI-AML3 treated with CM-272 cells showed a transcriptomic change compared to DMSO control (Figure 19A). The majority of changed genes were upregulated. OCI-AML3 was the most responsive cell line with the highest number of upregulated genes (947 total) followed by F-36P (328 total). MDS-L harbored the lowest amount of changed gene transcripts (143 total). When comparing the altered transcript pattern among the three cell lines, only two genes were commonly downregulated and 22 genes were commonly upregulated in the three cell lines demonstrated by Venn diagrams (Figure 19B). The commonly upregulated genes are either involved in an antiviral immune response (e.g. type I IFN signaling pathway), chromatin remodeling (e.g. nucleosome assembly), or TF activation (e.g. AP1 transcription factor complex). (Figure 19B)

In summary, CM-272 led to a transcriptional reprogramming of MDS/AML cells. These findings can be used to explain the underlying mechanisms behind the antitumor response of the cells.

Results

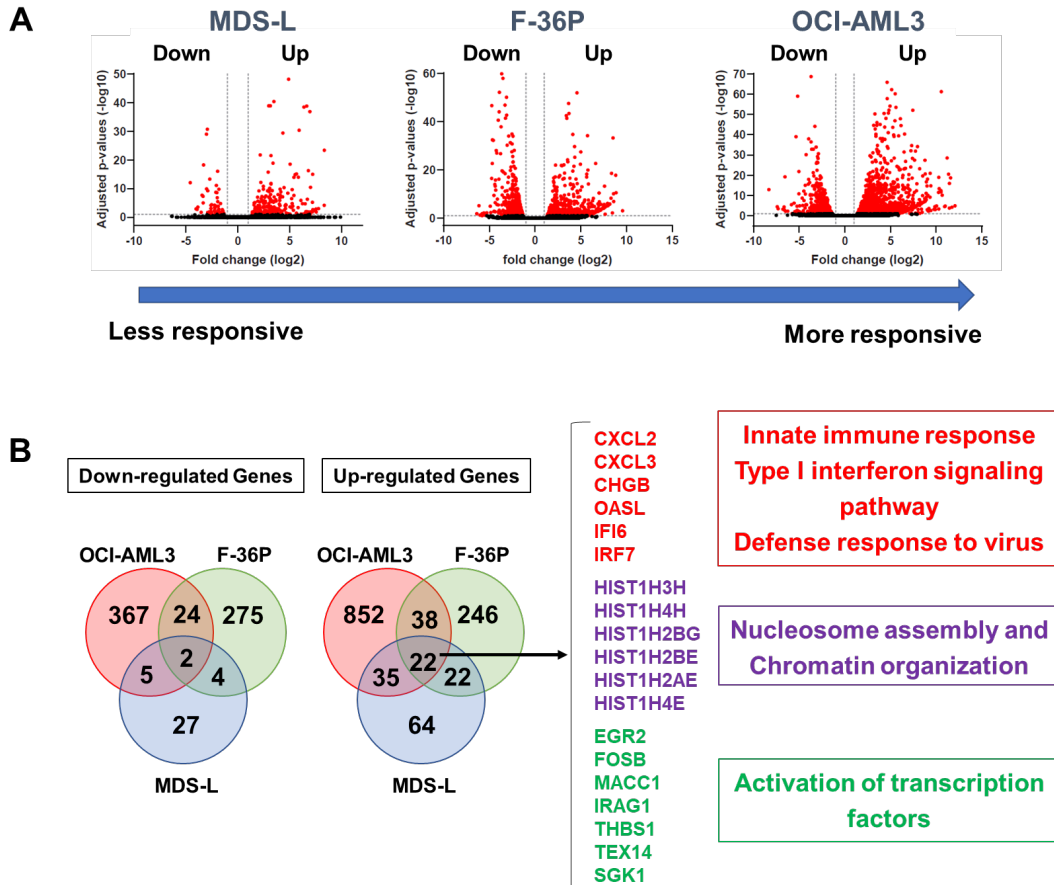


Figure 19: Commonly affected pathways in MDS-L, F-36P, and OCI-AML3 by CM-272 treatments.

(A) Volcano plots of RNA-Seq data of CM-272 treated MDS-L, F-36P and OCI-AML3 cells (72 h) of three biological replicates each. Up- and downregulated genes are reported as red dots and not differentially expressed genes (DEGs) are represented as black dots. P-threshold (=0.05) is indicated by the dotted line.

(B) Venn diagrams illustrate commonly up- and downregulated genes among the three drug-treated cell lines. 22 commonly upregulated genes are separately listed and assigned to specific signaling pathways.

6.3.1 Activation of an antiviral immune response of MDS/AML cell lines upon CM-272 treatment

As already seen in the previous RNA-Seq data, the antiviral immune response is one commonly upregulated signaling pathway upon CM-272 treatment in the MDS/AML cell lines. IFI6 and OASL, which are interferon-stimulated genes induced by various kinds of virus infections^{215,216} were shown to be commonly upregulated in CM-272 treated cells analyzed by RNA-Seq and confirmed by RT-qPCR (Figure 20A and B).

Furthermore, whole transcriptome analysis did not only provide data of mRNA expression but also dsRNA expression deriving from long terminal repeats (LTRs) of endogenous retroviruses (ERVs). LTR/ERV expression is associated with a type I IFN immune response and indeed, 85 LTR/ERVs were seen to be significantly upregulated including LTR7, MLT2A2, and LTR12C (Figure 20C).

Next, the cytokines IL-4, IL-8, and TNF α involved in viral defense mechanisms were explored in MDS-L, F-36P, and OCI-AML3 cells treated with DMSO or CM-272 for 48 h. The concentration of the secreted cytokines was determined by a Luminex assay. IL-8 secretion was highly significantly upregulated in MDS-L and OCI-AML3. IL-4 was moderately increased in MDS-L and OCI-AML3 and TNF α was seen to be slightly higher in the drug-treated F-36P and OCI-AML3 cells (Figure 20D).

These findings of CM-272-induced antiviral immune response in the MDS/AML cell lines confirmed the initial RNA-Seq analysis.

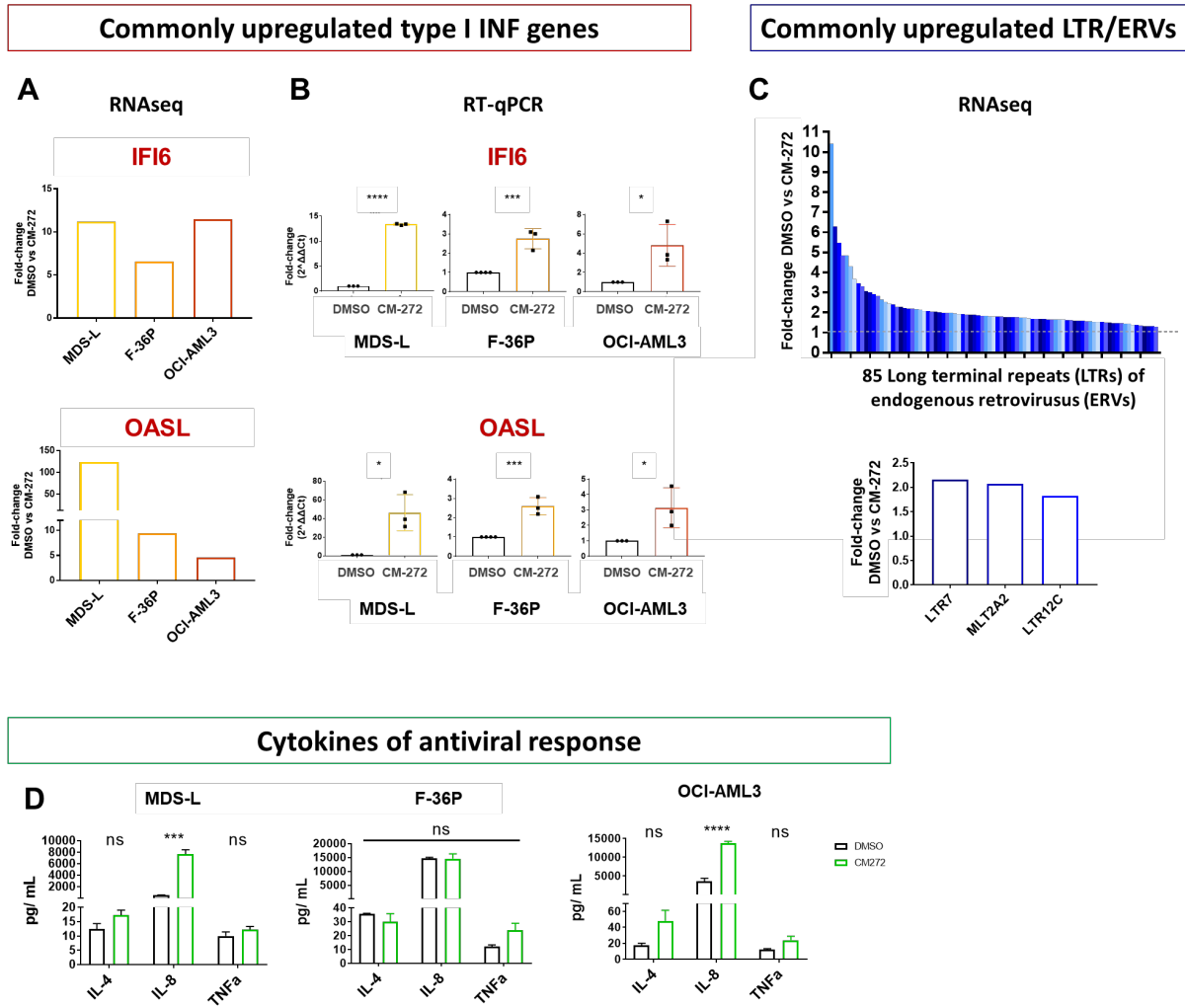


Figure 20: Antiviral immune response induced by CM-272 in MDS-L, F-36P, and OCI-AML3

(A) By RNA-Seq and (B) RT-qPCR, the mRNA expression of type I IFN-associated genes IFI6 and OASL was investigated in three cell lines treated with DMSO or CM-272 for 72 h. Gene expression of three biological replicates by RT-qPCR analysis was determined as described above (see Figure 16B). Statistical analysis was done using the unpaired t-test. (C) Upregulation of dsRNAs of LTR/ERV was also investigated by RNA-Seq. LTR7, MLT2A2, and LTR12C are upregulated LTR/ERVs associated with antiviral immune response and shown in a separate plot. (D) The cytokines IL-4, IL-8, and TNF α were investigated by a Luminex assay of MDS-L, F-36P, and OCI-AML3 treated with DMSO or CM-272 for 48 h (n=2). p-values: > 0.05 (ns); \leq 0.05 (*); \leq 0.01 (**); \leq 0.001 (***) ; \leq 0.0001 (****)

6.3.2 Myelomonocytic differentiation of OCI-AML3 upon CM-272 treatment

OCI-AML3 showed the most dramatic transcriptomic shift towards upregulation of genes (see 6.3) and the most significant effect on apoptosis, cell quiescence, and cell differentiation (see 6.1.3). Therefore, we were interested to better understand the underlying mode of action of CM-272 in OCI-AML3.

Twelve upregulated genes in CM-272-treated OCI-AML3 compared to the DMSO were found to be associated with myelomonocytic differentiation including FOSB and EGR2 (Figure 21A and B). By RT-qPCR, these myeloid TFs were also seen to increase in the treated samples. Furthermore, an upregulated gene signature specific for monocyte cell identity and an enhanced transcription of gene sets for myeloid cell differentiation could be identified by GSEA analysis of the RNA-Seq data (Figure 21C).

Functional assays including FACS and May-Grünwald + Giemsa stainings of OCI-AML3 treated with CM-272 supported the previous findings of myelomonocytic differentiation. The expression of monocytic differentiation markers CD14 and CD11b were both significantly upregulated upon CM-272 treatment. (Figure 21E) Treated cells also showed signs of cytological differentiation including increased cytoplasm-to-nucleus ratio and invagination of the nucleus. (Figure 21D)

In summary, these findings indicated that CM-272 mediated a myelomonocytic differentiation of OCI-AML3 cells. In the next chapter, the HOX/MEIS1 signaling axis was further investigated to find a mechanistic explanation for the myelomonocytic differentiation of OCI-AML3 upon CM-272 treatment.

Results

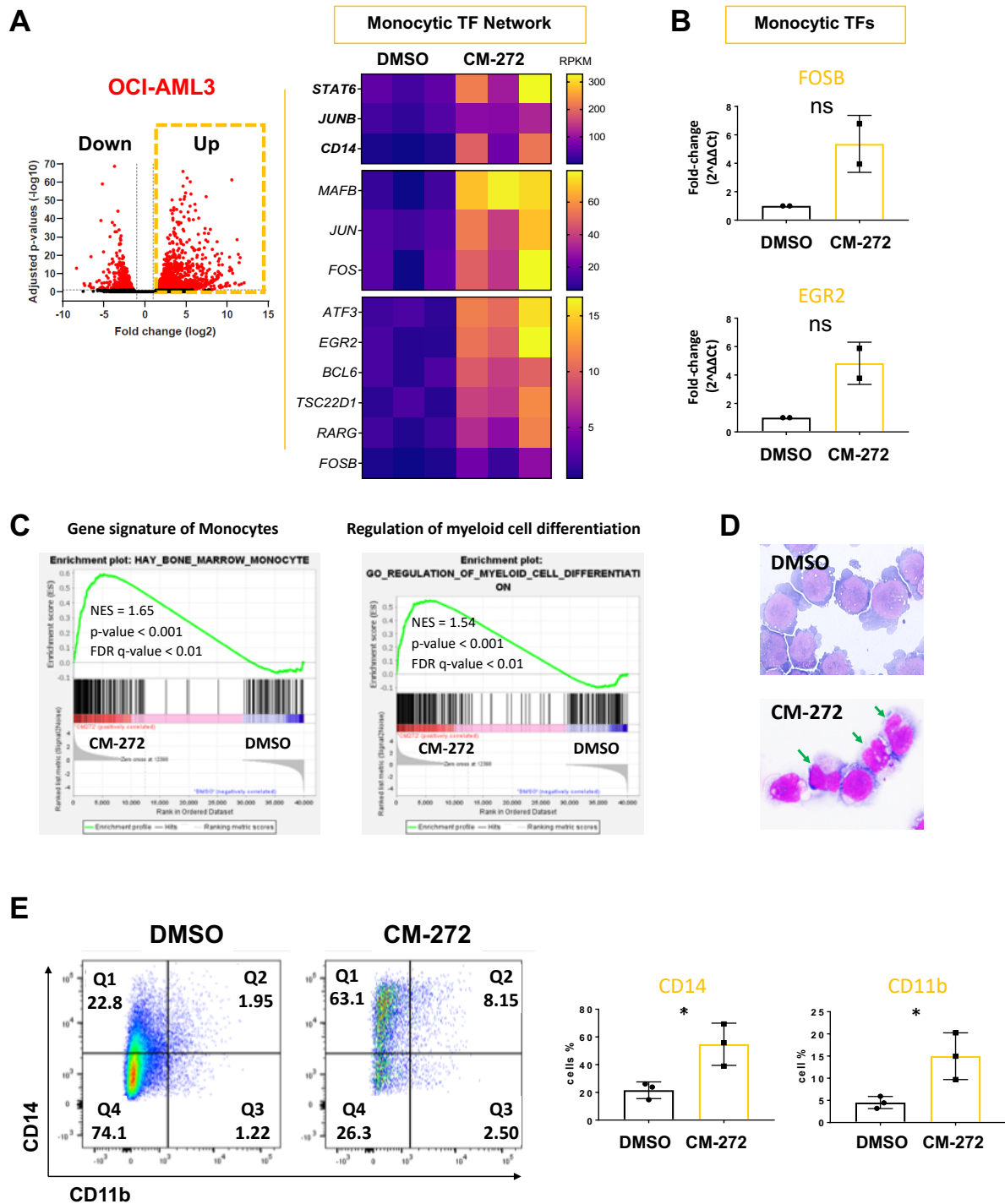


Figure 21: CM-272-mediated differentiation of OCI-AML3 cells.

(A) Volcano-plot and heat map of RNA-Seq data of CM-272 treated OCI-AML3 identified upregulated genes and their association with myelomonocytic differentiation. (B) Further validation of CM-272-treated cells (72 h) by RT-qPCR was done on myeloid TFs (FOSB and EGR2) and myeloid blockers/ HOX gene targets (PBX3 and MEIS1). Gene expression was analyzed as described above (Figure 16B). Statistical analysis was done using the unpaired t-test. Means with \pm SD of at least three biological replicates were examined. (C) GSEA analysis of the RNA-Seq data identified gene sets that are associated with monocytic differentiation of CM-272-treated OCI-AML3. (D) Cell morphology of DMSO or drug-treated cells after 72 h was examined by May-Grunwald + Giemsa staining. RGB pictures were taken with a 100x objective. (E) Differentiation markers CD14 and CD11b were investigated by FACS after 72 h drug treatment. CD14 and CD11b detection is depicted by representing scatter plots. All assays were performed in biological and technical triplicates and the mean with \pm SD was measured. p-values: > 0.05 (ns); \leq 0.05 (*); \leq 0.01 (**); \leq 0.001 (***) ; \leq 0.0001 (****)

6.3.3 CM-272 induces XPO1 downregulation, nuclear relocalization of NPM1c and decreased HOX gene expression in OCI-AML3

A mutation of the nuclear protein NPM1 gene in OCI-AML3 results in a loss of the NoLS (nucleolar localization signal) and the generation of a novel C-terminal nuclear export signal (NES) motif. Consequently, the mutated NPM1c dislocates via the nucleo-cytoplasmic transport protein XPO1 to the cytoplasm. This leads to aberrant upregulated HOX genes and reinforces an undifferentiated phenotype of AML blasts (Figure 22A). This disturbed molecular process was examined in CM-272-treated OCI-AML3 due to previous findings of myelomonocytic differentiation upon drug treatment.

RNA-Seq data revealed a significant downregulation of the mRNA expression of XPO1 upon CM-272 treatment (Figure 22B). Furthermore, the subcellular localization of NPM1c in DMSO and CM-272 samples was investigated by cell fractionation and western blot. The amount of NPM1c in the nucleus was 4-times higher in the treated cells than in the DMSO control (Figure 22C). As a response to the XPO1 downregulation and NPM1c relocalization, the myeloid blockers and HOX gene targets were downregulated in drug-treated OCI-AML3 (Figure 22D).

Together, these results indicate that repression of the XPO1 transporter, the relocalization of NPM1c and the downregulation of HOX genes is one very important CM-272-mediated mechanism contributing to the myelomonocytic differentiation of OCI-AML3.

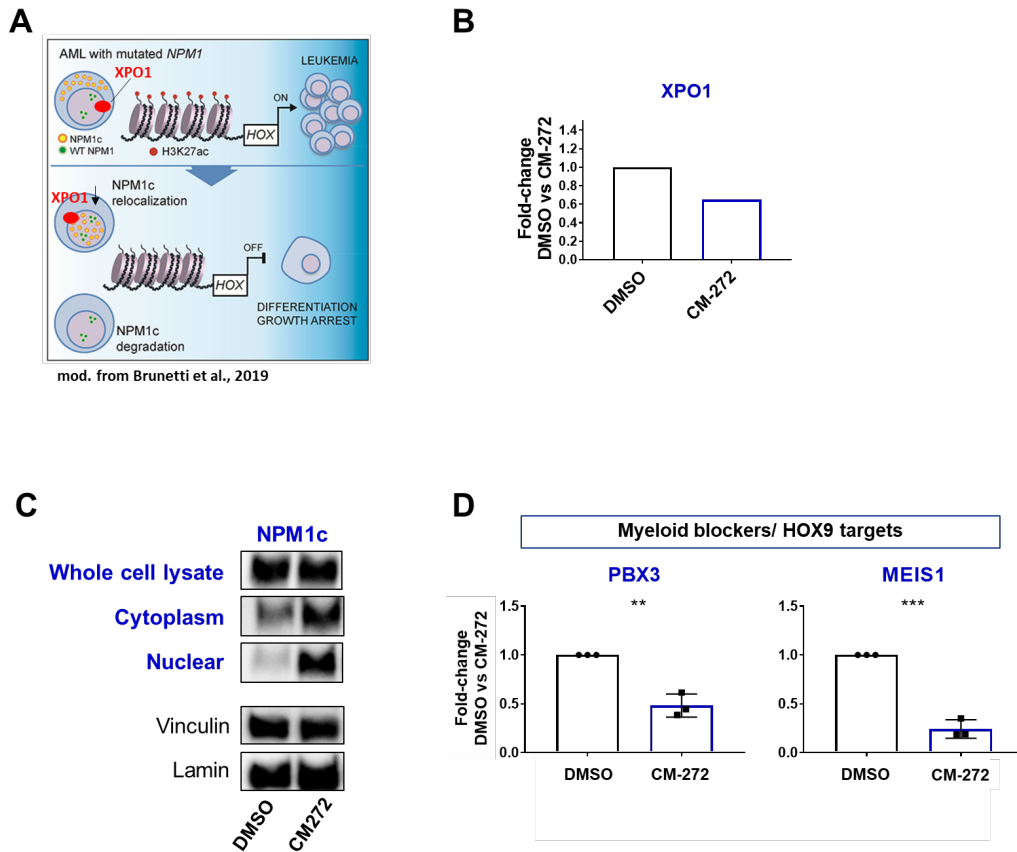


Figure 22: XPO1 downregulation leads to nuclear relocalization of NPM1c and decreased HOX gene expression in CM-272-treated OCI-AML3.

(A) In this schematic representation, the mechanism of decreased differentiation of AML blast harboring a NPM1 mutation is shown. **(B)** By RNA-Seq, the XPO1 transcription level was investigated in OCI-AML3 cells treated with DMSO or CM-272. **(C)** NPM1c was analyzed in whole cell lysate, cytoplasm, and nucleus in the CM-272 samples and compared to the protein proportion in the DMSO control (72 h treatment). Vinculin and lamin were used as loading controls (n=2). **(D)** mRNA expression of the myeloid blockers and HOX9 co-factors PBX3 and MEIS1 were investigated by RT-qPCR as described above (n=3). Statistical analysis using the unpaired t-test was performed to show statistical relevance of the data. Means with \pm SD of at least three biological replicates were examined. p-values: > 0.05 (ns); \leq 0.05 (*); \leq 0.01 (**); \leq 0.001 (***); \leq 0.0001 (****)

6.4 Generation of a suitable reporter gene cell line for screening of epigenetic agents

FDA- and EMA-approved drugs such as decitabine and azacitidine (DNMTi) were shown to reverse the hypermethylated state of transcriptionally silenced genes in tumor cells.¹⁸⁸ By a reporter gene cell line, the potency of different hypomethylating agents could be more feasibly investigated in a high-throughput manner to assess the temporal and dynamic changes in gene activation. For such drug screenings, a fluorescence reporter gene (mCherry) under the control of an epigenetically suppressed gene in an AML cell line could be used. In the figure below, the mechanism of the reporter gene cell line is illustrated.

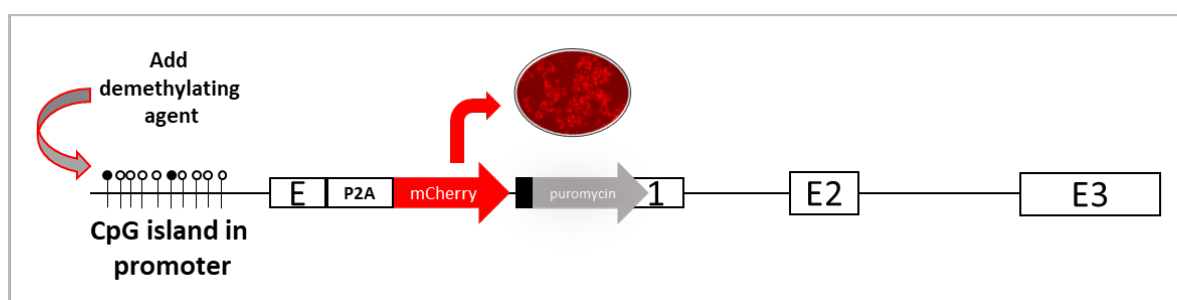


Figure 23: Schematic representation of the functionality of a reporter gene cell line for screening of epigenetic drugs.

A DNA fragment containing the reporter gene mCherry needs to be inserted downstream of an epigenetically suppressed gene promoter. Exon 1-3 (E1-3) represents the coding region of the analyzed gene SFRP1 in which mCherry has to be integrated. By applying demethylating agents, the hypermethylated promoter is demethylated, which reactivates the expression of the silenced gene together with the fluorescence gene mCherry. This reactivation can be visualized by fluorescence microscopy or FACS. Puromycin is supposed to be used as a selection marker for positively edited cells. A P2A sequence is used to separate the proteins SFRP1 and mCherry.

6.4.1 The SFRP1 gene can be used for epigenetic drug screening in AML

Previous findings of this work already showed that SFRP1 is downregulated by DNA and histone methylation in MDS and AML. CM-272 treatments of MDS-L, F-36P, and OCI-AML3 led to a reactivation of the SFRP1 expression (see Figure 16 and chapter 6.1.2). To generate a suitable AML reporter cell line, the link between downregulation of mRNA expression and DNA hypermethylation in SFRP1 was further investigated.

CpG islands within the promoter of SFRP1 were examined by two different DNA methylation methods. By pyrosequencing, the DNA methylation status of five CpG sites within the promoter of SFRP1 (Figure 24A) of two healthy tissues (MNC, placenta) and three AML cell lines (MOLM13, UoCM1, KG1a) were analyzed. All five CpG sites showed a much higher DNA methylation level in the diseased cells compared to MNCs and placenta (Figure 24B). These data were confirmed by the MassARRAY analysis investigating a larger region of the SFRP1 promoter (Figure 24A). The

Results

average DNA methylation level of five CpGs of healthy MNC and placenta cells were compared to MDS/AML cell lines (MDS-L, F-36P, MOLM13, KG1a, SKM1, UoCM1, OCI-AML3). The SFRP1 promoter was seen to be much higher methylated in cancer cells than in healthy cells. The DNA methylation of LINE1, which is composed of repetitive elements of interspersed DNA repeats, is commonly used as a surrogate marker for estimated global DNA methylation level. Here, LINE1 was also examined for global DNA methylation in healthy versus diseased cells, which was moderately high among all samples (Figure 24C).

The largest-to-date, public dataset of primary AML samples, so-called Beat AML, offers genomic data (n=451) that were analyzed to examine the mRNA expression of SFRP1 in primary cells. Healthy MNCs were compared to diseased samples including *de novo* or MDS-derived AML (MDS – or MDS +) along with other AML subtypes containing mutations in DNMT3A, STAG2, EZH2, TET2, and ASXL1. On transcriptional level, SFRP1 was seen to be significantly downregulated in MDS/AML samples versus healthy cells (Figure 24D).

Together with our previous results, these data could show that the suppressed mRNA expression of SFRP1 correlates with its epigenetically silenced promoter in a broad range of AML subtypes.

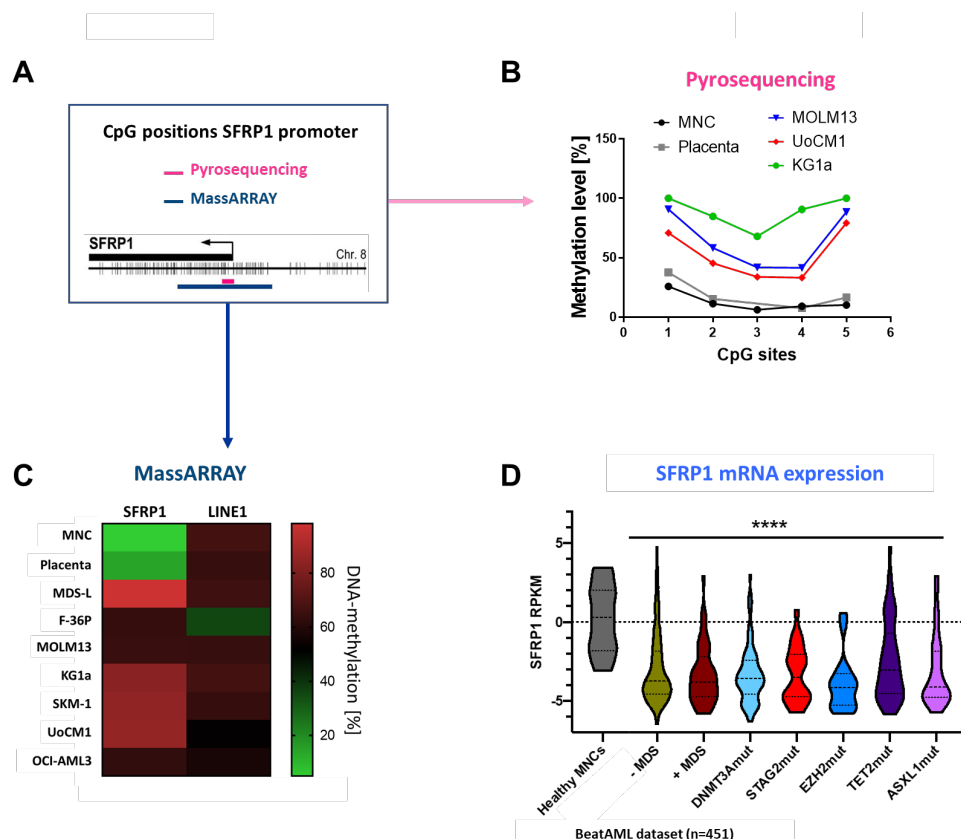


Figure 24: DNA hypermethylation correlates with SFRP1 gene silencing.

(A) Primers for pyrosequencing (pink) and MassARRAY (blue) bind in a CpG island within the promoter of SFRP1. (B) Five CpG sites were investigated in healthy primary cells (black and gray) and AML cell lines (colored) by pyrosequencing (n=1). (C) Using MassARRAY, the average of DNA methylation of five CpG sites was examined in healthy primary cells and MDS/AML cell lines (n=1). LINE1 was used as a control for DNA methylation. mRNA expression of SFRP1 was investigated by BeatAML dataset analysis of 451 primary healthy and AML samples. p-values: > 0.05 (ns); ≤ 0.05 (*); ≤ 0.01 (**); ≤ 0.001 (***); ≤ 0.0001 (****)

6.4.2 Identification of the optimal RNP targeting the SFRP1 gene

Three crRNAs obtained from web-based analysis were examined regarding their efficiency for target-directed binding in the PC3 cell line expressing SFRP1 endogenously. Without the addition of the SFRP1_mCherry_puro construct, the RNP complex was supposed to induce a SFRP1 gene KO only. This gene KO was investigated on protein and DNA level by western blot and a Surveyor nuclease assay, respectively.

PC-3 cells were transfected with one of the three RNPs containing crRNA #1, #2, or #3. Additionally, one sample was electroporated with a GFP vector to investigate the transfection efficiency (GFP sample). An untransfected control (UT control) contained the Cas9 electroporation enhancer only. After 24h, the GFP signal could be detected in our transfection control (Figure 25A). Interestingly, the cell proliferation was higher in the RNP-transfected samples compared to the UT and GFP controls after 72 h (Figure 25B).

The SFRP1 protein level in the crRNA #3 sample declined compared to the UT control and the samples for crRNA #1 and #2. Active β -catenin and cMYC are two downstream proteins of SFRP1 that are negatively regulated by SFRP1. In all three crRNA samples, the protein level of active β -catenin and cMYC were increased compared to the UT control (Figure 25C). Since only crRNA #3 showed a lowering of the SFRP1 protein level, this sample was further investigated by the Surveyor nuclease assay. DNA of the crRNA #3 sample was treated with the S1N, which specifically cleaves heteroduplexes caused by WT/indel mismatches during a PCR. According to the primer binding region and crRNA #3-specific binding site, three PCR bands of different sizes could be observed in sample crRNA #3 treated with the nuclease. The three PCR bands were a mix of PCR products containing a S1N-specific cleavage of heteroduplexes and no cleavage. This generated bands of 100 bp upstream of crRNA #3 binding site, 200 bp downstream of crRNA #3 binding site and a FL band without the S1N cleavage.

These assays indicated that crRNA #3 specifically binds SFRP1 with the highest affinity for the SFRP1 sequence compared to the other two crRNAs leading to the most efficient cleavage and KO by the Cas9 endonuclease (Figure 25D). Therefore, the crRNA #3 was selected for further HDR-based CRISPR/Cas9 editing at the SFRP1 gene site.

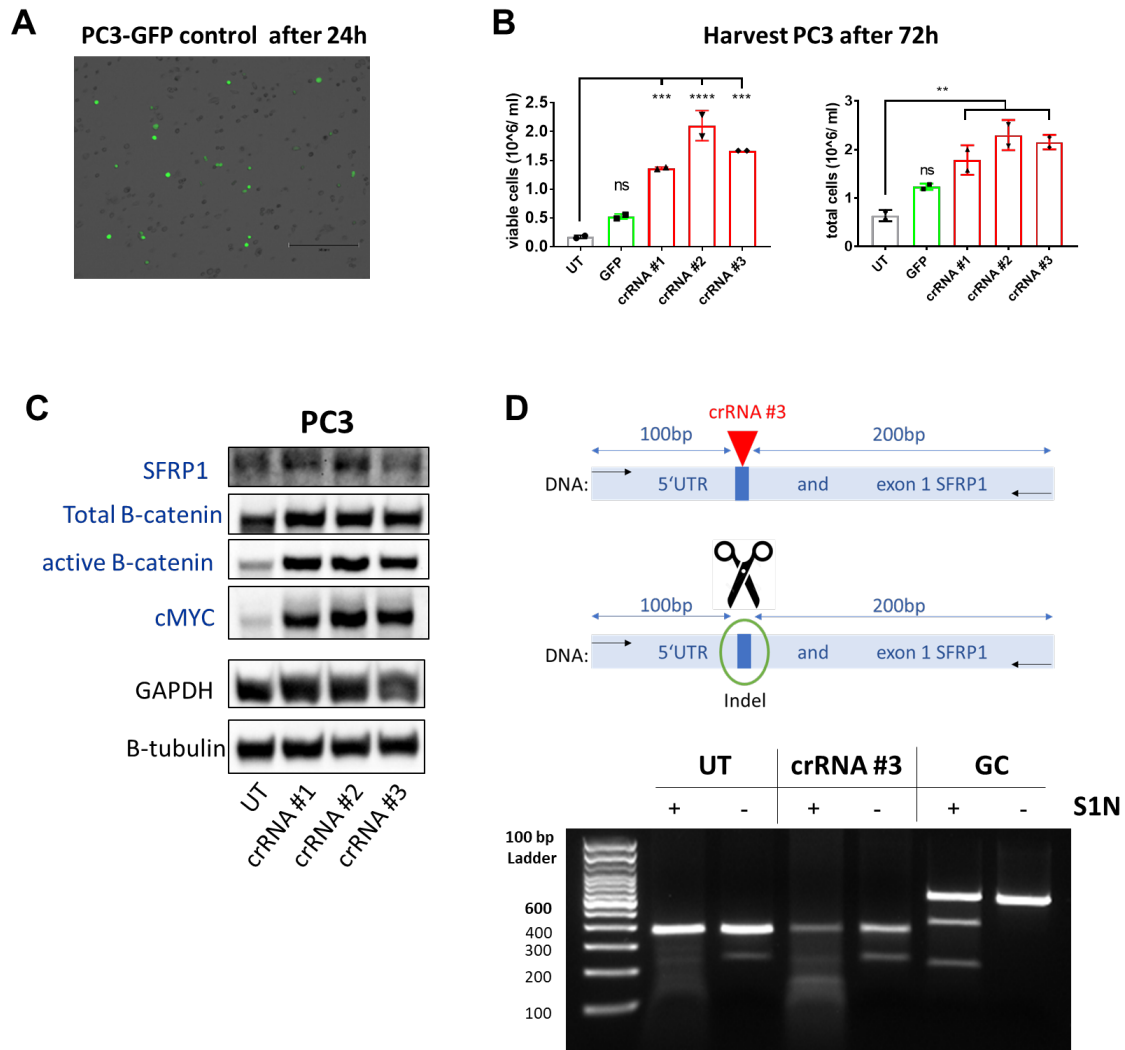


Figure 25: crRNA #3 is the optimal candidate for HDR-mediated CRISPR/Cas9 editing of SFRP1.

The PC-3 cell line was transfected with three different RNPs containing the crRNA #1, #2, and #3. A sample transfected with the GFP vector served as a transfection control. An UT control only contained the electroporation enhancer (UT sample). **(A)** After 24 h, the GFP signal of the transfection control was investigated by fluorescence microscopy in a 4x magnification. **(B)** After 72 h, cells were harvested for western blot and Surveyor nuclease assay. Cell number of harvested cells was determined by trypan blue staining and an automatic cell counting machine (n=2). **(C)** Protein level of SFRP1, total and active β -catenin and cMYC was examined by western blot. **(D)** The agarose gel showed PCR products of the UT control and the crRNA #3 sample treated with the S1N (+) or without (-). A GC control was used to test the nuclease activity. p-values: > 0.05 (ns); \leq 0.05 (*); \leq 0.01 (**); \leq 0.001 (***) ; \leq 0.0001 (****)

6.4.3 Molecular cloning of the SFRP1_mCherry_puro construct

Based on the crRNA #3 binding site within exon 1 of SFRP1, the SFRP1_mCherry_puro construct was generated. It was designed to contain the reporter gene mCherry being in frame and downstream of the SFRP1 promoter. Between SFRP1 and mCherry, a P2A sequence was inserted to avoid the transcription of one fusion protein but to generate two individually expressed proteins. A puromycin-resistant gene (puromycin-N-acetyltransferase) as a selectable marker was integrated downstream of SFRP1 and mCherry and had its own SV40 promoter to be constitutively active. Additionally, the construct consisted of a left and a right homologous arm (LHA and RHA) of SFRP1 being a prerequisite for the HDR-based CRISPR/Cas9 technology. (Figure 26A) Five DNA fragments containing all construct sections were amplified by PCR and assembled to one FL fragment, the SFRP1_mCherry_puro construct (Figure 26B and Table 23). The five PCRs for the fragments (F1-5) and the FL fragment were investigated by gel electrophoresis and sequencing (Figure 26C). Despite the slightly different band size of F3 in the agarose gel, the sequence of the FL fragment was almost 100 % correct. In the SFRP1 LHA region of the construct, three additional nucleotides were detected compared to the reference SFRP1 sequence. A point mutation was also seen in the SFRP1 LHA region that would not result in a frame shift or transcription termination. The exact sequence of the SFRP1_mCherry_puro fragment can be seen in appendix 12.2, Figure 32.

Therefore, the generated SFRP1_mCherry_puro construct was used for the HDR-based CRISPR/Cas9 editing of the SFRP1 gene site.

Results



Figure 26: Molecular cloning of the SFRP1_mCherry_puro construct.

(A) The designed SFRP1_mCherry_puro construct is depicted. P2A (gray) and mCherry (red) were designed in frame with two homologous arms (LHA and RHA) of the SFRP1 gene (blue). The mCherry had a SV40 polyA tail (dark gray). The puromycin-resistant gene (green) had its own SV40 promoter (bright green) and a SV40 polyA tail (dark green). Five fragments (F1-5 with corresponding bp size) were assembled to generate the SFRP1_mCherry_puro construct (2,673 bp total). **(B)** In the agarose gel picture, the five amplified PCR fragments and the SFRP1_mCherry_puro construct are shown. **(C)** The FL construct was sequenced in four parts. The nucleotides from the chromatograms were aligned to the reference sequence of all construct sections (taken from NCBI hg38).

6.4.4 THP-1 is a suitable AML reporter cell line for HDR-based CRISPR/Cas9 editing at the SFRP1 gene site

A suitable cell line for the HDR-based CRISPR/Cas9 editing of the SFRP1 gene had to fulfill two important criteria. First, the cell line needs to be transfectable and editable with such a large DNA fragment of ~ 2,7 kb by HDR-based CRISPR/Cas9. Second, the downregulated expression of SFRP1 has to be regulated by epigenetic processes including DNA methylation.

MDS/AML cell lines MDS-L, F-36P, OCI-AML3, HL-60, and THP-1 as well as the CML cell line K562 were electroporated and treated with puromycin. Only THP-1 and K562 cells survived the antibiotic selection. Both cell lines were further used to generate a reporter cell line. In this thesis, only the THP-1 data are shown.

Edited cells carrying the puromycin selection marker were selected until all negative cells died off determined by an untransfected control. To obtain single cell clones, a subcloning assay was performed in a 96-well plate containing a cell dilution of 0.3 and 0.1 cells per well. 20 single clones were picked, expanded and tested for their construct integration and mCherry expression by PCR and FACS. (Figure 27)

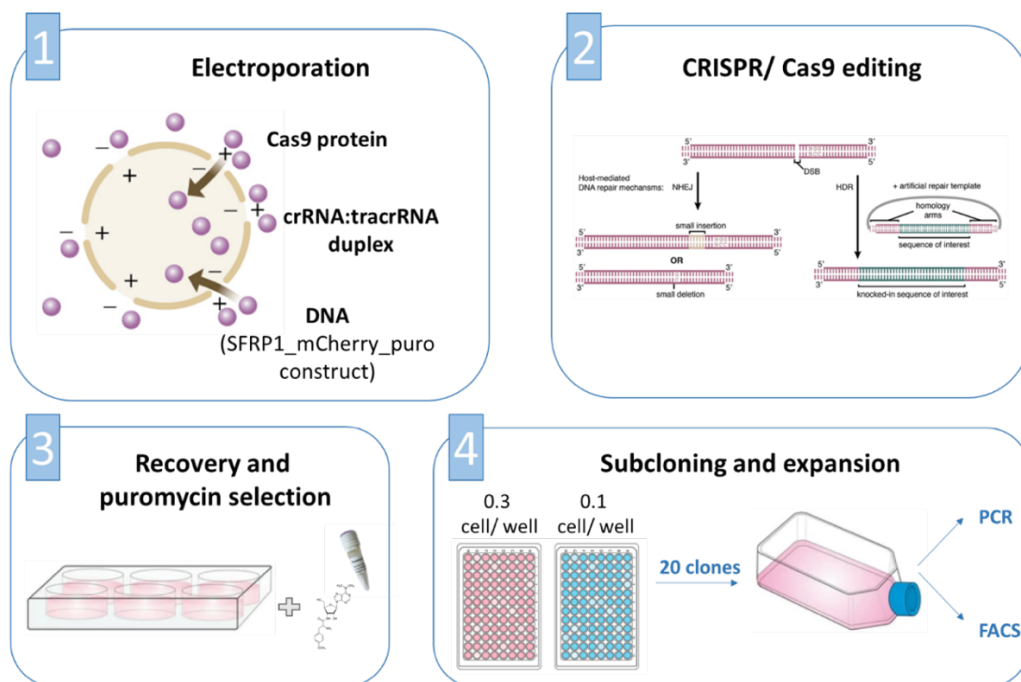


Figure 27: Overview of the transfection of THP-1 cells and obtaining single cell clones.

Schematic overview of how THP-1 single clones containing the SFRP1_mCherry_puro construct were generated. **(1)** Cells were transfected with the Cas9 protein, a crRNA:tracrRNA duplex and the purified SFRP1_mCherry_puro construct by electroporation. (image modified from ²¹⁷) **(2)** A DSB was induced by CRISPR/Cas9 editing which was repaired by the cellular repair mechanisms. NHEJ created indels/KOs and HDR resulted in an integration of the SFRP1_mCherry_puro construct. (image modified from ²¹⁸) **(3)** After a recovery time, cells were selected by puromycin to obtain a mixed population of KI cells. **(4)** By subcloning, 20 clones were picked, expanded and harvested for PCR and FACS analysis. (images created with BioRender.com)

Results

At the same time, THP-1 wild type (WT) cells were treated with DAC (daily dose) and CM-272 (single dose) for 72 h. Dose-response curves revealed no toxicity for DAC and an IC₅₀-value of 458 nM for CM-272 (Figure 28A). Both hypomethylating agents led to a significant re-expression of SFRP1 mRNA of up to 10-fold (Figure 28B).

Therefore, the THP-1 cell line could be used to establish a reporter cell line as a model for drug-induced re-activation of SFRP1 expression.

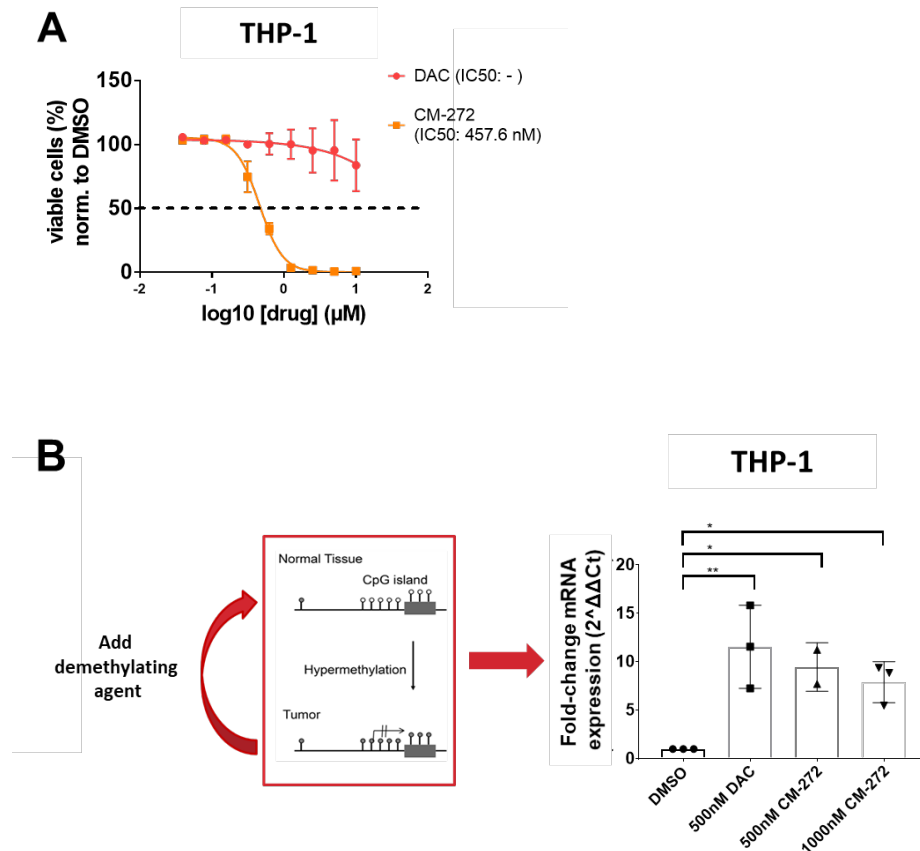


Figure 28: DAC and CM-272 induced a SFRP1 reactivation in THP-1 WT cells.

(A) Dose-response curves of THP-1 WT cells treated with DAC (daily) and CM-272 (once) for 72 h (n=2). **(B)** For 72 h, THP-1 WT cells were treated with DAC, CM-272, or the DMSO control. SFRP1 mRNA expression was analyzed by RT-qPCR (n=3). One-way ANOVA was performed for statistical evaluation. p-values: > 0.05 (ns); ≤ 0.05 (*); ≤ 0.01 (**); ≤ 0.001 (***) ; ≤ 0.0001 (****)

6.4.5 Validation of single cell clones of THP-1 by genotyping and FACS

The genotype of 20 cell clones of THP-1 was determined by PCR. We assumed that all clones carried at least one knockin (KI) allele after puromycin selection. Therefore, three different genotypes were possible: SFRP1^{ki/ki}, SFRP1^{ki/ko}, and SFRP1^{ki/WT}.

In PCR 1, the LHA and RHA region of SFRP1 was flanked by primers ~350 bp upstream and downstream of the crRNA #3 binding site. The elongation time of the PCR was 30 sec, so that only sequences up to 1 kb could be amplified. This would generate amplicons that derived from a WT or indel/KO allele and excluded the KI allele. According to the agarose gel of PCR 1, all clones harbored at least one WT or KO allele. To investigate a potential KI allele with the sequences for mCherry and puromycin, two primer pairs were designed at both sides of the insertion. By PCR 2, the LHA and mCherry region was investigated while PCR 3 was used to examine the puromycin and RHA region. Clone 1, 2, 4, 16, and 20 did not show an amplification for the LHA/mCherry region indicating a lack of correct insertion by small mutations within the primer binding region or bigger deletions of the construct. Consequently, the mRNA transcription, protein folding and function of mCherry could be disturbed in these five clones. In some of the clones, the bands were slightly higher (e.g. 9) or lower (e.g. 10) which can be associated with minor nucleotide changes. The puromycin/RHA region could be detected in all clones by PCR 3.

These results indicated that all clones carried one allele with a WT or KO and another allele with a partial or complete KI (Figure 29A).

In the next part, the 20 clones were additionally validated by DAC treatments (daily for 72 h) to examine their response to the demethylation. DAC is widely used to investigate re-expression of epigenetically silenced genes and can be applied in a broad range of concentrations that are not toxic to THP-1 cells (Figure 28A). Furthermore, DAC were seen to re-activate SFRP1 in previous RT-qPCR assays of WT THP-1 cells (Figure 28B). In future experiments, DAC should serve as a reference compound for gene reactivation that will be compared to new components. Therefore, the fold-change mCherry expression of DMSO control versus DAC treatment was analyzed by FACS. The change in fluorescence intensity (MFI) as well as the amount of mCherry positive cells of all single clones compared to WT THP-1 were measured to determine a correct gating strategy (Figure 29B). Interestingly, THP-1 clones reacted differently to the DAC treatment. The amount of mCherry positive cells was 2- to 4-times higher in clones 2, 10, 15 and 16 after DAC treatments. Highest MFI changes were seen in clone 7 and 16 (Figure 29C).

Considering both the PCR and FACS results, we continued to investigate clone 7 and 15. Clone 7 showed the highest MFI changes, but did not alter the amount of mCherry positive cells. Clone 15 increased the proportion of the mCherry population upon DAC treatment in contrast to clone 7. However, the MFI change of clone 15 was lower than in clone 7.

Results

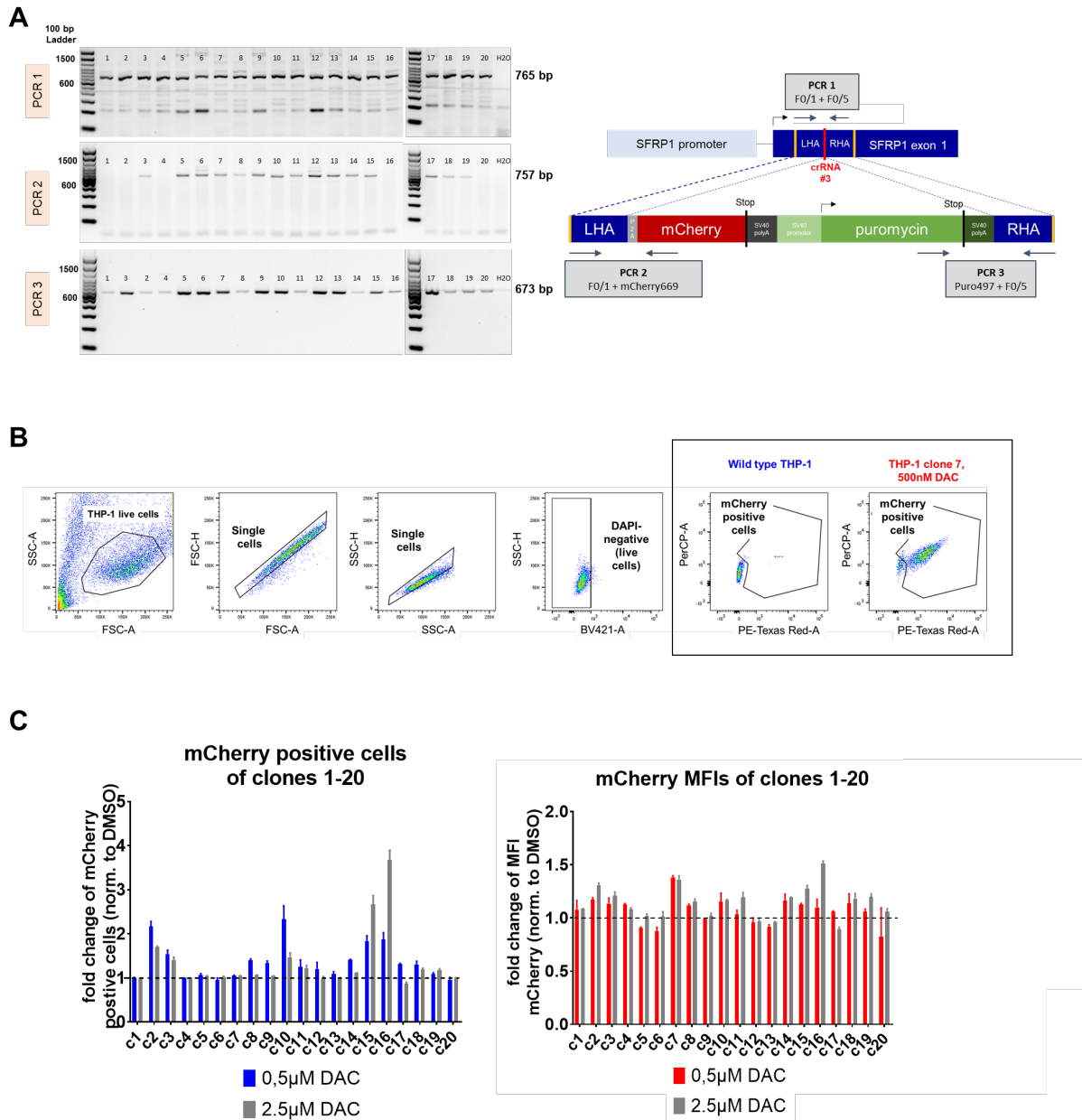


Figure 29: Investigating THP-1 single cell clones by PCR and FACS.

(A) Agarose gels of PCR 1, 2, and 3 (left) and primer binding sites (right) of 20 subcloned samples are depicted. (B) The mCherry signal was investigated on single and live (DAPI-negative) cells by FACS. mCherry cells of the transfected THP-1 clones were distinguished from mCherry negative cells by a THP-1 WT control. (C) For 72 h, 20 single cell clones were treated with DMSO or DAC followed by FACS analysis. The percentage of mCherry cells and the fluorescence intensity (MFIs) of DAC treated clones were normalized to the corresponding DMSO controls to determine the fold-change expression (n=3).

6.5 Investigating the potential of DAC and CM-272 to reactivate SFRP1 in clone 7 and 15 by fluorescence microscopy and FACS

In previous RT-qPCR experiments of THP-1 WT cells, the DNMT1/G9a inhibitor CM-272 could already be seen to re-activate SFRP1 (Figure 28B). In this chapter, this mechanism should be investigated on protein level by comparing the mCherry signal after DAC and CM-272 treatments. In response to DAC treatments, clone 7 changed the mCherry signal intensity and clone 15 elevated the amount of mCherry positive cells, which were used to test the drugs.

For fluorescence microscopy, DAC was applied daily and CM-272 only once on the day of cell plating. mCherry expression of the treated cells was investigated after 24 h, 48 h, 72 h, and 96 h (data not shown). The strongest fluorescence with moderate cell death was seen at 72 h. It could be also shown that the fluorescence intensity and/or the amount of mCherry positive cells of clone 7 increased similarly by both drugs in a dose-dependent manner. Only few mCherry positive cells of clone 15 were detectable for all conditions. Interestingly, the cell size enlarged, as seen in the trans-channel. (Figure 30A)

Next, applications of DAC and CM-272 were quantitatively examined by FACS using THP-1 clone 7 and 15 again. The drugs were either applied once or daily for 72 h to test which is the most efficient treatment schedule to re-activate SFRP1. MFIs as well as percentages of mCherry positive cells were explored. Percentages of mCherry positive cells of clone 7 increased after single treatments of DAC and CM-272, not after three doses. In clone 15, the number of mCherry positive cells was elevated with one- and three-time treatment of DAC, not with CM-272.

MFIs increased after single and daily CM-272 treatment as well as after daily treatment of DAC in clone 7. In clone 15, the mCherry signal intensity inclined upon single treatment of DAC and CM-272 as well as daily treatment with DAC (Figure 30B).

In summary, both drugs induced a reactivation of the SFRP1 promoter detectable by a shift of the mCherry MFIs and the amount of mCherry positive cells. Clone 7 and 15 partly responded differently to the drugs and the treatment regimen. These results indicated that analysis of the MFIs for clone 7 and percentages of mCherry positive cells for clone 15 show the most reliable data.

Results

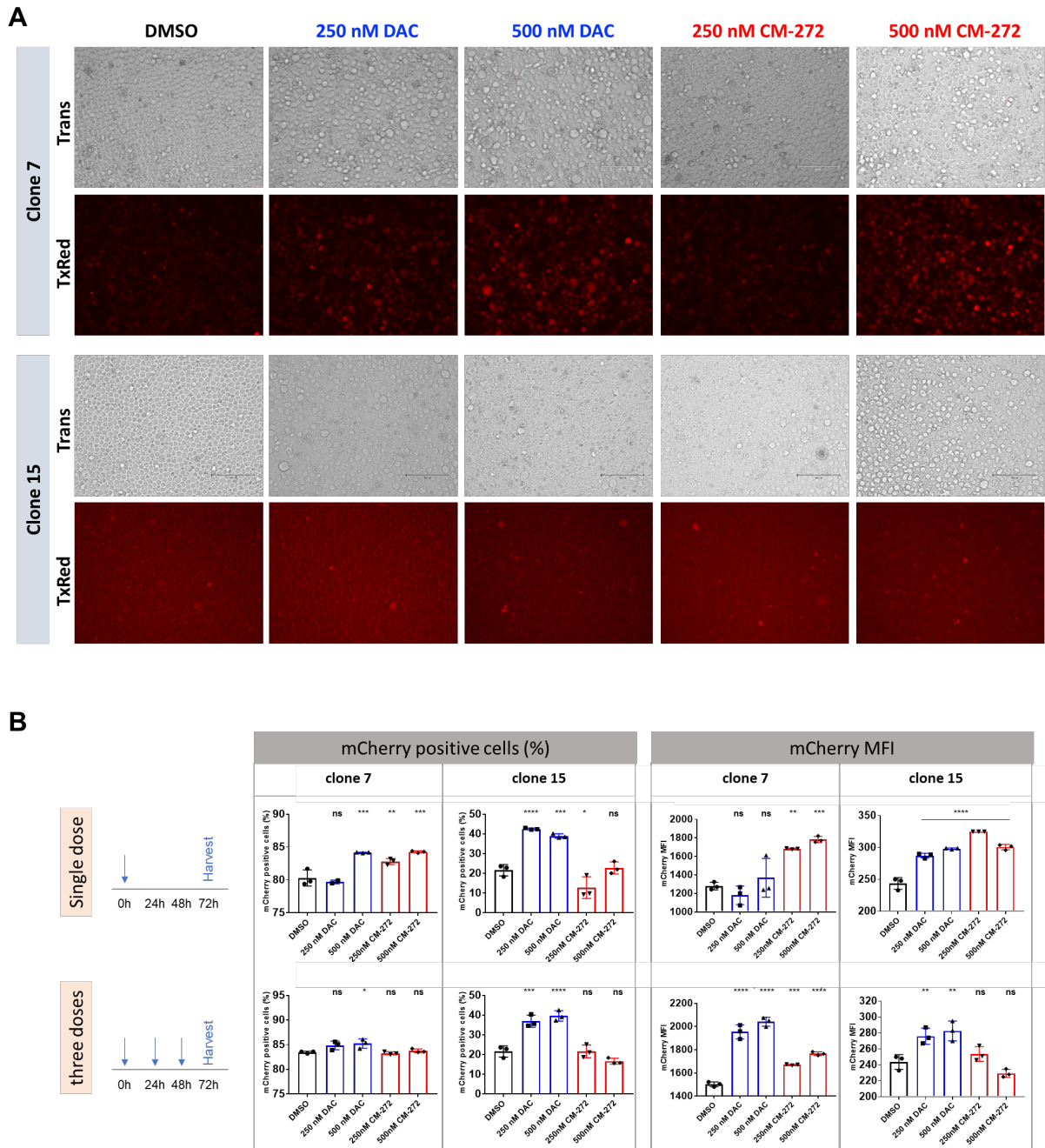


Figure 30: Fluorescence microscopy and FACS of DAC-/ CM-272-treated THP-1 clones 7 and 15.

(A) The mCherry signal of THP-1 clones 7 and 15 after DMSO, DAC (daily) and CM-272 (once) treatments was observed in the TxRed channel using the 20x objective. **(B)** FACS analysis of clone 7 and 15 treated daily or once with DMSO, DAC and CM-272 for 72 h was performed. For statistical evaluation, one-way ANOVA was carried out using 3 technical replicates.

p-values: > 0.05 (ns); ≤ 0.05 (*); ≤ 0.01 (**); ≤ 0.001 (***); ≤ 0.0001 (****)

7 Discussion

AML is a genetically heterogeneous malignancy that can arise from a dysplastic state (MDS). Genomic and epigenomic alterations have been identified to contribute to AML initiation and maintenance. Dysregulated activity of DNMT and G9a in MDS/AML are associated with transcriptionally silencing of TSGs as well as tumor metastasis, increased proliferation, and cancer progression. MDS and AML patients with poor-prognosis show clinical benefits when treated with azanucleosides (azacytidine and decitabine) that inhibit DNMT1 and reverse critical epigenetic events driving the cancer phenotype. A new first-in-class reversible dual small molecule inhibitor against DNMTs and G9a called CM-272 was discovered as an improved approach in cancer therapeutics.

The goal of this study is to identify AML disease-specific epigenetic vulnerabilities that can be targeted by inhibition of the DNMT/KMT complex in order to understand the molecular and functional consequences for therapeutic applications. Specifically, we aim to examine the response of dual DNMT/G9a inhibition in various MDS/AML cell line models and primary human AML cells with heterogenous mutational background. Moreover, a reporter gene cell line based on the epigenetically suppressed TSG SFRP1 should be generated to use it for epigenetic drug screenings and optimizing treatment schedules in AML. It was initially used to compare the potential of DAC and CM-272 to reactivate SFRP1.

7.1 CM-272 highly affected many different MDS/AML subtypes due to dual inhibition of G9a and DNMTs

Our first experiments revealed that CM-272 treatment already induced cytotoxicity and/or anti-proliferative effects within 24 h in almost all tested MDS/AML cell lines and reached its maximum after 72 h. The drug was shown to be highly potent in a broad range of MDS/AML cell lines with IC50s at nM concentrations (~ 100-500 nM) which was also seen in previous studies on different hematological cancer cell lines¹⁸⁴. We could not see strong cytotoxic differences of CM-272 between MDS, MDS-derived AML, and *de novo* AML cells indicating a universal activity against DNMT/G9a among MDS/AML cells. Notable, the cell lines OCI-AML2 and OCI-AML3 harboring a DNMT3A mutation responded more sensitively to the treatment suggesting a correlation between altered DNMT3A and response. In addition, the dual inhibitors CM-579 and CM-272 caused the highest cell toxicity in MDS, MDS-derived AML and *de novo* AML cell lines in comparison with the DNMTi DAC and SGI-1027. Thus, modification of two epigenetic processes

Discussion

seemed to have a higher killing capacity than DNA demethylation only as described in previous studies.¹⁸⁴

CM-272 and CM-579 were designed to reversibly inactivate DNMT/G9a activity by physically interfering with their protein interaction. The irreversible cytosine-substitute DAC is known to mediate proteasomal DNMT degradation through a suicide complex. Surprisingly, DAC treatment also induced G9a degradation in MDS-L and OCI-AML3 either directly by forming a suicide complex of DAC with both interacting enzymes DNMT and G9a or indirectly by downstream signals. In breast cancer cell lines, DAC was also shown to significantly decrease promoter H3K9 di-methylation of TSGs demonstrating its complimentary mechanism of action in gene reactivation in a manner independent of DNA methylation.¹⁵⁶ Similar to DAC treatments, CM-272 does not only inactivate DNMT/G9a but also induced their degradation shown in this study. However, CM-579 seemed to be less potent than DAC and CM-272. The G9a-associated histone methylation mark H3K9me2/3 was demethylated upon CM-272 treatment after 72 h in OCI-AML3 but not in the other two cell lines. As all epigenetic marks, histone methylation is a reversible modification²¹⁹ that underlies complex and dynamic processes. Therefore, investigating the histone methylation at a different time point could have resulted in a G9a-degradation-specific increase of H3K9me2/3 in MDS-L and F-36P after CM-272 and CM-579. In those two cell lines, H3K9 may be remethylated as a way to compensate for the lack of DNMTs and/or G9a. Other KMTs including GLP, SETDB1, and Suv39h1 are known to be recruited to multiple G9a target genes showing compensatory activity in G9a null cells.²²⁰ At time point 72 h however, the TSGs WNT5A, DKK1, and SFRP1 got upregulated by CM-272 in all three cell lines seen on mRNA and/or protein level. Although cells were treated daily with DAC and once with CM-579 and CM-272, DAC did not lead to an upregulation of the SFRP1 expression indicating that targeting histone methylation was necessary to reactivate this TSG under these treatment conditions. A second explanation could be that only longer treatments with DAC could have resulted in an increase of gene expression. In fact, DAC acts as a cytosine-substitute during replication causing an indirect inhibition of DNMT1 and long, passive demethylation.²²¹

The missing MDS-L mRNA data could have resulted from a methodical error of the RT-qPCR (primer design, method not sensitive enough, difficult DNA structure). However, SFRP1 could be detected on protein level and seen to be re-expressed by CM-579 and CM-272 treatments in MDS-L.

Taken together, these results revealed a strong impact of CM-272 on the epigenetic regulators that was linked to the regulation of H3K9me2/3 in OCI-AML3 and the transcriptional reactivation of downregulated genes in all investigated cell lines. CM-272 induced a potent therapeutic response *in vitro* due to its inhibitory effect against methyltransferase activity of G9a and DNMTs.

7.2 DNA and histone demethylation had the strongest effect on OCI-AML3 harboring a DNMT3A and NPM1 mutation

As discussed above, OCI-AML3 was one of the most responsive AML cell lines regarding cytotoxicity, DNMT/G9a degradation, histone demethylation and TSG upregulation upon dual inhibition by CM-272. These findings were complemented by functional assays. DNMT/G9a inhibition induced highly significant apoptotic effects resulting in a strong reduction of the colony forming potential in a dose-dependent manner in OCI-AML3. Anti-proliferative effects were also predominantly seen in OCI-AML3 which were caused by an increase of quiescent cells in the G0/G1 phase. MDS-L and F-36P exhibited a tendency of induced apoptosis and anti-proliferation. In previous studies, hypomethylating agents such as DAC also promoted anti-neoplastic effects including cell cycle arrest, pro-apoptosis, and anti-proliferation in AML cell lines. In contrast to CM-272, DAC was seen to cause DNA damage as a result to its irreversible incorporation into DNA.^{169,222} As a reversible inhibitor targeting DNMTs and G9a directly, CM-272 caused anti-tumor effect without DNA-damage. In previous studies on an ALL (CEMO-1), an AML (MV4-11), and a DLBCL (OCI-Ly10) cell line, CM-272 also showed inhibition of cell proliferation and cell cycle progression as well as induction of apoptosis.¹⁸⁴

As expected, transcriptome analysis by RNA-Seq revealed that DNA and histone demethylation resulted rather in an increased transcriptional activation of genes than downregulation in MDS-L, F-36P, and OCI-AML3. Upregulation of TSG was already seen by the initial RT-qPCR experiments of the WNT antagonists WNT5A, DKK1, and SFRP1. Hypomethylating agents such as DAC and AZA are known to induce re-expression of silenced TSGs and stimulate tumor cell reprogramming by reversing aberrant epigenetic modifications.²¹³ We can assume that reactivating suppressed TSGs contributed to the anti-tumor effects including pro-apoptosis, anti-proliferation, and cell cycle arrest seen in OCI-AML3 particularly. Fewer genes were upregulated in MDS-L and F-36P that can be associated with their weaker anti-tumor response.

OCI-AML3 harbors two very important AML-specific driver mutations including DNMT3A^{R882} and NPM1c that are relevant for the pathogenesis of AML.³⁹ The presence of a DNMT3A mutation has been suggested to have a predicting drug response to HMA in AML. In a small, retrospective series, AML cohorts were analyzed to investigate the relationship between DNMT3A mutations and HMA response. A significantly higher complete remission rate (CR) has been identified in AML patients harboring DNMT3A mutations or DNMT3A/NPM1 co-mutations who were treated in the front line setting with HMAs. Patients with a wild type DNMT3A showed a lower CR rate when HMA-treated.^{223,224} The double mutation of DNMT3A and NPM1 in OCI-AML3 could also be responsible for the stronger response to the dual inhibition by CM-272.

All in all, one can say that the monocytic *de novo* AML cell line OCI-AML3 showed the strongest therapeutic response upon dual inhibition of DNA and histone methylation, which can be associated with its AML-specific driver mutations via a DNMT3A epigenetic vulnerability.

7.3 Upregulated endogenous dsRNAs of LTR/ERVs could be linked to viral mimicry and anti-tumor effects in leukemia cells

In CM-272 treated MDS-L, F-36P, and OCI-AML3 cells, a transcriptomic shift could be observed causing down- or upregulation of genes and a reprogramming of these tumor cells. Upregulation of genes by demethylating agents is traditionally associated with reactivation of epigenetically silenced TSGs and the main mode of action of this drug group. However, transcriptome analyses recently revealed that DAC-treatments can also decrease gene expression including genes regulated by c-MYC as well as genes involved in metabolic processes.^{225,226}

Here, it was focused on commonly upregulated genes in MDS-L, F-36P, and OCI-AML3 upon CM-272 treatment because the majority of the altered genes were reactivated. By demethylation of DNA and histones, the chromatin architecture was changed and TFs were activated, two mechanisms that contribute to an elevated transcription of genes.

Interestingly, genes associated with the induction of an antiviral immune response were seen to be upregulated in all three MDS/AML cell lines. More precisely, the type I interferon (IFN) signaling pathway of the innate immune response was shown to be activated. It is the first line of defense against viral infections and plays a central role in the regulation of innate immunity. This defense system limits the viral spread shortly after infection and also activates multifaceted antitumor immunity.²²⁷ Previously, another group could also show that CM-272 induces IFN response and immunogenic cell death in the hematopoietic cell lines CEMO (ALL), MV4-11 (AML), and OCI-Ly10 (DLBCL).¹⁸⁴ In different cohorts with hematologic cancers, a clinical response to AZA was linked to the activation of transposable elements and innate immunity.²²⁸ These results indicated a universal reprogramming of the innate immune system in different subgroups of leukemia by DNMTi alone and dual DNMT/G9a blockage.

Many studies have already described different anticancer effects upon type I IFN activation in malignant cells. It turned out that this antiviral immune response exerts directly anticancer effects by activating homodimeric IFN α / β receptor 1 (IFNAR) signaling pathway.²²⁹ Thereby it could be shown that the cycle progression is inhibited, terminal differentiation is promoted, and the apoptosis is induced. These previous studies stand in line with the findings of the phenotypic changes of OCI-AML3 upon CM-272 treatment in this work.

Moreover, the anti-tumor effects by epigenetic agents were linked to the reactivation of epigenetic silenced ERVs and the induction of the viral mimicry in ovarian and colorectal cancer cells.^{181,182} Upon treatment with epigenetic modulators, an upregulation of endogenous dsRNAs was seen, followed by an induction of type I and III IFN responses.²³⁰ This could also be explored in the AML cell lines U937, HL60, and KG1a showing an induction of genes involved in a type I IFN response upon DAC treatment.²³¹ In fact, we also found 85 different dsRNAs originating from LTR/ERVs including LTR7, MLT2A2 and LTR12C to be upregulated in our MDS/AML *in vitro* models. Daskalakis et al. also described an activation of the ERV LTR12C upon treatment with DNMT- and HDAC-inhibitors in different human cancer cell lines as well as in healthy human cells²³².

Another group also found that treatment with AZA increased the representation of ERVs in a cohort of MDS and CMML patients compared to healthy donors. Controversially, this did not correlate with response. Instead, they suggested that activating latent differentiation programs play a more important role in the AZA mechanism of action than induction of ERVs expression, which is rather considered as a bystander effect.²³³

Taken together, these findings showed that DNA/histone demethylation by CM-272 may promote an anti-tumor effect in AML cells through re-activated ERVs and a type I IFN response described as viral mimicry. However, this link between anti-tumor effect and viral mimicry remains to be fully explored.

7.4 Dual inhibition of DNMT/G9a led to myelomonocytic differentiation of OCI-AML3 through reduced HOX9/MEIS1 activity

It has been known for decades that low-dose-HMA treatments promote terminal differentiation with subsequent apoptosis in leukemic cells due to DNA hypomethylation and transcriptional reprogramming.²³⁴⁻²³⁶ In this thesis, similar effects of OCI-AML3 cells upon DNMT/G9a blockage were observed. Strong pro-apoptotic and anti-proliferative effects, as well as cell-cycle arrest of OCI-AML3 upon DNMT/G9a inhibition may result from a transcriptional reprogramming of these blast cells towards monocytic differentiation. In fact, TFs associated with myelomonocytic differentiation (FOS, JUNB, PU.1) became reactivated in OCI-AML3 upon DNMT/G9a inhibition. The expression of these TFs was also linked to the suppressed formation of AML stem cells observed in previous studies.^{237,238} Treated cells responded by morphological changes towards cell maturation and an activation of a monocytic-specific immunophenotype²³⁹ identified by CD14 and CD11b upregulation.

In addition to an elevated monocytic TF network, myeloid blockers involved in the HOX9/MEIS1 pathway (PBX3, MEIS1) were seen to be downregulated. This may enhance the potential of treated OCI-AML3 cells to differentiate. This downregulation of HOX genes could be caused directly by a CM-272-specific transcriptional reprogramming or indirectly by altered molecules regulating the HOX/MEIS1 pathway.

Besides a DNMT3A mutation, this cell line also harbors a NPM1 mutation (NPM1c) leading to its abnormal cytoplasmic localization being highly relevant for the disease progression. NPM1 mutant AML cells highly express members of the stem cell gene signature including HOXA and HOXB genes and MEIS1.²⁴⁰ An immediate downregulation of HOX genes can be caused by a loss of NPM1c from the cytoplasm either through nuclear re-localization or targeted degradation. In previous studies, it could be shown that re-localization of NPM1c induces cell growth arrest and differentiation in OCI-AML3.²⁴¹ Here, OCI-AML3 with a dual DNMT/G9a blockage showed an increased amount of NPM1c within the nuclear fraction which may cause the HOX gene downregulation and monocytic differentiation.

The cytoplasmic transport of NPM1 is mediated by the nucleo-cytoplasmic transporter exportin 1 (XPO1). Its inhibition results in nuclear re-localization of NPM1c demonstrated by a nuclear export inhibitor KPT-330 of another study. As a consequence of XPO1 inhibition, a loss of HOX gene expression and differentiation of the OCI-AML3 could be seen.²⁴¹ It is possible that XPO1 expression and/or activity is affected by the DNMT/G9a inhibition leading to an accumulation of NPM1c within the nucleus in OCI-AML3.

In summary, our data indicated that myelomonocytic differentiation in OCI-AML3 upon CM-272 is caused by a re-localization of NPM1c that mediates a downregulation of HOX genes. However, the exact mechanism of how NPM1c is re-localized into the nucleus upon CM-272 treatment needs to be further investigated.

7.5 CM-272 induced anti-neoplastic effects in primary AML blasts

CM-272 treatments of five primary AML samples of different origin and mutational background initially revealed similar anti-tumor effects as seen in our cell line models of MDS and AML. In general, the treatment caused Caspase 3/7 mediated apoptosis, a reduction of the colony forming potential and morphological signs of differentiation in the blast cells. Furthermore, the *in vitro* experiments already suggested that AML cells with NPM1 and DNMT3A mutations are more sensitive to the CM-272 treatment. However, a clear link between mutation and response could not be determined by patient-derived AML samples. More samples need to be investigated that would enable a stable, statistical analysis of mutations and responders. Primary AML samples are

more difficult to culture and the fitness of different samples can highly vary which can lead to drug-independent effects that need to be considered when further experiments.

7.6 Generation of the SFRP1-specific reporter gene cell line as an epigenetic drug screening model for AML

A recombinant reporter system was generated based on a *in situ* modification of the endogenous locus of the TSG SFRP1, decisive regulator of the WNT pathway. This system was suggested to have the utility for rapid, quantitative, and visual readout for effects of “epigenetic therapy” agents on the abnormally silenced promoter of SFRP1 in AML.

SFRP1 is found to be downregulated in different cancer entities (CRC, prostate cancer, and renal cell cancer, and leukemia) which was associated with tumor development. Not only in solid cancers but also in leukemia including AML, promoter hypermethylation has been described as the common mechanism underlying the SFRP1 suppression.¹⁰⁸⁻¹¹² Here, specific CpG sites in a CpG island within the promoter region of SFRP1 were also seen to be hypermethylated in AML cell lines compared to healthy cells. *In silico* analysis of healthy MNCs and several AML subtypes of patient samples confirmed previous findings of the transcriptional downregulation of SFRP1. Therefore, the recombinant reporter system was based on the epigenetically suppressed SFRP1 gene.

A DNA fragment of ~ 2.7 kb containing the reporter gene mCherry and the selection marker puromycin was successfully generated by molecular cloning. Minor changes of the SFRP1 sequence upstream of mCherry did not lead to frame shift and its disturbed expression. Further experiments could verify the functionality of mCherry.

There are three major genome editing technologies including zinc-finger nucleases (ZFNs), transcription activator-like effector nucleases (TALENs) and clustered regularly interspaced short palindromic repeat (CRISPR)-Cas-associated nucleases. CRISPR/Cas9 has the important advantage that the nuclease Cas9 can be used independently of the target sequence in contrast to the other two endonuclease-based tools. Different DNA regions can be targeted by designing complementary guide RNAs that form a complex with the Cas9 protein. Furthermore, ZFNs and TALENs are much more laborious and expensive.²⁴² Therefore, we decided to use the HDR-based CRISPR/Cas9 technology for targeted integration of a DNA fragment at the exon 1 of SFRP1 to generate a recombinant reporter cell line. A major problem of this method are off-targets. Their occurrence was minimized by using crRNAs based on online crRNA-designing tools that predict the probability for off-targets. Transfection of PC3 cells, endogenously expressing SFRP1, with

Discussion

RNPs containing the crRNA #3 resulted in a KO of the SFRP1 gene. This led to an activated WNT pathway seen by an elevated β -Catenin and c-Myc expression and increased cell proliferation. To modify leukemia cell lines, the nucleofection technology was used, which is a physical, electroporation-based transfection method. In general, gene delivery technologies can be broadly classified into three groups: chemical (e.g. lipofection), biological (e.g. lentiviral transduction), and physical methods (e.g. electroporation). The nucleofection uses specific voltages and reagents to create temporary pores on the cell membrane to transfer DNA or RNA into cells. Once you have optimized all conditions, nucleofection takes only a few minutes to deliver DNA or RNA to cells. In contrast, the standard biological method, lentiviral transduction, needs two weeks to produce recombinant viruses, which can be used for cell transduction and stable DNA integration. Moreover, nucleofection yields rapid transfection of a large number of cells compared to the chemical method, lipofection. This lipid-based method is not an effective delivery strategy for all kinds of cell lines.^{243,244}

In various MDS/AML cell lines including MDS-L, F-36P, OCI-AML3, HL-60, and THP-1 as well as the CML cell line K562, a KO could be easily generated by nucleofection. However, a stable and correct KI of the ~ 2.7 kb SFRP1_mCherry_puro construct was much more difficult. The challenge was to find a leukemia cell line that favors the repair mechanism HDR instead of NHEJ. In fact, NHEJ was observed to be generally more active, because it acts throughout the cell cycle of a variety of cell types including division and post-mitosis. HDR is primarily restricted to the S/G2 phase limiting transfections for precise editing to actively dividing cells. Importantly, the presence of functional p53 being frequently mutated in cancer and AML is found to be necessary for efficient HDR activity.²⁴⁵ To enhance the HDR efficiency, key enzymes involved in the NHEJ can be inhibited including DNA ligase IV, KU70, and KU80.²⁴² Even without NHEJ inhibition, the cell lines THP-1 (AML) and K-562 (CML) were finally found to be editable by the HDR-based CRISPR/Cas9 method. In both cell lines, gene expression of SFRP1 was seen to be upregulated upon treatment with DAC and CM-272, thus suitable for HMA-based drug screenings.

After puromycin-selection of positively transfected THP-1 cells, several single cell clones were characterized regarding their genotype and mCherry expression under basal condition and in response to DAC. All clones were heterozygous with one allele carrying the SFRP1_mCherry_puro construct. The SFRP1 was not completely epigenetically silenced in THP-1 seen by a basal mCherry expression in untreated cells. Notable, the large DNA fragment of 2.7 kb could not always be correctly inserted which was identified by PCRs of a missing or altered mCherry gene region. Consequently, the signal intensity of mCherry differed from one clone to another. Genetic alterations due to varied integrations or epigenetic modifications could influence the mCherry gene expression. Additionally, most of the samples showed a heterogenous cell population of mCherry

expressing cells and mCherry negative cells. It cannot be excluded a methodical mistake during the single cell preparation that resulted in an expansion of more than one clone in a well. Another reason could be the formation of subclones due to spontaneous genetic alterations during culturing after a successful single cell preparation.

After initial drug testing with DAC, clones 7 and 15 were chosen for further drug screenings. Clone 7 showed already a high basal SFRP1 promoter activity of the majority of cells. Their mCherry expression could be elevated by HMAs. In comparison to clone 7, clone 15 was comprised of only a few cells expressing mCherry without treatment. The inactivated promoter was turned on upon HMA application seen by an increased number of mCherry positive cells. Depending on the two different responses, the parameters MFI or cell percentage should be considered for analysis by FACS. For fluorescence microscopy, only clone 7 can be used because of its high mCherry intensity. The fluorescence signal of clone 15 is too low with or without drug treatment.

In summary, we obtained two recombinant THP-1 clones that either changed the fluorescence intensity with equal number of positive cells or increased the amount of mCherry expressing cells upon DAC and CM-272 treatment.

7.7 The gold standard treatment of DAC and CM-272 was verified by the reporter cell lines THP-1 clone 7 and 15

The two recombinant THP-1 clones 7 and 15 were used to compare DAC with CM-272. DAC has a short half-life and acts by incorporation into the DNA during S-phase. Therefore, DAC is commonly applied daily assuming that it does not accumulate over time. CM-272 is a direct inhibitor of the methyltransferases and acts independently of the cell cycle phases, thus applied only once in this thesis. Both treatment regimens were seen to upregulate SFRP1 mRNA expression in WT THP-1 cells investigated by RT-qPCR. This schedule should be used as the gold standard for DAC and CM-272 treatment and verified by the two THP-1 clones.

As described above, only clone 7 could be examined by fluorescence microscopy due its high mCherry intensity. mCherry positive cells of clone 7 increased their mCherry expression upon DAC and CM-272 treatment similarly. There are also other weaknesses of this protein detection method: THP-1 are suspension cells that do not grow in a monolayer so that counting and quantification of mCherry expressing cells is very difficult especially over time when using real-time microscopy. Moreover, the fluorescence intensity within a cell cannot easily be quantified and one cannot distinguish between live and dead mCherry positive cells without further live/dead staining.

Discussion

Both, percentage of positive cells and signal intensity could be precisely determined in a high-throughput manner by FACS. Considering the gold standard treatment regime of DAC (daily) and CM-272 (once), clone 7 responded to the drugs as expected by significantly increasing the fluorescence intensity. Only DAC induced an SFRP1 promoter activation in clone 15 seen by an increased number of mCherry positive cells.

All in all, these initial drug experiments showed the principal functionality of the newly generated reporter gene cell line that can be used to examine SFRP1 promoter activation by epigenetic modulator.

8 Conclusion

Dual inhibition of DNMT/G9a affected a wide range of MDS/AML cell lines with different genetic backgrounds seen by cytotoxicity assays. OCI-AML3 was identified as one of the most responding AML cell lines being a model for the AML-driver mutations DNMT3A and NPM1. Our experiments revealed that the induction of myelomonocytic differentiation as well as viral mimicry are connected to anti-tumor effects in OCI-AML3 cells treated with CM-272. We suggested that OCI-AML3 differentiation resulted from an accumulation of the mutated NPM1 protein in the nucleus by XPO1 downregulation causing a reduced activity of the HOX9/MEIS1 axis. Additionally, endogenous dsRNAs of LTR/ERVs were shown to be upregulated upon DNMT/G9a blockage in MDS-L, F-36P, and OCI-AML3. Thereby, the IFN signaling pathway of the innate immune response was shown to be activated, which may contribute to the anti-tumor effects in the AML cells. Initial experiments on primary AML cells showed similar anti-cancer effects.

In the second part of this thesis, an AML-reporter cell line based on the epigenetically suppressed SFRP1 gene was successfully generated to screen different epigenetic drugs and to identify optimal treatment regimen. High-throughput analysis by FACS was performed to further characterized two different THP-1 clones. DAC and CM-272 treatments of the two clones either turned on or increased the promoter activity of SFRP1 by promoter hypomethylation.

9 Outlook

The first-in-class reversible dual inhibitor CM-272 examined in our MDS/AML *in vitro* models showed promising anti-tumor effects in nM range among different leukemia subtypes with various mutational backgrounds. Moreover, it is important to test how healthy cell types such as HSPC and immune cells are affected by the dual blockage. In particular, cytotoxicity and changes in gene expression in these cells should be investigated to detect possible side effects of this drug at an early stage of testing.

It is known that the type I IFNs can also have immunostimulatory effects on all types of immune cells such as DCs, CTLs, NK cells and macrophages, and thereby enhance anticancer immune responses in MDS/AML cells.²²⁹ Our transcriptome data already indicated a CM-272-specific activation of this type of immune response in MDS-L, F-36P, and OCI-AML3. This effect can be further investigated by CM-272-treated MDS/AML cells cocultured with immune cells.

So far, an insufficient number of primary AML patient samples were analyzed with the dual inhibitor. A larger number of samples could be stratified in different AML subtypes based on their mutational background to verify the data on MDS/AML cell lines (cytotoxicity, DNMT/G9a protein degradation, and functional assays).

Targeting epigenetic regulators as monotherapy has shown a limited therapeutic efficacy. Therefore, combinational treatments of CM-272 with other epigenetic inhibitors (e.g. HDACi), conventional chemotherapy (e.g. cytarabine), immunotherapy (e.g. PD-1/PD-L1 inhibitor), or other forms of targeted therapies such as FLT3 inhibitors or BCL-2 inhibitor (venetoclax) are currently in different stages of clinical testing.^{246,247} In MDS/AML cell lines, CM-272 could also be combined to discover a synergistic effect of the two drugs.

To extend the findings of the RNA-Seq and the transcriptional changes, it should also be examined which genomic regions are affected by hypo/hypermethylation upon CM-272 treatment in MDS and AML. For example, the Infinium MethylationEPIC BeadChip is a comprehensive genome-wide method at single-nucleotide resolution for the detection of methylated CpGs. In this work, it could be shown that TFs and genes associated with chromatin remodeling are upregulated in MDS-L, F-36P and OCI-AML3. These findings could be further investigated using ChIP-Seq by which genome-wide DNA binding sites for TFs and other proteins can be identified. In addition, valuable insights of chromatin accessibility and gene regulation can be provided by ATAC-Seq. Through all these sequencing analyses, we would gain a comprehensive understanding of the mechanism of CM-272 in MDS and AML. We suggested that accumulated NPM1c protein mediates the downregulation of the HOX9A/MEIS1 axis and thereby inducing differentiation in OCI-AML3. Another possible biological process causing the CM-272-specific anti-tumor response could be the

Outlook

activated viral mimicry in those cells. By DNA methylation analysis, ChIP-Seq, and ATAC-Seq, these processes should be more intensively investigated.

The next important steps would be to investigate the dual inhibition of the methyltransferases *in vivo*. Previous studies, AML, ALL, and DLBCL xenogeneic models showed a significantly prolonged survival when treated with CM-272.¹⁸⁴ Here, drug response of OCI-AML3 has been intensively investigated *in vitro*, thus it is also suitable for the establishment of a xenogeneic model. Using a recombinant OCI-AML3 cell line containing a reporter gene such as luciferase, the tumor growth of the injected and engrafted cells could be monitored much effectively.

In the second part of this thesis, a recombinant THP-1 reporter cell line was generated to test epigenetic drugs and optimize treatment schedules. The investigated clones 7 and 15 were composed of cells heterogeneously expressing the reporter gene mCherry. To obtain a homogenous cell population of 100 % mCherry negative or positive cells, FACS cell sorting should be performed. Samples with only negative cells would turn on their SFRP1 promoter activity upon drug treatment and increase their number of positive cells. In a sample with 100% mCherry positive cells, the signal intensity would increase that could be quantified by the MFI in FACS.

Finally, vast range of epigenetic drugs could be applied to the reporter cell line alone or in combination with another drug. Thereby, different dosages, exposure time, and treatment regimens could be tried out to identify the conditions with the strongest response seen by the mCherry signal. Epigenetic drugs and combinations could be compared with each other, which would provide a better understanding of the mode of actions of the drugs. The most responsive drugs could be used for *in vitro* experiments with wild type cell lines and primary AML cells, as well as for *in vivo* models.

10 List of Figures

Figure 1: The hierarchical blood system from HSCs to differentiated blood cells.	2
Figure 2: Frequency of mutated genes in MDS having prognostic and therapeutic significance.	3
Figure 3: Transformation of MDS to secAML by clonal evolution.....	4
Figure 4: Normal hematopoiesis and different types of leukemia.....	5
Figure 5: NPM1wt and NPM1c shuttle between cellular compartments.....	9
Figure 6: Mechanisms of leukemic evolution.....	10
Figure 7: An overview of the epigenetic mechanisms: DNA methylation, histone modification and ncRNAs.	13
Figure 8: SFRP1 antagonizes the WNT signaling pathway.	16
Figure 9: Gene regulation by DNA methylation of normal and cancer cells.....	17
Figure 10: G9a is a multipotent regulator of gene expression.....	19
Figure 11: Gene downregulation by a cross-talk between DNA methylation and H3K9me2/3.	20
Figure 12: DNMTi AZA and DAC versus dual inhibitor CM-272.	25
Figure 13: Cell cycle analysis by DAPI and BrDU staining.....	49
Figure 14: Schematic overview of the SFRP1_mCherry_puro construct.	63
Figure 15: Cytotoxicity assays of MDS/AML cell lines treated with hypomethylating drugs. .	73
Figure 16: Impact of epigenetic inhibition on DNMTs, G9a, WNT antagonists, and H3K9me2/3.	75
Figure 17: Functional assays with MDS/AML cell lines upon CM-272 treatment.	77
Figure 18: Functional assays with CM-272 treated patient-derived AML blasts.	79
Figure 19: Commonly affected pathways in MDS-L, F-36P, and OCI-AML3 by CM-272 treatments.	81
Figure 20: Antiviral immune response induced by CM-272 in MDS-L, F-36P, and OCI-AML3 .	83
Figure 21: CM-272-mediated differentiation of OCI-AML3 cells.....	85
Figure 22: XPO1 downregulation leads to nuclear relocalization of NPM1c and decreased HOX gene expression in CM-272-treated OCI-AML3.	87
Figure 23: Schematic representation of the functionality of a reporter gene cell line for screening of epigenetic drugs.....	88

List of Figures

Figure 24: DNA hypermethylation correlates with SFRP1 gene silencing.....	89
Figure 25: crRNA #3 is the optimal candidate for HDR-mediated CRISPR/Cas9 editing of SFRP1.	91
Figure 26: Molecular cloning of the SFRP1_mCherry_puro construct.	93
Figure 27: Overview of the transfection of THP-1 cells and obtaining single cell clones	94
Figure 28: DAC and CM-272 induced a SFRP1 reactivation in THP-1 WT cells.....	95
Figure 29: Investigating THP-1 single cell clones by PCR and FACS.	97
Figure 30: Fluorescence microscopy and FACS of DAC-/ CM-272-treated THP-1 clones 7 and 15.....	99
Figure 31: Sequence to analyze for MassARRAY.	xxi
Figure 32: Sequence of SFRP1_mCherry_puro construct.	xxii
Figure 33: Alignment of sequenced amplicons of clone 7 and 15 for genotyping.	xxiii

11 List of Tables

Table 1: Proportion of new cases of leukemia subtypes in women and men in Germany in 2015-2016.....	6
Table 2: Notable mutated genes, their classification and frequency in AML. ⁴⁰	7
Table 3: General equipment.....	27
Table 4: Consumables.....	30
Table 5: Chemicals and reagents.	32
Table 6: Prepared buffer solutions.	34
Table 7: Kits.....	35
Table 8: Prokaryotic cell line.....	36
Table 9: Cytokines/ Inhibitor for cultivating MDS/AML cell lines and primary AML cells.	36
Table 10: Media.....	36
Table 11: Supplements for Methocult media for colony forming Unit (CFU) assay.....	36
Table 12: Media composition of eukaryotic cell lines.....	37
Table 13: Primary AML samples.....	38
Table 14: Supplements for SpemSpan media for primary AML culturing.	38
Table 15: Epigenetic drugs.....	39
Table 16: Antibodies for Flow Cytometry.....	40
Table 17: Primary antibodies for western blot.....	40
Table 18: Secondary antibodies for western blot.....	40
Table 19: Primer for RT-qPCR.	41
Table 20: Primer for pyrosequencing.....	41
Table 21: Primer for MassARRAY.....	42
Table 22: Primer for Surveyor assay.	42
Table 23: Primer for molecular cloning.....	43
Table 24: Primer for sequencing of SFRP1_mCherry_puro construct in pcDNA TOPO-vector.	44
Table 25: Primers for genotyping of the expected size for WT/KO/KI alleles of SFRP1	44
Table 26: Templates for molecular cloning.....	44
Table 27: crRNA candidates for HDR-based CRISPR/Cas9 editing of the SFRP1 gene.....	45
Table 28: Software.	45

List of Tables

Table 29: PCR program with a Hot Start Taq polymerase for a MassARRAY assay.....	56
Table 30: Components and concentrations of a PCR for the MassARRAY assay.	56
Table 31: Components for RNA conversion and cleavage.	57
Table 32: Hybridization procedure with slowly decreasing temperature to form heteroduplexes.	61
Table 33: PCR program for Q5 polymerase.	64
Table 34: Component and concentrations for a standard PCR reaction.	64
Table 35: Components and volume of Colony-PCR.	66
Table 36: PCR-Program of Colony-PCR.....	66
Table 37: Limiting dilutions for subcloning.	68

12 Appendix

12.1 Sequence to analyze for MassARRAY

ORIGINAL SEQUENCE

CCCTGTTATTTAAAGCGCAAGGCTTTGTTTCAGGTATGGGAAAGGCGAAGTTGGATCCCAGGAAGAGCGGCTCCGGGGACCACAGCGAGTCCCTGCGAGGCCAAGGCGCAGAGCTGCCTCCCGGGCCAGCCC CGCTGCACCTGGGT
 CGCGAGGGGCGCTGAGCGATACCTGGGACAGACCAGACGCGCTTAGGAATCACTGCACAGCATGCGAGCAACCT
 CGGGCCCTCAGTCCCCAGCACCGGGACCCAGCGGCGGGCGGGCGTAGGGTGGCGCGGGTCTCTCTGCAGCTCCGG
 CCGGGGATGGAGGGGGCGGCTCGCGCACGTGGGAGGAGGCA GCCTTACCTTGGGGCTTGGAGGCTT CGGTGGCA
 TTGGGCGGCGTCATGGCGATGCAGACGTCCCCCTCGGGAACTTGTACACTTAAGCATCTCGGGCCAGTAGAAG
 CCGAAGAACTGCATGACCGGCTCGCACGAGT CGCGCACG GCTCGCAGAGCCAGCGACA CGGGTAGATGGGC CGG
 TCCAGGCAGA CGGGCGCGAAGAGCGAGCAGAGGAAGACCTGGGTGC CGGCGTGGCAGTTCTTGTGAGCAGGGGC
 ACCCAGCTGCTGGCCTGCTGCTTCACCTCCGCGATGGTCTCGTGCTCCAGCAGGTTGGGCAGCACCATCTTCTTG
 TAGCCCACTTGTGGCACAGCCGAGGTC CGCGGGGATGTCCA CGCACTGAGGTGGCTTGGTGTAGAAGCGCCCG
 CTCTGGTACCGGGCGATGTCCGACTGGAAGCTCACTAGTCTACTCGCTGGCCGAGCCCA CGGCCAGAAGCGCC
 CGCCAGCGCCAGCAGCA CGCCAGGGCTGCCCGCGCGGCCCCCTCGCTGCGCCCGATGCCATGCCCGGCT
 CTGCGCCCTGTTCTCGCGACGT CGGGCTGCCCTCGCCGCTCCCGCGCGCGTCCCTGCGCAAACTTCCAGGG
 ACCTCGGGGACAAAAGGCGCAGTCCCAGCGTTGCCCGGCTCGCGGC CGCAAGCTGCTGCCCGTCCCCCGG
 CCAGTGGCGGCCCTCGGCTCGGT CGGAGGCGCGCGGGCGGGAGGCGGCGCTGCGGGCTGGGTGCGCCCGG
 CTCCCGGAGGTGCGGCGAGCAGGAAGGCGCGGGCGGCGGGCGCGCGGCACTGACTCGGAGGCTGCAGGGCTGG
 AGTGCGCGGGGCTCCTACGCGCGAGCCCTCGGAGCCCGCCCGCGCAGCCAATCAGCTCCCGGCGGGGCGAGCCG
 ACTCGTTACCACTCGTCCGTCACCGGCGCGGGAGCCAATCGCTCCCTCGCGAGCGGTTCGGTTTACTAGAACCAG
 ACGCGGCTCAACACCCCTTAAAAAACAAAACCAAAAAATAC

CONVERTED SEQUENCE

TTTTGTTATTTAAAGCGTAAGGTTTTGTTTTAGGTATGGGAAAGGCGAAGTTGGATTTTAGGAAGAGCGGTTTCGGGGATTATAGCGAGTTTTTTGCGAGGTTAAGGCGTAGAGTTGTCTTTTTCGGGTTAGTTTCGTCTGTATTTGGGT
 CGCGAGGGGCGTTGAGCGATATTTGGGATAGATTAGA CGCGTTTAGGAATTA CGTGATAGTATGCGAGTAATTT
 CGGGTTTTTAGTTTTTAGTATCGGGATTTAGCGGCGGGCGGGCGTAGGGTGGCGCGGGTTTTTTTTGTAGTTTTCGG
 TCGGGGATGGAGGGGGCGGTTCGCGTACGTGGGAGGAGGTA GTTTTTATTTTTGGGGTTTTGGAGGTTTT CGGTGGTA
 TTGGGCGGCGTTATGGCGATGTAGA CTTTTTTTTCGGGAAATTTGTTATATTTAAGTATTTCGGGTTAGTAGAAG
 TCGAAGAAATGTATGATCGGTTCTACGAGT CGCGTACGTTTCGTAGAGTTAGCGATA CGGGTAGATGGGT CGG
 TTTAGGTAGA CGGGCGCGAAGAGCGAGTAGAGGAAGATTTGGGTGT CGGCGTGGTAGTTTTTTGTTGAGTAGGGGT
 ATTTTAGTTGTTGGTTTTGTTTTTTTTTTTTATTTTTCTTTATTTTTCTTTATGTTTTCTGTTTTTAGTAGGTTGGGTAGTATTATTTTTTTG
 TAGTTTA CTTGTGTTATAGTCTTAGGTT CGCGGGGATGTTTACGTATTGAGGTGGTTTTGGTGTAGAAGCGTTTCG
 TTTTGGTACGGGT CGATGTTCGATTGGAAGTTTACGTAGTCTATTCTTTGGT CGAGTTTACGGTTAGAAGCGTTC
 GCGTTTAGCGTTAGTAGTACGTTTAGGGTTGTTTTCGCGCGGTTTTTTTTCTTTGCGTTTCGATGTTTATGTCTGTT
 TTGCGTTTTGTTTTTCGCGACGT CGGGTTGTTTTCTCGTTTTTTTCGCGCGCGTTTTGTCTAAATTTTTAGGG
 ATTTTTCGGGATAAAAAGGCGTAGTTTTTTAGCGTTGTTCTGTTTTCGCGGTCTAAGTTGTGTTCTGTTTTTTTCGG
 TTAGTGGCGTTTTTCGTTTTGCGGT CGGAGGCGGCGCGGGCGGGAGGCGGCGTTGCGGGTTGGGTGCGTTTTCGG
 TTTT CGGAGGTGCGGCGAGTAGGAAGGCGCGGGCGGCGGGCGCGCGGTATTGATTTCGGAGGTTGTAGGGTTGG
 AGTGCGCGGGGTTTTTA CGGT CGAGTTTTCGGAGTCTTT CGCGTAGTTAATTAGTTTTCGGCGGGGCGAGTCTG
 ATTCTTATTA CTTCTGTTATCGGCGCGGGAGTTAATCTTTTTTTTCGCGAGCGGTTCTGTTTATTAGAATTAG
 ACGCGGTTTTAATTTTTTTTTAAAAATAAAAATAAAAATAT

Figure 31: Sequence to analyze for MassARRAY.

This is the SFRP1 gene region (chromosome 8: 41165786-41167175, hg19, SFRP1 promoter) that was investigated by MassARRAY. In red, the potential methylated CpGs are highlighted. The upper sequence is the original sequence and below after bisulfite conversion. The forward primer is in green and the reverse primer in blue.

12.2 Sequence of SFRP1_mCherry_puro construct

LHA of SFRP1; P2A, mCherry, SV40 poly A mCherry, SV40 promoter puromycin, Puromycin, SV40 poly A Puromycin, RHA SFRP1

```

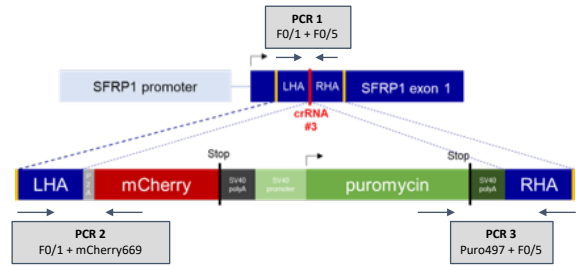
CTCCCCGCCCCGCGCCGCTCCGACCGCAGGCCGAGGGCCGCCACTGGCCGGGGGACCAGGGCAGCAGC
TTGCGGCCGCGGAGCCGGGCAACGCTGGGGACTGCGCCTTTTGTCCCCGGAGGTCCCTGGAAGTTTGC
GGCAGGACGCGCGCGGGGAGGCCGGGAGGCAGCCCCGACGTCGCGGAGAACAGGGCGCAGAGCCGGC
ATGGGCATCGGGCGCAGCGAGGGGGGCCGCCGCGGGGNNCCCTGGGCGTGCTGCTGGCGCTGGGCGC
GGCGCTTCTGGCCGTGGGCTCGGCMAGCGGAAGCGGAGCTACTAACTTCAGCCTGCTGAAGCAGGCTG
GAGACGTGGAGGAGAACCCTGGACCTATGGTGAGCAAGGGCGAGGAGGATAACATGGCCATCATCAAG
GAGTTCATGCGCTTCAAGGTGCACATGGAGGGCTCCGTGAACGGCCACGAGTTCGAGATCGAGGGCGA
GGGCGAGGGCCGCCCTACGAGGGCACCCAGACCGCCAAGCTGAAGGTGACCAAGGGTGGCCCCCTGC
CCTTCGCCTGGGACATCCTGTCCCCTCAGTTCATGTACGGCTCCAAGGCCTACGTGAAGCACCCCGCC
GACATCCCCGACTACTTGAAGCTGTCTTCCCCGAGGGCTTCAAGTGGGAGCGCGTGATGAACCTCGA
GGACGGCGGGCGTGGTGACCGTGACCCAGGACTCCTCCCTGCAGGACGGCGAGTTCATCTACAAGGTGA
AGCTGCGCGGCACCAACTTCCCCTCCGACGGCCCCGTAATGCAGAAGAAGACCATGGGCTGGGAGGCC
TCCTCCGAGCGGATGTACCCCGAGGACGGCGCCCTGAAGGGCGAGATCAAGCAGAGGCTGAAGCTGAA
GGACGGCGGCCACTACGACGCTGAGGTCAAGACCACCTACAAGGCCAAGAAGCCCGTGCAGCTGCCCCG
GCGCCTACAACGTCAACATCAAGTTGGACATCACCTCCACAACGAGGACTACACCATCGTGGAACAG
TAGAACCGCGCCGAGGGCCGCCACTCCACCGCGGCATGGACGAGCTGTACAAGTAAACTTGTTTAT
TGCAGCTTATAATGGTTACAAATAAAGCAATAGCATCACAAATTCACAAATAAAGCATTTTTTTCAC
TGCATTCTAGTTGTGGTTTGTCCAAACTCATCAATGTATCTTATGGTGTGGAAAGTCCCAGGCTCCC
CAGCAGGCAGAAGTATGCAAAGCATGCATCTCAATTAGTCAGCAACCAGGTGTGGAAAGTCCCAGGC
TCCCAGCAGGCAGAAGTATGCAAAGCATGCATCTCAATTAGTCAGCAACCATAGTCCCGCCCTAAC
TCCGCCCATCCCGCCCTAACTCCGCCAGTTCGCCCCATCTCCGCCCATGGCTGACTAATTTTTTT
TTATTTATGCAGAGGCCGAGGCCGCTCTGCCTCTGAGCTATTCCAGAAGTAGTGAGGAGGCTTTTTT
GGAGGCCTAGGCTTTTGCAAAATGACCGAGTACAAGCCACGGTGCGCCTCGCCACCCGCGACGACGT
CCCCAGGGCCGTACGCACCCTCGCCGCCGCGTTCGCCGACTACCCCGCCACGCGCCACACCGTCGATC
CGGACCGCCACATCGAGCGGGTCAACCGAGCTGCAAGAACTCTTCTCACGCGCGTTCGGGCTCGACATC
GGCAAGGTGTGGTTCGCGGACGACGGCGCCGCGGTGGCGGTCTGGACCAGCCGGAGAGCGTCAAGC
GGGGGCGGTGTTCCCGAGATCGGCCCCGCGCATGGCCGAGTTGAGCGGTTCCCGGCTGGCCGCGCAGC
AACAGATGGAAGGCTCCTGGCGCCGCACCGGCCAAGGAGCCCGGTGGTTCCTGGCCACCGTCGGC
GTCTCGCCCCGACCACAGGGCAAGGGTCTGGGCAGCGCGTCTGCTCCCCGAGTGGAGGCGGCCGA
GCGCGCCGGGGTGCCCGCCTTCTGGAGACCTCCGCGCCCCGCAACCTCCCCTTCTACGAGCGGCTCG
GCTTACCGTCAACCGGACGTCGAGGTGCCGAAGGACCGCGCACCTGGTGCATGACCCGCAAGCCC
GGTGCCTAAACTTGTATTTATGTCAGCTTATAATGGTTACAAATAAAGCAATAGCATCACAAATTTAC
AAATAAAGCATTTTTTTCACTGCATTCTAGTTGTGGTTTGTCCAAACTCATCAATGTATCTTGAGTAC
GACTACGTGAGCTTCCAGTCGGACATCGGCCCGTACCAGAGCGGGCGCTTCTACACCAAGCCACCTCA
GTGCGTGGACATCCCCGCGGACCTGCGGCTGTGCCACAACGTGGGCTACAAGAAGATGGTGTGCCCCA
ACCTGCTGGAGCACGAGACCATGGCGGAGGTGAAGCAGCAGGCCAGCAGCTGGGTGCCCTGCTCAAC
AAGAACTGCCACGCCGGCACCCAGGTCTTCTCTGCTCGTCTTCCGCGCCCGTCTGCTGGACCGGCC
CATCTACCCGTGTGCTGGCTCAA

```

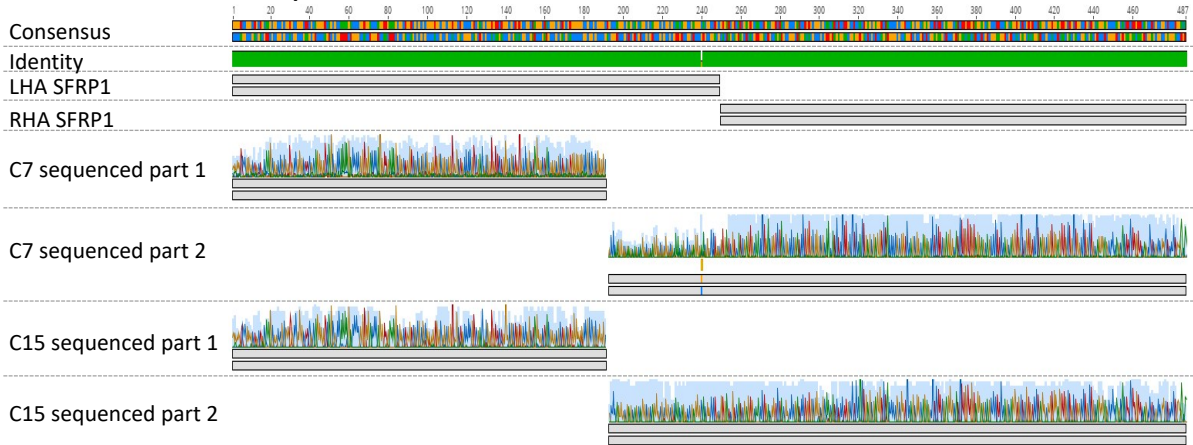
Figure 32: Sequence of SFRP1_mCherry_puro construct.

By molecular cloning, the SFRP1_mCherry_puro construct was generated. It contains left and right homologous arms of SFRP1 (LHA in gray and RHA in blue), a P2A segment (yellow), mCherry gene (red), SV40 polyA tail for mCherry (violet), SV40 promoter for puromycin (dark gray), puromycin gene (green), and a SV40 polyA tail for puromycin (dark green).

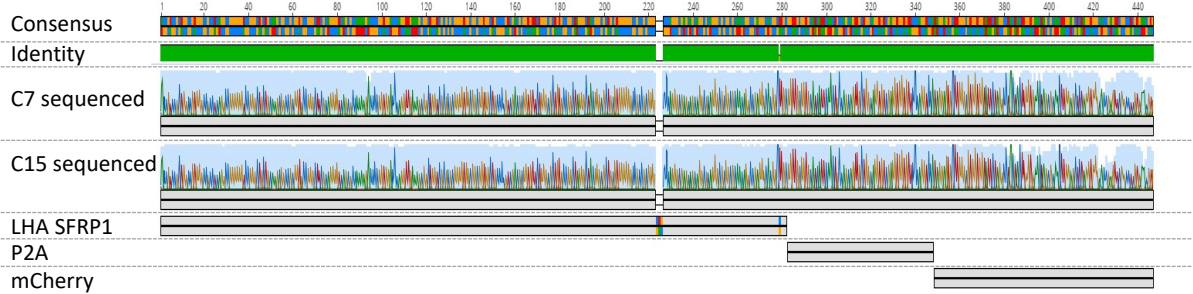
12.3 Sequencing of PCR 1, 2, and 3 of clone 7 and 15



PCR 1 F0/1.fw-F0/5.rv, Seq: F0/1.fw, F0/5.rv



PCR 2 F0/1.fw-mCherry699.rv, Seq:mCherry153.rv



PCR 3 puro497-F0/5, seq:puro497.fw

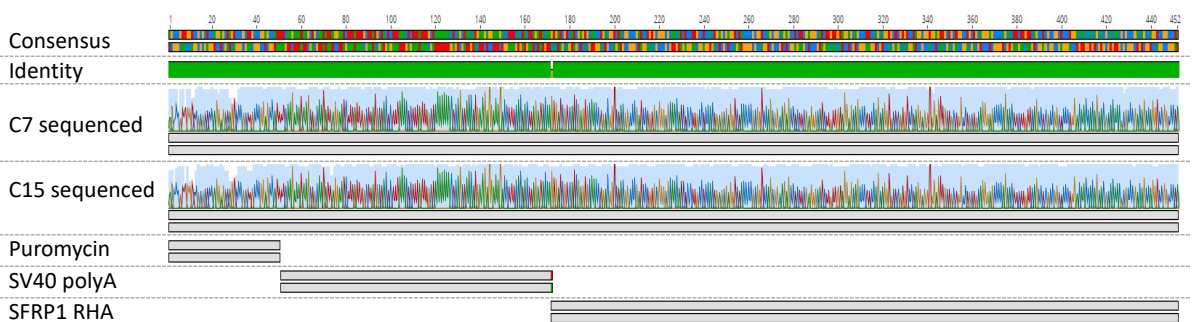


Figure 33: Alignment of sequenced amplicons of clone 7 and 15 for genotyping.

The regions that were investigated by three PCRs are depicted in the scheme of the construct above. Below, the alignment of the chromatograms of the sequenced region with the reference sequence for the different construct sections is shown.

13 Acknowledgement

At this point I would like to express my great gratitude to all the people who supported me in writing my dissertation.

My special thanks go to Dr. Borhane Guezzeguez for the intensive supervision throughout the entire work and the unique opportunity to work on exciting research projects. He gave me almost unlimited opportunities to expand both my professional knowledge and personal skills. I found our regular discussions about our current research and the willingness to incorporate my own ideas particularly stimulating. I would also like to thank him for allowing me to participate in many conferences and courses and to exchange ideas with other researchers. These experiences broadened my horizons in many areas of my life.

I would also like to thank Prof. Dr. Matthias Theobald and Prof. Dr. Thomas Hankeln for discussing and evaluating the progress of my work with me in a constructive and competent manner. Their feedback was guiding for my research.

A big thank you also goes to the German Cancer Research Center and the TransMed Graduate School, which provided me with a lot of support and encouragement as a doctoral student on my way to graduation.

I would also like to thank everyone in my research group. Our time, which I will never forget, was characterized by helpfulness, mutual consideration and respect for each other.

Last but not least, I would like to express a big thank you to my family, without whom I would not have come this far. I thank my parents above all for being a constant in my life and always offering me a home of peace and refueling. I would also like to thank my dear husband Johannes, who has supported me so much, especially in the difficult times, through his empathy and humor. Finally, I would like to thank our daughter Nora for her smile, which makes me infinitely happy.

14 Bibliography

- 1 Jagannathan-Bogdan, M. & Zon, L. I. Hematopoiesis. *Development* 140, 2463-2467, doi:10.1242/dev.083147 (2013).
- 2 Doulatov, S., Notta, F., Laurenti, E. & Dick, J. E. Hematopoiesis: a human perspective. *Cell Stem Cell* 10, 120-136, doi:10.1016/j.stem.2012.01.006 (2012).
- 3 Kondo, M. Lymphoid and myeloid lineage commitment in multipotent hematopoietic progenitors. *Immunol Rev* 238, 37-46, doi:10.1111/j.1600-065X.2010.00963.x (2010).
- 4 Kuhn, V. et al. Red Blood Cell Function and Dysfunction: Redox Regulation, Nitric Oxide Metabolism, Anemia. *Antioxid Redox Signal* 26, 718-742, doi:10.1089/ars.2016.6954 (2017).
- 5 Tigner, A., Ibrahim, S. & Murray, I. (ed Treasure Island (FL): StatPearls Publishing) (Treasure Island (FL): StatPearls Publishing, Updated 2020 Sep 25).
- 6 Jurk, K. & Kehrel, B. in *Seminars in thrombosis and hemostasis* Vol. 31 381-392 (Thieme Medical Publishers, 2005).
- 7 Pinho, S. & Frenette, P. S. Haematopoietic stem cell activity and interactions with the niche. *Nat Rev Mol Cell Biol* 20, 303-320, doi:10.1038/s41580-019-0103-9 (2019).
- 8 Zhang, P. et al. The physical microenvironment of hematopoietic stem cells and its emerging roles in engineering applications. *Stem Cell Res Ther* 10, 327, doi:10.1186/s13287-019-1422-7 (2019).
- 9 Gill, H., Leung, A. Y. & Kwong, Y. L. Molecular and Cellular Mechanisms of Myelodysplastic Syndrome: Implications on Targeted Therapy. *Int J Mol Sci* 17, 440, doi:10.3390/ijms17040440 (2016).
- 10 Hasserjian, R. P. Myelodysplastic Syndrome Updated. *Pathobiology* 86, 7-13, doi:10.1159/000489702 (2019).
- 11 Swerdlow, S. H. et al. The 2016 revision of the World Health Organization classification of lymphoid neoplasms. *Blood* 127, 2375-2390, doi:10.1182/blood-2016-01-643569 (2016).
- 12 Neukirchen, J. et al. Incidence and prevalence of myelodysplastic syndromes: Data from the Düsseldorf MDS-registry. *Leukemia Research* 35, 1591-1596 (2011).
- 13 Zeidan, A. M., Shallis, R. M., Wang, R., Davidoff, A. & Ma, X. Epidemiology of myelodysplastic syndromes: Why characterizing the beast is a prerequisite to taming it. *Blood Reviews* 34, 1-15, doi:https://doi.org/10.1016/j.blre.2018.09.001 (2019).
- 14 Zhang, L., Padron, E. & Lancet, J. The molecular basis and clinical significance of genetic mutations identified in myelodysplastic syndromes. *Leukemia Research* 39, 6-17, doi:https://doi.org/10.1016/j.leukres.2014.10.006 (2015).
- 15 Lee, E.-J., Podoltsev, N., Gore, S. D. & Zeidan, A. M. The evolving field of prognostication and risk stratification in MDS: Recent developments and future directions. *Blood Reviews* 30, 1-10, doi:https://doi.org/10.1016/j.blre.2015.06.004 (2016).
- 16 Kennedy, J. A. & Ebert, B. L. Clinical Implications of Genetic Mutations in Myelodysplastic Syndrome. *J Clin Oncol* 35, 968-974, doi:10.1200/JCO.2016.71.0806 (2017).
- 17 Menssen, A. J. & Matthew, W. J. Genetics of progression from MDS to secondary leukemia. *Blood* 136 (1), 50-60 (2020).
- 18 Bispo, J. A. B., Pinheiro, P. S. & Kobetz, E. K. Epidemiology and Etiology of Leukemia and Lymphoma. *Cold Spring Harb Perspect Med* 10, doi:10.1101/cshperspect.a034819 (2020).
- 19 Velten, L. et al. Identification of leukemic and pre-leukemic stem cells by clonal tracking from single-cell transcriptomics. *Nat Commun* 12, 1366, doi:10.1038/s41467-021-21650-1 (2021).

Bibliography

- 20 Pelayo, R., Dorantes-Acosta, E., Vadillo, E. & Fuentes-P, E. in *Advances in Hematopoietic Stem Cell Research* Ch. Chapter 5, (2012).
- 21 Ahmed, N., Yigit, A., Isik, Z. & Alpkocak, A. Identification of Leukemia Subtypes from Microscopic Images Using Convolutional Neural Network. *Diagnostics (Basel)* 9, doi:10.3390/diagnostics9030104 (2019).
- 22 Khoury, J. D. et al. The 5th edition of the World Health Organization Classification of Haematolymphoid Tumours: Myeloid and Histiocytic/Dendritic Neoplasms. *Leukemia* 36, 1703-1719, doi:10.1038/s41375-022-01613-1 (2022).
- 23 Arber, D. A. et al. The 2016 revision to the World Health Organization classification of myeloid neoplasms and acute leukemia. *Blood* 127, 2391-2405, doi:10.1182/blood-2016-03-643544 (2016).
- 24 Vardiman, J. W. The World Health Organization (WHO) classification of tumors of the hematopoietic and lymphoid tissues: An overview with emphasis on the myeloid neoplasms. *Chemico-Biological Interactions* 184, 16-20, doi:https://doi.org/10.1016/j.cbi.2009.10.009 (2010).
- 25 Brunning, R. D. Classification of acute leukemias. *Semin Diagn Pathol* 20, 142-153, doi:10.1016/s0740-2570(03)00031-5 (2003).
- 26 RKI. Krebs in Deutschland. (Robert Koch-Institut, Berlin, 2019).
- 27 Miranda-Filho, A. et al. Epidemiological patterns of leukaemia in 184 countries: a population-based study. *Lancet Haematol* 5, e14-e24, doi:10.1016/s2352-3026(17)30232-6 (2018).
- 28 Snyder, R. Leukemia and benzene. *Int J Environ Res Public Health* 9, 2875-2893, doi:10.3390/ijerph9082875 (2012).
- 29 Friedman, D. L. et al. Subsequent neoplasms in 5-year survivors of childhood cancer: the Childhood Cancer Survivor Study. *J Natl Cancer Inst* 102, 1083-1095, doi:10.1093/jnci/djq238 (2010).
- 30 Stieglitz, E. & Loh, M. L. Genetic predispositions to childhood leukemia. *Ther Adv Hematol* 4, 270-290, doi:10.1177/2040620713498161 (2013).
- 31 Davis, A. S., Viera, A. J. & Mead, M. D. Leukemia: An Overview for Primary Care. *American Family Physician* 89 (2014).
- 32 Sanz, M. A. et al. Management of acute promyelocytic leukemia: recommendations from an expert panel on behalf of the European LeukemiaNet. *Blood* 113, 1875-1891, doi:10.1182/blood-2008-04-150250 (2009).
- 33 Stein, E. M. & Tallman, M. S. Emerging therapeutic drugs for AML. *Blood* 127, 71-78, doi:10.1182/blood-2015-07-604538 (2016).
- 34 Jabbour, E. & Kantarjian, H. Chronic myeloid leukemia: 2018 update on diagnosis, therapy and monitoring. *Am J Hematol* 93, 442-459, doi:10.1002/ajh.25011 (2018).
- 35 Hallek, M., Shanafelt, T. D. & Eichhorst, B. Chronic lymphocytic leukaemia. *Lancet* 391, 1524-1537, doi:10.1016/s0140-6736(18)30422-7 (2018).
- 36 Medinger, M., Heim, D., Lengerke, C., Halter, J. P. & Passweg, J. R. [Acute lymphoblastic leukemia - diagnosis and therapy]. *Ther Umsch* 76, 510-515, doi:10.1024/0040-5930/a001127 (2019).
- 37 Siegel, R. L., Miller, K. D. & Jemal, A. Cancer Statistics, 2017. *CA Cancer J Clin* 67, 7-30, doi:10.3322/caac.21387 (2017).
- 38 Patel, J. P. et al. Prognostic relevance of integrated genetic profiling in acute myeloid leukemia. *N Engl J Med* 366, 1079-1089, doi:10.1056/NEJMoa1112304 (2012).
- 39 Cancer Genome Atlas Research, N. et al. Genomic and epigenomic landscapes of adult de novo acute myeloid leukemia. *N Engl J Med* 368, 2059-2074, doi:10.1056/NEJMoa1301689 (2013).
- 40 Yamada, O. & Kawachi, K. The role of the JAK-STAT pathway and related signal cascades in telomerase activation during the development of hematologic malignancies. *JAKSTAT* 2, e25256, doi:10.4161/jkst.25256 (2013).

Bibliography

- 41 Cook, A. M. et al. Role of altered growth factor receptor-mediated JAK2 signaling in growth and maintenance of human acute myeloid leukemia stem cells. *Blood* 123, 2826-2837, doi:10.1182/blood-2013-05-505735 (2014).
- 42 Ghoshal Gupta, S., Baumann, H. & Wetzler, M. Epigenetic regulation of signal transducer and activator of transcription 3 in acute myeloid leukemia. *Leuk Res* 32, 1005-1014, doi:10.1016/j.leukres.2007.11.035 (2008).
- 43 Grisendi, S., Mecucci, C., Falini, B. & Pandolfi, P. P. Nucleophosmin and cancer. *Nat Rev Cancer* 6, 493-505, doi:10.1038/nrc1885 (2006).
- 44 Falini, B., Brunetti, L., Sportoletti, P. & Martelli, M. P. NPM1-mutated acute myeloid leukemia: from bench to bedside. *Blood* 136, 1707-1721, doi:10.1182/blood.2019004226 (2020).
- 45 Odenike, O., Anastasi, J. & Le Beau, M. M. Myelodysplastic syndromes. *Clin Lab Med* 31, 763-784, doi:10.1016/j.cl.2011.08.005 (2011).
- 46 Figueroa, M. E. et al. DNA methylation signatures identify biologically distinct subtypes in acute myeloid leukemia. *Cancer Cell* 17, 13-27, doi:10.1016/j.ccr.2009.11.020 (2010).
- 47 Yang, L., Rau, R. & Goodell, M. A. DNMT3A in haematological malignancies. *Nat Rev Cancer* 15, 152-165, doi:10.1038/nrc3895 (2015).
- 48 Ley, T. J. et al. DNMT3A mutations in acute myeloid leukemia. *N Engl J Med* 363, 2424-2433, doi:10.1056/NEJMoa1005143 (2010).
- 49 Russler-Germain, D. A. et al. The R882H DNMT3A mutation associated with AML dominantly inhibits wild-type DNMT3A by blocking its ability to form active tetramers. *Cancer Cell* 25, 442-454, doi:10.1016/j.ccr.2014.02.010 (2014).
- 50 Qu, Y. et al. Differential methylation in CN-AML preferentially targets non-CGI regions and is dictated by DNMT3A mutational status and associated with predominant hypomethylation of HOX genes. *Epigenetics* 9, 1108-1119, doi:10.4161/epi.29315 (2014).
- 51 Lu, R. et al. Epigenetic Perturbations by Arg882-Mutated DNMT3A Potentiate Aberrant Stem Cell Gene-Expression Program and Acute Leukemia Development. *Cancer Cell* 30, 92-107, doi:10.1016/j.ccell.2016.05.008 (2016).
- 52 Shlush, L. I. et al. Identification of pre-leukaemic haematopoietic stem cells in acute leukaemia. *Nature* 506, 328-333, doi:10.1038/nature13038 (2014).
- 53 Spencer, D. H. et al. CpG Island Hypermethylation Mediated by DNMT3A Is a Consequence of AML Progression. *Cell* 168, 801-816 e813, doi:10.1016/j.cell.2017.01.021 (2017).
- 54 Yang, X., Wong, M. P. M. & Ng, R. K. Aberrant DNA Methylation in Acute Myeloid Leukemia and Its Clinical Implications. *Int J Mol Sci* 20, doi:10.3390/ijms20184576 (2019).
- 55 Garg, S. et al. Hepatic leukemia factor is a novel leukemic stem cell regulator in DNMT3A, NPM1, and FLT3-ITD triple-mutated AML. *Blood* 134, 263-276 (2019).
- 56 Zarka, J., Short, N. J., Kanagal-Shamanna, R. & Issa, G. C. Nucleophosmin 1 Mutations in Acute Myeloid Leukemia. *Genes (Basel)* 11, doi:10.3390/genes11060649 (2020).
- 57 Berger, S. L., Kouzarides, T., Shiekhattar, R. & Shilatifard, A. An operational definition of epigenetics. *Genes Dev* 23, 781-783, doi:10.1101/gad.1787609 (2009).
- 58 John, R. M. & Rougeulle, C. Developmental Epigenetics: Phenotype and the Flexible Epigenome. *Front Cell Dev Biol* 6, 130, doi:10.3389/fcell.2018.00130 (2018).
- 59 Allis, C. D. & Jenuwein, T. The molecular hallmarks of epigenetic control. *Nature Reviews Genetics* 17, 487-500, doi:10.1038/nrg.2016.59 (2016).
- 60 Quina, A. S., Buschbeck, M. & Di Croce, L. Chromatin structure and epigenetics. *Biochemical Pharmacology* 72, 1563-1569, doi:https://doi.org/10.1016/j.bcp.2006.06.016 (2006).
- 61 Li, B., Carey, M. & Workman, J. L. The role of chromatin during transcription. *Cell* 128, 707-719, doi:10.1016/j.cell.2007.01.015 (2007).

Bibliography

- 62 Rose, N. R. & Klose, R. J. Understanding the relationship between DNA methylation and histone lysine methylation. *Biochim Biophys Acta* 1839, 1362-1372, doi:10.1016/j.bbagr.2014.02.007 (2014).
- 63 O'Brien, J., Hayder, H., Zayed, Y. & Peng, C. Overview of MicroRNA Biogenesis, Mechanisms of Actions, and Circulation. *Front Endocrinol (Lausanne)* 9, 402, doi:10.3389/fendo.2018.00402 (2018).
- 64 Dana, H. et al. Molecular Mechanisms and Biological Functions of siRNA. *INTERNATIONAL JOURNAL of BIOMEDICAL SCIENCE* Vol. 13 (2017).
- 65 Statello, L., Guo, C. J., Chen, L. L. & Huarte, M. Gene regulation by long non-coding RNAs and its biological functions. *Nat Rev Mol Cell Biol* 22, 96-118, doi:10.1038/s41580-020-00315-9 (2021).
- 66 Zhang, J., Zhang, Y. Z., Jiang, J. & Duan, C. G. The Crosstalk Between Epigenetic Mechanisms and Alternative RNA Processing Regulation. *Front Genet* 11, 998, doi:10.3389/fgene.2020.00998 (2020).
- 67 Yang, Y. & Wang, Y. Role of Epigenetic Regulation in Plasticity of Tumor Immune Microenvironment. *Front Immunol* 12, 640369, doi:10.3389/fimmu.2021.640369 (2021).
- 68 Robertson, K. D. & Jones, P. A. DNA methylation: Past, present and future directions. *Carcinogenesis* 21, 461-467 (2000).
- 69 Turker, M. S. The establishment and maintenance of DNA methylation patterns in mouse somatic cells. *Semin Cancer Biol* 9, 329-337, doi:10.1006/scbi.1999.0133 (1999).
- 70 Jones, P. A. & Takai, D. The role of DNA methylation in mammalian epigenetics. *Science* 293, 1068-1070, doi:10.1126/science.1063852 (2001).
- 71 Bestor, T. H., Gundersen, G., Kolstø, A.-B. & Prydz, H. CpG islands in mammalian gene promoters are inherently resistant to de novo methylation. *Genetic Analysis: Biomolecular Engineering* 9, 48-53, doi:https://doi.org/10.1016/1050-3862(92)90030-9 (1992).
- 72 Cross, S. H. & Bird, A. P. CpG islands and genes. *Current Opinion in Genetics & Development* 5, 309-314, doi:https://doi.org/10.1016/0959-437X(95)80044-1 (1995).
- 73 Goll, M. G. & Bestor, T. H. Eukaryotic cytosine methyltransferases. *Annu Rev Biochem* 74, 481-514, doi:10.1146/annurev.biochem.74.010904.153721 (2005).
- 74 Bird, A. DNA methylation patterns and epigenetic memory. *Genes Dev* 16, 6-21, doi:10.1101/gad.947102 (2002).
- 75 Weber, M. et al. Distribution, silencing potential and evolutionary impact of promoter DNA methylation in the human genome. *Nature Genetics* 39, 457-466, doi:10.1038/ng1990 (2007).
- 76 Okano, M., Bell, D. W., Haber, D. A. & Li, E. DNA Methyltransferases Dnmt3a and Dnmt3b Are Essential for De Novo Methylation and Mammalian Development. *Cell* 99, 247-257 (1999).
- 77 Arand, J. et al. In vivo control of CpG and non-CpG DNA methylation by DNA methyltransferases. *PLoS Genet* 8, e1002750, doi:10.1371/journal.pgen.1002750 (2012).
- 78 Ji, H. et al. Comprehensive methylome map of lineage commitment from haematopoietic progenitors. *Nature* 467, 338-342, doi:10.1038/nature09367 (2010).
- 79 Farlik, M. et al. DNA Methylation Dynamics of Human Hematopoietic Stem Cell Differentiation. *Cell Stem Cell* 19, 808-822, doi:10.1016/j.stem.2016.10.019 (2016).
- 80 Bock, C. et al. DNA methylation dynamics during in vivo differentiation of blood and skin stem cells. *Mol Cell* 47, 633-647, doi:10.1016/j.molcel.2012.06.019 (2012).
- 81 Bröske, A.-M. et al. DNA methylation protects hematopoietic stem cell multipotency from myeloerythroid restriction. *Nature Genetics* 41, 1207-1215, doi:10.1038/ng.463 (2009).
- 82 Tadokoro, Y., Ema, H., Okano, M., Li, E. & Nakauchi, H. De novo DNA methyltransferase is essential for self-renewal, but not for differentiation, in hematopoietic stem cells. *J Exp Med* 204, 715-722, doi:10.1084/jem.20060750 (2007).

Bibliography

- 83 Trowbridge, J. J., Snow, J. W., Kim, J. & Orkin, S. H. DNA methyltransferase 1 is essential for and uniquely regulates hematopoietic stem and progenitor cells. *Cell Stem Cell* 5, 442-449, doi:10.1016/j.stem.2009.08.016 (2009).
- 84 Hodges, E. et al. Directional DNA methylation changes and complex intermediate states accompany lineage specificity in the adult hematopoietic compartment. *Mol Cell* 44, 17-28, doi:10.1016/j.molcel.2011.08.026 (2011).
- 85 Hogart, A. et al. Genome-wide DNA methylation profiles in hematopoietic stem and progenitor cells reveal overrepresentation of ETS transcription factor binding sites. *Genome Res* 22, 1407-1418, doi:10.1101/gr.132878.111 (2012).
- 86 Challen, G. A. et al. Dnmt3a is essential for hematopoietic stem cell differentiation. *Nat Genet* 44, 23-31, doi:10.1038/ng.1009 (2011).
- 87 Ma, H. S. et al. Overexpression of DNA (Cytosine-5)-Methyltransferase 1 (DNMT1) And DNA (Cytosine-5)-Methyltransferase 3A (DNMT3A) Is Associated with Aggressive Behavior and Hypermethylation of Tumor Suppressor Genes in Human Pituitary Adenomas. *Med Sci Monit* 24, 4841-4850, doi:10.12659/msm.910608 (2018).
- 88 Rajabi, H. et al. DNA methylation by DNMT1 and DNMT3b methyltransferases is driven by the MUC1-C oncoprotein in human carcinoma cells. *Oncogene* 35, 6439-6445, doi:10.1038/onc.2016.180 (2016).
- 89 Wong, K. K. DNMT1 as a therapeutic target in pancreatic cancer: mechanisms and clinical implications. *Cellular Oncology* 43, 779-792, doi:10.1007/s13402-020-00526-4 (2020).
- 90 Wong, K. K. DNMT1: A key drug target in triple-negative breast cancer. *Seminars in Cancer Biology* 72, 198-213, doi:https://doi.org/10.1016/j.semcancer.2020.05.010 (2021).
- 91 Wu, J. et al. Linc00152 promotes tumorigenesis by regulating DNMTs in triple-negative breast cancer. *Biomedicine & Pharmacotherapy* 97, 1275-1281, doi:https://doi.org/10.1016/j.biopha.2017.11.055 (2018).
- 92 Loo, S. K., Ab. Hamid, S. S., Musa, M. & Wong, K. K. DNMT1 is associated with cell cycle and DNA replication gene sets in diffuse large B-cell lymphoma. *Pathology - Research and Practice* 214, 134-143, doi:https://doi.org/10.1016/j.prp.2017.10.005 (2018).
- 93 Poole, C. J. et al. DNMT3B overexpression contributes to aberrant DNA methylation and MYC-driven tumor maintenance in T-ALL and Burkitt's lymphoma. *Oncotarget* 8, 76898-76920, doi:10.18632/oncotarget.20176 (2017).
- 94 Loo, S. K. et al. DNMT1 is predictive of survival and associated with Ki-67 expression in R-CHOP-treated diffuse large B-cell lymphomas. *Pathology* 49, 731-739, doi:10.1016/j.pathol.2017.08.009 (2017).
- 95 Benetatos, L. & Vartholomatos, G. On the potential role of DNMT1 in acute myeloid leukemia and myelodysplastic syndromes: not another mutated epigenetic driver. *Ann Hematol* 95, 1571-1582, doi:10.1007/s00277-016-2636-8 (2016).
- 96 Brunetti, L., Gundry, M. C. & Goodell, M. A. DNMT3A in Leukemia. *Cold Spring Harb Perspect Med* 7, doi:10.1101/cshperspect.a030320 (2017).
- 97 Wang, Z. et al. Acute myeloid leukemia immune escape by epigenetic CD48 silencing. *Clin Sci (Lond)* 134, 261-271, doi:10.1042/cs20191170 (2020).
- 98 Wong, K. K., Lawrie, C. H. & Green, T. M. Oncogenic Roles and Inhibitors of DNMT1, DNMT3A, and DNMT3B in Acute Myeloid Leukaemia. *Biomarker Insights* 14, 1-12 (2019).
- 99 Christiansen, D. H., Andersen, M. K. & Pedersen-Bjergaard, J. Methylation of p15INK4B is common, is associated with deletion of genes on chromosome arm 7q and predicts a poor prognosis in therapy-related myelodysplasia and acute myeloid leukemia. *Leukemia* 17, 1813-1819, doi:10.1038/sj.leu.2403054 (2003).
- 100 Sherr, C. J. Principles of Tumor Suppression. *Cell* 116, 235-246 (2004).

Bibliography

- 101 Singh, V., Sharma, P. & Capalash, N. DNA methyltransferase-1 inhibitors as epigenetic therapy for cancer. *Curr Cancer Drug Targets* 13, 379-399, doi:10.2174/15680096113139990077 (2013).
- 102 Fares, J., Wolff, L. & Bies, J. p15INK4b, a Tumor Suppressor in Acute Myeloid Leukemia 289-312 (IntechOpen, 2011).
- 103 Mizuno, S. et al. Expression of DNA methyltransferases DNMT1, 3A, and 3B in normal hematopoiesis and in acute and chronic myelogenous leukemia. *Blood* 97 (2001).
- 104 Bovolenta, P., Esteve, P., Ruiz, J. M., Cisneros, E. & Lopez-Rios, J. Beyond Wnt inhibition: new functions of secreted Frizzled-related proteins in development and disease. *J Cell Sci* 121, 737-746, doi:10.1242/jcs.026096 (2008).
- 105 Chong, J. M., Uren, A., Rubin, J. S. & Speicher, D. W. Disulfide bond assignments of secreted Frizzled-related protein-1 provide insights about Frizzled homology and netrin modules. *J Biol Chem* 277, 5134-5144, doi:10.1074/jbc.M108533200 (2002).
- 106 Nusse, R. & Clevers, H. Wnt/beta-Catenin Signaling, Disease, and Emerging Therapeutic Modalities. *Cell* 169, 985-999, doi:10.1016/j.cell.2017.05.016 (2017).
- 107 van Andel, H., Kocemba, K. A., Spaargaren, M. & Pals, S. T. Aberrant Wnt signaling in multiple myeloma: molecular mechanisms and targeting options. *Leukemia* 33, 1063-1075, doi:10.1038/s41375-019-0404-1 (2019).
- 108 Atschekzei, F. et al. SFRP1 CpG island methylation locus is associated with renal cell cancer susceptibility and disease recurrence. *Epigenetics* 7, 447-457, doi:10.4161/epi.19614 (2012).
- 109 Huang, J. et al. Down-regulation of SFRP1 as a putative tumor suppressor gene can contribute to human hepatocellular carcinoma. *BMC Cancer* 7, 126, doi:10.1186/1471-2407-7-126 (2007).
- 110 Kim, J. & Kim, S. In silico Identification of SFRP1 as a Hypermethylated Gene in Colorectal Cancers. *Genomics Inform* 12, 171-180, doi:10.5808/GI.2014.12.4.171 (2014).
- 111 Lim, D. H. K. & Maher, E. R. DNA methylation: a form of epigenetic control of gene expression. *The Obstetrician & Gynaecologist* 12, 37-42 (2011).
- 112 Fukui, T. et al. Transcriptional silencing of secreted frizzled related protein 1 (SFRP 1) by promoter hypermethylation in non-small-cell lung cancer. *Oncogene* 24, 6323-6327, doi:10.1038/sj.onc.1208777 (2005).
- 113 Kirstetter, P., Anderson, K., Porse, B. T., Jacobsen, S. E. & Nerlov, C. Activation of the canonical Wnt pathway leads to loss of hematopoietic stem cell repopulation and multilineage differentiation block. *Nat Immunol* 7, 1048-1056, doi:10.1038/ni1381 (2006).
- 114 Khan, N. I. & Bendall, L. J. Role of WNT signaling in normal and malignant hematopoiesis. *Histology and Histopathology* 21, 761-774 (2006).
- 115 Guo, H. et al. Hypermethylation of secreted frizzled-related proteins predicts poor prognosis in non-M3 acute myeloid leukemia. *Onco Targets Ther* 10, 3635-3644, doi:10.2147/OTT.S136502 (2017).
- 116 Gama-Sosa, M. A. et al. The 5-methylcytosine content of DNA from human tumors. *Nucleic Acids Research* 11, 6883-6894, doi:10.1093/nar/11.19.6883 (1983).
- 117 Bedford, M. T. & Helden, P. D. v. Hypomethylation of DNA in Pathological Conditions of the Human Prostate. *Cancer Research* 47, 5274-5276 (1987).
- 118 Feinberg, A. P., Gehrke, C. W., Kuo, K. C. & Ehrlich, M. Reduced genomic 5-methylcytosine content in human colonic neoplasia. *Cancer Research* 48, 1159-1161 (1988).
- 119 Beck, C. R., Garcia-Perez, J. L., Badge, R. M. & Moran, J. V. LINE-1 elements in structural variation and disease. *Annu Rev Genomics Hum Genet* 12, 187-215, doi:10.1146/annurev-genom-082509-141802 (2011).
- 120 Gaudet, F. et al. Induction of Tumors in Mice by Genomic Hypomethylation. *Science* 300, 489-492, doi:10.1126/science.1083558 (2003).

Bibliography

- 121 Eden, A., Gaudet, F., Waghmare, A. & Jaenisch, R. Chromosomal Instability and Tumors Promoted by DNA Hypomethylation. *Science* 300, 455-455, doi:10.1126/science.1083557 (2003).
- 122 Karpf, A. R. & Matsui, S. Genetic disruption of cytosine DNA methyltransferase enzymes induces chromosomal instability in human cancer cells. *Cancer Res* 65, 8635-8639, doi:10.1158/0008-5472.CAN-05-1961 (2005).
- 123 Feinberg, A. P. & Tycko, B. The history of cancer epigenetics. *Nature Reviews Cancer* 4, 143-153, doi:10.1038/nrc1279 (2004).
- 124 Epping, M. T. et al. The human tumor antigen PRAME is a dominant repressor of retinoic acid receptor signaling. *Cell* 122, 835-847, doi:10.1016/j.cell.2005.07.003 (2005).
- 125 Karpf, A. R., Bai, S., James, S. R., Mohler, J. L. & Wilson, E. M. Increased expression of androgen receptor coregulator MAGE-11 in prostate cancer by DNA hypomethylation and cyclic AMP. *Mol Cancer Res* 7, 523-535, doi:10.1158/1541-7786.MCR-08-0400 (2009).
- 126 Orichio, E. et al. Distinct roles for LINE-1 and HERV-K retroelements in cell proliferation, differentiation and tumor progression. *Oncogene* 26, 4226-4233, doi:10.1038/sj.onc.1210214 (2007).
- 127 Hillman, J. C. et al. BORIS Expression in Ovarian Cancer Precursor Cells Alters the CTCF Cistrome and Enhances Invasiveness through GALNT14. *Mol Cancer Res* 17, 2051-2062, doi:10.1158/1541-7786.MCR-19-0310 (2019).
- 128 Timp, W. & Feinberg, A. P. Cancer as a dysregulated epigenome allowing cellular growth advantage at the expense of the host. *Nat Rev Cancer* 13, 497-510, doi:10.1038/nrc3486 (2013).
- 129 Paro, R., Grossniklaus, U., Santoro, R. & Wutz, A. Introduction to Epigenetics. (2021).
- 130 Zhao, Z. & Shilatifard, A. Epigenetic modifications of histones in cancer. *Genome Biol* 20, 245, doi:10.1186/s13059-019-1870-5 (2019).
- 131 Rea, S. et al. Regulation of chromatin structure by site-specific histone H3 methyltransferases. *Nature* 406, 593-599, doi:10.1038/35020506 (2000).
- 132 Schultz, D. C., Ayyanathan, K., Negorev, D., Maul, G. G. & Rauscher, F. J., 3rd. SETDB1: a novel KAP-1-associated histone H3, lysine 9-specific methyltransferase that contributes to HP1-mediated silencing of euchromatic genes by KRAB zinc-finger proteins. *Genes Dev* 16, 919-932, doi:10.1101/gad.973302 (2002).
- 133 Tachibana, M., Sugimoto, K., Fukushima, T. & Shinkai, Y. Set domain-containing protein, G9a, is a novel lysine-preferring mammalian histone methyltransferase with hyperactivity and specific selectivity to lysines 9 and 27 of histone H3. *J Biol Chem* 276, 25309-25317, doi:10.1074/jbc.M101914200 (2001).
- 134 Martin, C. & Zhang, Y. The diverse functions of histone lysine methylation. *Nature Reviews Molecular Cell Biology* 6, 838-849, doi:10.1038/nrm1761 (2005).
- 135 Shinkai, Y. & Tachibana, M. H3K9 methyltransferase G9a and the related molecule GLP. *Genes Dev* 25, 781-788, doi:10.1101/gad.2027411 (2011).
- 136 Minkovsky, A. et al. The Mbd1-Atf7ip-Setdb1 pathway contributes to the maintenance of X chromosome inactivation. *Epigenetics & Chromatin* 7:12 (2014).
- 137 Karimi, M. M. et al. DNA methylation and SETDB1/H3K9me3 regulate predominantly distinct sets of genes, retroelements, and chimeric transcripts in mESCs. *Cell Stem Cell* 8, 676-687, doi:10.1016/j.stem.2011.04.004 (2011).
- 138 Du, J., Johnson, L. M., Jacobsen, S. E. & Patel, D. J. DNA methylation pathways and their crosstalk with histone methylation. *Nat Rev Mol Cell Biol* 16, 519-532, doi:10.1038/nrm4043 (2015).
- 139 Casciello, F., Windloch, K., Gannon, F. & Lee, J. S. Functional Role of G9a Histone Methyltransferase in Cancer. *Front Immunol* 6, 487, doi:10.3389/fimmu.2015.00487 (2015).

Bibliography

- 140 Shankar, S. R. et al. G9a, a multipotent regulator of gene expression. *Epigenetics* 8, 16-22, doi:10.4161/epi.23331 (2013).
- 141 Lachner, M., O'Carroll, D., Rea, S., Mechtler, K. & Jenuwein, T. Methylation of histone H3 lysine 9 creates a binding site for HP1 proteins. *Nature* 410, 116-120, doi:10.1038/35065132 (2001).
- 142 Lehnertz, B. et al. The methyltransferase G9a regulates HoxA9-dependent transcription in AML. *Genes Dev* 28, 317-327, doi:10.1101/gad.236794.113 (2014).
- 143 Zhang, J. et al. Down-regulation of G9a triggers DNA damage response and inhibits colorectal cancer cells proliferation. *Oncotarget* 6 (2015).
- 144 Hua, K.-T. et al. The H3K9 methyltransferase G9a is a marker of aggressive ovarian cancer that promotes peritoneal metastasis. *Molecular Cancer* 13 (2014).
- 145 Nan, X. et al. Transcriptional repression by the methyl-CpG-binding protein MeCP2 involves a histone deacetylase complex. *Nature* 393, 386-389, doi:10.1038/30764 (1998).
- 146 Hendrich, B. & Bird, A. Identification and Characterization of a Family of Mammalian Methyl-CpG Binding Proteins. *MOLECULAR AND CELLULAR BIOLOGY* 18, 6538–6547 (1998).
- 147 Fuks, F. et al. The methyl-CpG-binding protein MeCP2 links DNA methylation to histone methylation. *J Biol Chem* 278, 4035-4040, doi:10.1074/jbc.M210256200 (2003).
- 148 Okitsu, C. Y. & Hsieh, C. L. DNA methylation dictates histone H3K4 methylation. *Mol Cell Biol* 27, 2746-2757, doi:10.1128/MCB.02291-06 (2007).
- 149 Tamaru, H. & Selker, E. U. A histone H3 methyltransferase controls DNA methylation in *Neurospora crassa*. *Nature* 414, 277-283, doi:10.1038/35104508 (2001).
- 150 Feldman, N. et al. G9a-mediated irreversible epigenetic inactivation of Oct-3/4 during early embryogenesis. *Nature Cell Biology* 8, 188-194, doi:10.1038/ncb1353 (2006).
- 151 Lehnertz, B. et al. Suv39h-Mediated Histone H3 Lysine 9 Methylation Directs DNA Methylation to Major Satellite Repeats at Pericentric Heterochromatin. *Current Biology* 13, 1192-1200, doi:10.1016/s0960-9822(03)00432-9 (2003).
- 152 Smallwood, A., Esteve, P. O., Pradhan, S. & Carey, M. Functional cooperation between HP1 and DNMT1 mediates gene silencing. *Genes Dev* 21, 1169-1178, doi:10.1101/gad.1536807 (2007).
- 153 Esteve, P. O. et al. Direct interaction between DNMT1 and G9a coordinates DNA and histone methylation during replication. *Genes Dev* 20, 3089-3103, doi:10.1101/gad.1463706 (2006).
- 154 McCabe, M. T., Brandes, J. C. & Vertino, P. M. Cancer DNA methylation: molecular mechanisms and clinical implications. *Clin Cancer Res* 15, 3927-3937, doi:10.1158/1078-0432.CCR-08-2784 (2009).
- 155 Tachibana, M., Matsumura, Y., Fukuda, M., Kimura, H. & Shinkai, Y. G9a/GLP complexes independently mediate H3K9 and DNA methylation to silence transcription. *EMBO J* 27, 2681-2690, doi:10.1038/emboj.2008.192 (2008).
- 156 Wozniak, R. J., Klimecki, W. T., Lau, S. S., Feinstein, Y. & Futscher, B. W. 5-Aza-2'-deoxycytidine-mediated reductions in G9A histone methyltransferase and histone H3 K9 di-methylation levels are linked to tumor suppressor gene reactivation. *Oncogene* 26, 77-90, doi:10.1038/sj.onc.1209763 (2007).
- 157 Sharma, S. et al. Lysine methyltransferase G9a is not required for DNMT3A/3B anchoring to methylated nucleosomes and maintenance of DNA methylation in somatic cells. *Epigenetics and Chromatin* 5 (2012).
- 158 Kondo, Y. Epigenetic cross-talk between DNA methylation and histone modifications in human cancers. *Yonsei Med J* 50, 455-463, doi:10.3349/ymj.2009.50.4.455 (2009).
- 159 Greenberg, P. L. et al. Revised international prognostic scoring system for myelodysplastic syndromes. *Blood* 120, 2454-2465, doi:10.1182/blood-2012-03-420489 (2012).

Bibliography

- 160 Tobinsson, M. & Kittang, A. O. Treatment of myelodysplastic syndrome in the era of next-generation sequencing. *J Intern Med* 286, 41-62, doi:10.1111/joim.12893 (2019).
- 161 Giagounidis, A. et al. Results of a randomized, double-blind study of romiplostim versus placebo in patients with low/intermediate-1-risk myelodysplastic syndrome and thrombocytopenia. *Cancer* 120, 1838-1846, doi:10.1002/cncr.28663 (2014).
- 162 Garelius, H. K. et al. Erythropoiesis-stimulating agents significantly delay the onset of a regular transfusion need in nontransfused patients with lower-risk myelodysplastic syndrome. *J Intern Med* 281, 284-299, doi:10.1111/joim.12579 (2017).
- 163 Zhou, L. et al. Inhibition of the TGF-beta receptor I kinase promotes hematopoiesis in MDS. *Blood* 112, 3434-3443, doi:10.1182/blood-2008-02-139824 (2008).
- 164 Cimmino, L. et al. Restoration of TET2 Function Blocks Aberrant Self-Renewal and Leukemia Progression. *Cell* 170, 1079-1095 e1020, doi:10.1016/j.cell.2017.07.032 (2017).
- 165 Stahl, M. & Zeidan, A. M. Lenalidomide use in myelodysplastic syndromes: Insights into the biologic mechanisms and clinical applications. *Cancer* 123, 1703-1713, doi:10.1002/cncr.30585 (2017).
- 166 Ball, B. J. et al. Venetoclax and hypomethylating agents (HMAs) induce high response rates in MDS, including patients after HMA therapy failure. *Blood Adv* 4, 2866-2870, doi:10.1182/bloodadvances.2020001482 (2020).
- 167 Bewersdorf, J. P., Stahl, M. & Zeidan, A. M. Immune checkpoint-based therapy in myeloid malignancies: a promise yet to be fulfilled. *Expert Rev Anticancer Ther* 19, 393-404, doi:10.1080/14737140.2019.1589374 (2019).
- 168 Assi, R. et al. A phase II trial of ruxolitinib in combination with azacytidine in myelodysplastic syndrome/myeloproliferative neoplasms. *Am J Hematol* 93, 277-285, doi:10.1002/ajh.24972 (2018).
- 169 Hollenbach, P. W. et al. A comparison of azacitidine and decitabine activities in acute myeloid leukemia cell lines. *PLoS One* 5, e9001, doi:10.1371/journal.pone.0009001 (2010).
- 170 Patel, A. A., Cahill, K., Saygin, C. & Odenike, O. Cedazuridine/decitabine: from preclinical to clinical development in myeloid malignancies. *Blood Adv* 5, 2264-2271, doi:10.1182/bloodadvances.2020002929 (2021).
- 171 Dohner, H. et al. Diagnosis and management of AML in adults: 2017 ELN recommendations from an international expert panel. *Blood* 129, 424-447, doi:10.1182/blood-2016-08-733196 (2017).
- 172 Dombret, H. & Gardin, C. An update of current treatments for adult acute myeloid leukemia. *Blood* 127, 53-61, doi:10.1182/blood-2015-08-604520 (2016).
- 173 Jurcic, J. G. What Happened to Anti-CD33 Therapy for Acute Myeloid Leukemia? *Current Hematologic Malignancy Reports* 7, 65-73, doi:10.1007/s11899-011-0103-0 (2012).
- 174 Levis, M. Midostaurin approved for FLT3-mutated AML. *Blood* 129, 3403-3406, doi:10.1182/blood-2017-05-782292 (2017).
- 175 Fenaux, P. et al. Azacitidine prolongs overall survival compared with conventional care regimens in elderly patients with low bone marrow blast count acute myeloid leukemia. *J Clin Oncol* 28, 562-569, doi:10.1200/JCO.2009.23.8329 (2010).
- 176 Pelcovits, A. & Niroula, R. Acute Myeloid Leukemia: A Review. *RHODE ISLAND MEDICAL JOURNAL* (2020).
- 177 Giralt, S. & Bishop, M. R. Principles and overview of allogeneic hematopoietic stem cell transplantation. *Cancer Treat Res* 144, 1-21, doi:10.1007/978-0-387-78580-6_1 (2009).
- 178 Robertson, K. D. DNA methylation and human disease. *Nature Reviews Genetics* 6, 597-610, doi:10.1038/nrg1655 (2005).
- 179 Baylin, S. B. & Jones, P. A. A decade of exploring the cancer epigenome — biological and translational implications. *Nature Reviews Cancer* 11, 726-734, doi:10.1038/nrc3130 (2011).

Bibliography

- 180 Diesch, J. et al. A clinical-molecular update on azanucleoside-based therapy for the treatment of hematologic cancers. *Clin Epigenetics* 8, 71, doi:10.1186/s13148-016-0237-y (2016).
- 181 Chiappinelli, K. B. et al. Inhibiting DNA Methylation Causes an Interferon Response in Cancer via dsRNA Including Endogenous Retroviruses. *Cell* 162, 974-986, doi:10.1016/j.cell.2015.07.011 (2015).
- 182 Roulois, D. et al. DNA-Demethylating Agents Target Colorectal Cancer Cells by Inducing Viral Mimicry by Endogenous Transcripts. *Cell* 162, 961-973, doi:10.1016/j.cell.2015.07.056 (2015).
- 183 Issa, J. P. & Kantarjian, H. M. Targeting DNA methylation. *Clin Cancer Res* 15, 3938-3946, doi:10.1158/1078-0432.CCR-08-2783 (2009).
- 184 Jose-Eneriz, E. S. et al. Discovery of first-in-class reversible dual small molecule inhibitors against G9a and DNMTs in hematological malignancies. *Nat Commun* 8, 15424, doi:10.1038/ncomms15424 (2017).
- 185 Foulks, J. M. et al. Epigenetic drug discovery: targeting DNA methyltransferases. *J Biomol Screen* 17, 2-17, doi:10.1177/1087057111421212 (2012).
- 186 Barcena-Varela, M. et al. Dual Targeting of Histone Methyltransferase G9a and DNA-Methyltransferase 1 for the Treatment of Experimental Hepatocellular Carcinoma. *Hepatology* 69, 587-603, doi:10.1002/hep.30168 (2019).
- 187 Segovia, C. et al. Inhibition of a G9a/DNMT network triggers immune-mediated bladder cancer regression. *Nat Med* 25, 1073-1081, doi:10.1038/s41591-019-0499-y (2019).
- 188 Pleyer, L. & Greil, R. Digging deep into "dirty" drugs - modulation of the methylation machinery. *Drug Metab Rev* 47, 252-279, doi:10.3109/03602532.2014.995379 (2015).
- 189 Chiba, S. et al. Establishment and erythroid differentiation of a cytokine-dependent human leukemic cell line F-36: a parental line requiring granulocyte- macrophage colony-stimulating factor or interleukin-3, and a subline requiring erythropoietin. *Blood* 78, 2261-2268, doi:10.1182/blood.V78.9.2261.2261 (1991).
- 190 Andersson, L. C., Nilsson, K. & Gahmberg, C. G. K562—A human erythroleukemic cell line. *International Journal of Cancer* 23, 143-147, doi:https://doi.org/10.1002/ijc.2910230202 (1979).
- 191 Asou, H. et al. Establishment of a Human Acute Myeloid Leukemia Cell Line (Kasumi-1) With 8;2 Chromosome Translocation. *Blood* 77, 2031-2036 (1991).
- 192 Furley, A. J. et al. Divergent molecular phenotypes of KG1 and KG1a myeloid cell lines. *Blood* 68, 1101-1107, doi:10.1182/blood.V68.5.1101.bloodjournal6851101 (1986).
- 193 Matsuoka, A. et al. Lenalidomide induces cell death in an MDS-derived cell line with deletion of chromosome 5q by inhibition of cytokinesis. *Leukemia* 24, 748-755, doi:10.1038/leu.2009.296 (2010).
- 194 Matsuo, Y. et al. Two acute monocytic leukemia (AML-M5a) cell lines (MOLM-13 and MOLM-14) with interclonal phenotypic heterogeneity showing MLL-AF9 fusion resulting from an occult chromosome insertion, ins(11;9)(q23;p22p23). *Leukemia* 11, 1469-1477 (1997).
- 195 Lanotte, M. et al. NB4, a maturation inducible cell line with t(15;17) marker isolated from a human acute promyelocytic leukemia (M3). *Blood* 77, 1080-1086, doi:10.1182/blood.V77.5.1080.1080 (1991).
- 196 Tiacci, E. et al. The NPM1 wild-type OCI-AML2 and the NPM1-mutated OCI-AML3 cell lines carry DNMT3A mutations. *Leukemia* 26, 554-557, doi:10.1038/leu.2011.238 (2012).
- 197 Tai, S. et al. PC3 is a cell line characteristic of prostatic small cell carcinoma. *Prostate* 71, 1668-1679, doi:10.1002/pros.21383 (2011).
- 198 Nakagawa, T. & Matozaki, S. The SKM-1 leukemic cell line established from a patient with progression to myelomonocytic leukemia in myelodysplastic syndrome (MDS)-

Bibliography

- contribution to better understanding of MDS. *Leuk Lymphoma* 17, 335-339, doi:10.3109/10428199509056841 (1995).
- 199 Tsuchiya, S. et al. Establishment and characterization of a human acute monocytic leukemia cell line (THP-1). *International Journal of Cancer* 26, 171-176, doi:https://doi.org/10.1002/ijc.2910260208 (1980).
- 200 Allen, R. et al. Establishment and characterization of a megakaryoblast cell line with amplification of MLL. *Leukemia* 12, 1119-1127 (1998).
- 201 Reins, J. et al. Transcriptional down-regulation of the Wnt antagonist SFRP1 in haematopoietic cells of patients with different risk types of MDS. *Leuk Res* 34, 1610-1616, doi:10.1016/j.leukres.2010.04.013 (2010).
- 202 Biotec, M. CD34 MicroBead Kit, human, (2021).
- 203 McKinnon, K. M. Flow Cytometry: An Overview. *Curr Protoc Immunol* 120, 5 1 1-5 1 11, doi:10.1002/cpim.40 (2018).
- 204 Stark, R., Grzelak, M. & Hadfield, J. RNA sequencing: the teenage years. *Nat Rev Genet* 20, 631-656, doi:10.1038/s41576-019-0150-2 (2019).
- 205 Inc, T. F. S. Real-time PCR handbook. (2014).
- 206 MilliporeSigma. Protein blotting handbook. (2017).
- 207 Busó, E. J. & Iborra, M. in *Epigenetic Biomarkers and Diagnostics* 137-153 (2016).
- 208 Goodier, J. L. Restricting retrotransposons: a review. *Mob DNA* 7, 16, doi:10.1186/s13100-016-0070-z (2016).
- 209 Qiagen. Pyrosequencing Rechnology and Platform Overview. (2021).
- 210 Ran, F. A. et al. Double nicking by RNA-guided CRISPR Cas9 for enhanced genome editing specificity. *Cell* 154, 1380-1389, doi:10.1016/j.cell.2013.08.021 (2013).
- 211 -Ran, F. A. et al. Genome engineering using the CRISPR-Cas9 system. *Nat Protoc* 8, 2281-2308, doi:10.1038/nprot.2013.143 (2013).
- 212 Salem, T. Z. et al. The Influence of SV40 polyA on Gene Expression of Baculovirus Expression Vector Systems. *PLoS One* 10, e0145019, doi:10.1371/journal.pone.0145019 (2015).
- 213 Stomper, J., Rotondo, J. C., Greve, G. & Lubbert, M. Hypomethylating agents (HMA) for the treatment of acute myeloid leukemia and myelodysplastic syndromes: mechanisms of resistance and novel HMA-based therapies. *Leukemia*, doi:10.1038/s41375-021-01218-0 (2021).
- 214 Datta, J. et al. A new class of quinoline-based DNA hypomethylating agents reactivates tumor suppressor genes by blocking DNA methyltransferase 1 activity and inducing its degradation. *Cancer Res* 69, 4277-4285, doi:10.1158/0008-5472.CAN-08-3669 (2009).
- 215 Sajid, M. et al. The Functional and Antiviral Activity of Interferon Alpha-Inducible IFI6 Against Hepatitis B Virus Replication and Gene Expression. *Front Immunol* 12, 634937, doi:10.3389/fimmu.2021.634937 (2021).
- 216 Leisching, G., Wiid, I. & Baker, B. The Association of OASL and Type I Interferons in the Pathogenesis and Survival of Intracellular Replicating Bacterial Species. *Front Cell Infect Microbiol* 7, 196, doi:10.3389/fcimb.2017.00196 (2017).
- 217 OpenStax. 10.01 Microbes and the Tools of Genetic Engineering, (2021).
- 218 Verzi, S., Krishnakumar, R., Levin, D., Krofcheck, D. & Williams, K. *Data Science and Machine Learning for Genome Security.*, (2021).
- 219 Greer, E. L. & Shi, Y. Histone methylation: a dynamic mark in health, disease and inheritance. *Nat Rev Genet* 13, 343-357, doi:10.1038/nrg3173 (2012).
- 220 Fritsch, L. et al. A subset of the histone H3 lysine 9 methyltransferases Suv39h1, G9a, GLP, and SETDB1 participate in a multimeric complex. *Mol Cell* 37, 46-56, doi:10.1016/j.molcel.2009.12.017 (2010).
- 221 Tsai, H. C. et al. Transient low doses of DNA-demethylating agents exert durable antitumor effects on hematological and epithelial tumor cells. *Cancer Cell* 21, 430-446, doi:10.1016/j.ccr.2011.12.029 (2012).

Bibliography

- 222 Abou Najem, S., Khawaja, G., Hodroj, M. H., Babikian, P. & Rizk, S. Adjuvant Epigenetic Therapy of Decitabine and Suberoylanilide Hydroxamic Acid Exerts Anti-Neoplastic Effects in Acute Myeloid Leukemia Cells. *Cells* 8, doi:10.3390/cells8121480 (2019).
- 223 Coombs, C. C., Sallman, D. A. & Rapaport, F. Mutational correlates of response to hypomethylating agent therapy in acute myeloid leukemia. *haematologica*, e457-e460 (2016).
- 224 Metzeler, K. H. et al. DNMT3A mutations and response to the hypomethylating agent decitabine in acute myeloid leukemia. *Leukemia* 26, 1106-1107, doi:10.1038/leu.2011.342 (2012).
- 225 Sato, T., Issa, J. J. & Kropf, P. DNA Hypomethylating Drugs in Cancer Therapy. *Cold Spring Harb Perspect Med* 7, doi:10.1101/cshperspect.a026948 (2017).
- 226 Yang, X. et al. Gene body methylation can alter gene expression and is a therapeutic target in cancer. *Cancer Cell* 26, 577-590, doi:10.1016/j.ccr.2014.07.028 (2014).
- 227 Wolff, F., Leisch, M., Greil, R., Risch, A. & Pleyer, L. The double-edged sword of (re)expression of genes by hypomethylating agents: from viral mimicry to exploitation as priming agents for targeted immune checkpoint modulation. *Cell Commun Signal* 15, 13, doi:10.1186/s12964-017-0168-z (2017).
- 228 Ohtani, H. et al. Activation of a Subset of Evolutionarily Young Transposable Elements and Innate Immunity Are Linked to Clinical Responses to 5-Azacytidine. *Cancer Res* 80, 2441-2450, doi:10.1158/0008-5472.CAN-19-1696 (2020).
- 229 Zitvogel, L., Galluzzi, L., Kepp, O., Smyth, M. J. & Kroemer, G. Type I interferons in anticancer immunity. *Nat Rev Immunol* 15, 405-414, doi:10.1038/nri3845 (2015).
- 230 Kordella, C., Lamprianidou, E. & Kotsianidis, I. Mechanisms of Action of Hypomethylating Agents: Endogenous Retroelements at the Epicenter. *Front Oncol* 11, 650473, doi:10.3389/fonc.2021.650473 (2021).
- 231 David J Nicholas, Pragya Srivastava, AlMujtaba AlShangity & Nemeth, M. J. DNMTi Decitabine Induces a Type I Interferon Resposne in Leukemia Cell lines. *The FASEB Journal* (2018).
- 232 Daskalakis, M. et al. Reactivation of endogenous retroviral elements via treatment with DNMT- and HDAC-inhibitors. *Cell Cycle* 17, 811-822, doi:10.1080/15384101.2018.1442623 (2018).
- 233 Kazachenka, A. et al. Epigenetic therapy of myelodysplastic syndromes connects to cellular differentiation independently of endogenous retroelement derepression. *Genome Med* 11, 86, doi:10.1186/s13073-019-0707-x (2019).
- 234 Judith K. Christman, N. M., David Herzog, and Natalie Schneiderman. Effect of 5-Azacytidine on Differentiation and DNA Methylation in Human P r o m y e l o c y t i c L e u k e m i a Cells (HL-60) *Cancer Research* 43, 763-769 (1983).
- 235 Stubbins, R. J. & Karsan, A. Differentiation therapy for myeloid malignancies: beyond cytotoxicity. *Blood Cancer J* 11, 193, doi:10.1038/s41408-021-00584-3 (2021).
- 236 S Negrotto et al. CpG methylation patterns and decitabine treatment response in acute myeloid leukemia cells and normal hematopoietic precursors. *Leukemia* 26, 244-254 (2012).
- 237 Somervaille, T. C. & Cleary, M. L. PU.1 and Junb: suppressing the formation of acute myeloid leukemia stem cells. *Cancer Cell* 10, 456-457, doi:10.1016/j.ccr.2006.11.009 (2006).
- 238 Santaguida, M. et al. JunB protects against myeloid malignancies by limiting hematopoietic stem cell proliferation and differentiation without affecting self-renewal. *Cancer Cell* 15, 341-352, doi:10.1016/j.ccr.2009.02.016 (2009).
- 239 Zhu, Y. P., Thomas, G. D. & Hedrick, C. C. 2014 Jeffrey M. Hoeg Award Lecture: Transcriptional Control of Monocyte Development. *Arterioscler Thromb Vasc Biol* 36, 1722-1733, doi:10.1161/ATVBAHA.116.304054 (2016).

Bibliography

- 240 Alcalay, M. et al. Acute myeloid leukemia bearing cytoplasmic nucleophosmin (NPMc+ AML) shows a distinct gene expression profile characterized by up-regulation of genes involved in stem-cell maintenance. *Blood* 106, 899-902, doi:10.1182/blood-2005-02-0560 (2005).
- 241 Brunetti, L. et al. Mutant NPM1 Maintains the Leukemic State through HOX Expression. *Cancer Cell* 34, 499-512 e499, doi:10.1016/j.ccell.2018.08.005 (2018).
- 242 Li, H. et al. Applications of genome editing technology in the targeted therapy of human diseases: mechanisms, advances and prospects. *Signal Transduct Target Ther* 5, 1, doi:10.1038/s41392-019-0089-y (2020).
- 243 Synthego. *How To Use CRISPR: Your Guide to Successful Genome Engineering; Chapter 06: How to Select the Best CRISPR Transfection Protocol*, (2022).
- 244 PellegriniBenchling, R. *How to express CRISPR in your target cells*, (2016).
- 245 Conti, A. & Di Micco, R. p53 activation: a checkpoint for precision genome editing? *Genome Med* 10, 66, doi:10.1186/s13073-018-0578-6 (2018).
- 246 Cheng, Y. et al. Targeting epigenetic regulators for cancer therapy: mechanisms and advances in clinical trials. *Signal Transduct Target Ther* 4, 62, doi:10.1038/s41392-019-0095-0 (2019).
- 247 Bewersdorf, J. P., Shallis, R., Stahl, M. & Zeidan, A. M. Epigenetic therapy combinations in acute myeloid leukemia: what are the options? *Ther Adv Hematol* 10, 2040620718816698, doi:10.1177/2040620718816698 (2019).